Sunali Bhatnagar

St. Anne's College

Supervised by:

Professor Constantin-C. Coussios

CAVITATION-ENHANCED TRANSDERMAL VACCINE DELIVERY BY ULTRASOUND

A thesis submitted to the Department of Engineering Science for the degree of Doctor of Philosophy

Michaelmas 2014

Abstract

Currently, the most common route for vaccine delivery is by intramuscular injection with a needle and syringe. Injection has a number of disadvantages, such as risk of infection at the injection site, needle prick injuries, and needle phobia that leads to significant levels of patient non-compliance. Therefore, the focus of this thesis is the development of an alternative ultrasound-assisted transdermal vaccine delivery system. To do so, we target immunological Langerhans cells in the epidermal layer of the skin that efficiently provoke an immune response. The stratum corneum (SC) is a barrier that prevents conventional transdermal vaccine delivery. Methods such as microneedles, iontophoresis and thermal ablation are presented in literature for the permabilisation of this layer.

Sonophoresis is the use of ultrasound to transport molecules through a medium. Previous studies have demonstrated that the key underpinning mechanism is inertial cavitation, which leads to permeabilisation of the SC and facilitates transdermal delivery. Most studies to date have pre-exposed the skin to ultrasound prior to delivery of a vaccine in liquid form as a droplet placed on the skin. This approach is not practical for widespread use, but more importantly fails to take advantage of the potential of cavitation-mediated micro streaming to enhance active transport of molecules beyond the permeabilised skin. The focus of the present work is the development of a complete system that enables storage of the vaccine in a readily useable gel form whilst promoting and monitoring cavitation activity to simultaneously permeabilise the skin and enhance transdermal vaccine transport.

Through initial *in vitro* studies, we first demonstrated that inertial cavitation can be exploited to promote the active transport of molecular entities such as vaccine molecules from a gel into a biological medium. A gel vaccine dosage formulation is utilised in order to mimic current clinically approved and established clinical ultrasound coupling gel formulations. By comparing the effects mediated at two ultrasound frequencies (0.256 MHz vs 1 MHz) which preferentially promote cavitational microstreaming or acoustic streaming, ultrasound parameters most conducive to producing high levels of inertial cavitation were identified as 0.256 MHz and peak rarefactional pressures on the order of 1 MPa. Three vaccine loaded gels were then formulated with either micro- or nano-sized cavitation nuclei and assessed for the optimal acoustic and chemical characteristics at the predetermined ultrasound parameters. Nano-sized nuclei were shown to be most effective at lowering the inertial cavitation threshold, as well as instigating the highest and most sustained levels of inertial cavitation as indicated

by broadband acoustic emissions at the ultrasound focus, without causing any structural damage to the vaccine molecules themselves.

Ex vivo data has shown that nanoscale-nucleated inertial cavitation at the skin surface delivered a model vaccine Ovalbumin (OVA) to depths of 500 μm into porcine skin. Novel nanoparticles produced in-house used to enhance and instigate cavitation at lower pressures penetrated to depths of up to 700 μm, due to their small size and unique ability to self-propel. Delivery profiles were obtained using multi-photon microscopy of skin sections immediately after treatment. Analysis of acoustic emissions from the focus showed substantial correlation between high delivery dose and depth, and significant amounts of inertial cavitation (i.e. broadband acoustic emissions from the focus).

In vivo studies showed that the delivery achieved to murine skin was significantly ($p<0.05$) higher in the nanoparticle-assisted ultrasound transdermal vaccination group than the chemical penetration enhancer (positive control) group, with delivery of doses up to 1 μg /treatment, compared to 400 ng in the positive control group. This dose was sufficient to trigger an antigen-specific immune response. Specific anti-OVA IgG antibody levels in the ultrasound-assisted vaccine delivery group were significantly ($p<0.05$) higher than in all other control groups, and substantially higher than the current gold standard in transdermal delivery – chemical penetration enhancers. Although a low level antibody response was observed transdermally compared to the subcutaneous injection group (indicative of 100% delivery response), it is believed that optimisation of this system will lead to a viable and non-invasive delivery platform for vaccines that can be used both in a primary care setting, and eventually for self-vaccination at home.

Statement of Originality

I hereby declare that this submission is my own work and, to the best of my knowledge, it contains no materials previously published or written by another person, or substantial proportions of material which have been accepted for the award of any other degree of diploma at the University of Oxford or any other educational institution, except where due acknowledgement is made in the thesis.

Any contribution made to the research by others, with whom I have worked at the University of Oxford or elsewhere, is explicitly acknowledged in the thesis.

I also declare that the intellectual content of this thesis is a product of my own work, except to the extent that assistance from others in the project's design and conception or in style, presentation and linguistic expression is acknowledged.

Sunali Bhatnagar

January 2015

Acknowledgements

This thesis is dedicated to my family because I would not be at this juncture without them. Since childhood, my parents nourished my growth and wisdom, and this achievement is a testament to their relentless encouragement, belief and personal effort to see me succeed. My sister, Dr. Rupali Bhatnagar, is credited with getting me through the peaks and troughs of my DPhil journey as both my most enthusiastic cheerleader and my harshest critic.

Within BUBBL, I would like to express my thanks to my primary supervisor, Professor Constantin Coussios, for guiding my journey from an inexperienced masters student to a scientist with the ability to independently explore new research ideas. Constantin's passion for biomedical research served as a key source of inspiration throughout my DPhil studies, and his valuable expertise in ultrasound as well as the general practice of research science has been fundamental in shaping the direction of my own research. I would also like to thank Dr Heiko Schiffter for his advice and expertise in the initial stages of my project.

The *in vivo* studies described in Chapter 6 of this thesis would not have been possible without the guidance and assistance of Dr Robert Carlisle. The time, expertise and good humour that I have received from Bob has made the final (and most challenging) part of my DPhil both enjoyable and highly educational. Senior members of BUBBL must also be credited for their patience and understanding with my unfamiliarity with lab techniques, particularly Dr Jamie Collin for his help with all things ultrasound and Dr Nikolas Weissmuller for all things biological. Completion of this thesis would have taken a lot longer had Jamie and Nik not been around.

Much of this research would never have been possible if not for the expert craftsmanship and indomitable high spirits of our workshop technicians, Jim Fisk and David Salisbury. Their presence throughout my DPhil has been both a valuable support to, and a very enjoyable reprieve from, the focussed nature of my research. I would also like to thank every member of BUBBL, past and present, as everyone has helped me in some way and made coming to the lab every day so enjoyable. I move forward from this lab with more treasured friendships than I could have imagined.

The highlight of my DPhil experience was my summer research placement at the University of Santa Barbara, California. The constant support of my host, Professor Samir Mitragotri, and his research group encouraged and inspired me to learn about new ideas, concepts and techniques in drug delivery which I never would have encountered otherwise, thus relegating the constant sunshine to my second favourite part of the summer. I would also like to take this opportunity to thank the Centre for Doctoral Training in Healthcare Innovation and the Oxford Martin School, both for the opportunity to undertake a research placement abroad and for their generous financial support throughout my DPhil.

Finally, one significant member of BUBBL has made the latter half of my time in Oxford my most enjoyable. I would like to thank my best friend and partner, Dr James Kwan, for his unfailing companionship, mentorship and encouragement through the writing of this thesis and the research described therein.

Research Dissemination

Peer-Reviewed Journal Papers

S. Bhatnagar, H. Schiffter and C.-C. Coussios, “Exploitation of Acoustic Cavitation-Induced Microstreaming to Enhance Molecular Transport”, J. Pharm. Sci. 103(6): 1903–1912 (2014).

Conference Presentations

S. Bhatnagar & C.-C Coussios "The effect of cavitation nuclei in a protein loaded gel for ultrasound-assisted transdermal delivery". The 14th International Symposium on Therapeutic Ultrasound, Las Vegas, USA. 2-5 April 2014.

S. Bhatnagar, C.-C. Coussios and H. Schiffter, “Molecular Transport Mechanisms in Ultrasound Assisted Transdermal Drug and Vaccine Delivery; A Mechanistic Study” The 12th International Symposium on Therapeutic Ultrasound, Heidelberg, Germany (2012).

Contents

List of Figures

List of Common Acronyms

BSA	Bovine Serum Albumin
NC	Nanocup
OVA	Ovalbumin
SC	Stratum corneum
DC	Duty cycle
HIFU	High-intensity focussed ultrasound
PCD	Passive cavitation detector
PRF	Pulse repetition frequency
PRFP	Peak rarefactional focal pressure
SDS	Sodium dodecyl sulphate
US	Ultrasound
TMM	Tissue mimicking material

1 Introduction

1.1 Vaccine Delivery: State of the art

Over the last 200 years, vaccinations have been one of the most successful medical interventions in the reduction of infectious diseases (Ada 2003). Research consequent to the discovery of the smallpox vaccine in 1798 uncovered the properties of a successful vaccine: the capability to elicit a strong, protective immune response, without being potent enough to overcome the immune response and cause the disease. In addition to the development of vaccines themselves, administration routes have also been the subject of significant research interest, with non-invasive routes widely regarded as the preferred solution.

The vast majority of vaccines are administered by intramuscular or subcutaneous injection. Injection requires syringes and needles, which necessitate careful disposal to avoid unintended harm. Moreover, the significant risk of cross-contamination during needle use demands adherence to strict guidelines and protocols for which trained personnel are required. Injection can be painful and cause stress, especially in children; for paediatric vaccination programs, poor compliance is one of the reasons for incomplete vaccine coverage (Jacobson, Swan et al. 2001). Finally, muscle and subcutaneous tissue contain less antigen presenting cells (APCs) than skin tissue, indicating that they are sub-optimal sites for vaccination (Bal, Ding et al. 2010). These disadvantages of injectable vaccines have boosted the research on alternative delivery routes, such as oral, mucosal and transdermal delivery systems in the search for safer and more effective vaccines. Each of these routes are briefly explained and assessed below.

Research in the area of oral vaccine delivery is fuelled by advantages such as ease of administration without any complex devices and high patient compliance. The gastro intestinal environment is the main barrier to the widespread adoption of oral vaccine delivery. The acidic environment results in poor delivery efficiency of antigen in crossing the intestinal wall (Russell-Jones 2000). As a result, strategies

for oral vaccine administration regimens include repeated large dose administration, but this is unsuitable for the majority of protein antigens due to both cost and availability. Other systems utilise nanoparticles and other proteins as mucosal binding carriers for oral vaccines to transport them across the intestinal wall unharmed (Russell-Jones, Veitch et al. 1999). With the exception of the large dose administration, these methods are currently the subject of research to determine their effectiveness and viability.

Mucosal sites represent the major portal of entry for infectious disease causing human pathogens. It is estimated that 70% of infectious agents enter the host via mucosal tissues such as the lungs, nasal, oral or vaginal and rectal epithelium (Woodrow, Bennett et al. 2012). However, challenges associated with this route of delivery include poor patient compliance, the dilution of mucosal vaccines in mucosal fluid, and the effect of bulk flow that limits effective deposition on the epithelium(Neutra and Kozlowski 2006). Additionally, mucosal vaccines become trapped within the mucus gel (due to gel viscosity and pore size) and are subsequently degraded. Dose control in mucosal vaccination is also difficult due to the variability in the mucosal environment between individuals. A recent study by Rajapaksa et al (2010) has suggested designing vaccines to mimic physicochemical properties of opportunistic pathogens, specifically charge and size, to increase efficiency via this route(Rajapaksa, Bennett et al. 2010).

The transdermal route has shown potential for non-invasive vaccine delivery with clinical and commercial success in the delivery of small drug molecules, such as lidocaine for anaesthesia (Meier, Wasner et al. 2003) and nicotine (Moolchan, Robinson et al. 2005) in patches. Additionally, the skin has important immunological functions and contains skin residing antigen presenting cells (APCs). Langerhans cells and dermal dendritic cells found in the epidermis (see section 1.2.2 for further detail) communicate with elements of the systemic immune system offering potential for mounting the immune response required from a vaccine.

However, the barrier to widespread transdermal vaccine delivery is widely recognised as the uppermost layer of the skin, the stratum corneum (SC) which has very low permeability to molecules larger than 500 Da (Prausnitz, Mitragotri et al. 2004). Vaccines that are on the order of kilodaltons therefore cannot pass. Nonetheless, strategies for increasing the permeability of this layer, or bypassing it altogether include iontophoresis (Deshpande and Wagh 2013), solid or hollow microneedles (Indermun, Luttge et al. 2014), thermal ablation therapies (Biradar and Sanghavi 2014), and sonophoresis (the use of ultrasound to increase the permeability of a medium). These techniques are discussed further in section 1.2.3.

Transdermal systems also have the benefits of (1) avoiding the pain and apprehension felt by patients when receiving injections, (2) reducing the risk of needle-stick injury and re-use of needle and syringe, and (3) administration by minimally trained personnel or patients themselves, leading to high patient compliance. Many skin vaccination methods use vaccines in a dry state, enabling vaccine stabilisation without the need for refrigeration and reconstitution by trained personnel. Transdermal vaccination methods may also reduce the package size of the dosage form compared to a needle, syringe and vaccine vial, which facilitates lower cost and infrastructure needs for storage, transport and disposal (Kim and Prausnitz 2011).

Disadvantages associated with the transdermal route mainly revolve around cost of wide scale application. Methods based on physical techniques that require particular devices might pose constraints for adoption in developing countries. Similarly, the use of electrical power may limit the widespread use of these methods. However, in developed countries, where the risks associated with needle use are still present and indeed prevalent, transdermal delivery could be a viable method for vaccine delivery. For these reasons, transdermal vaccine delivery offers potential for development as a non-invasive vaccine delivery route, and is therefore the focus of this thesis.

1.2 Transdermal delivery

1.2.1 Skin structure and function

The skin is the body's outermost physical barrier to the surrounding environment, offering protection from mechanical damage, ultraviolet radiation, dehydration and micoorganisms. The skin consists of three main layers, the epidermis, dermis and subcutaneous fat tissue (figure 1.1). The epidermis is the outermost layer of the skin, varying in thickness from 50-150μm, depending on the site of the body. Underneath the epidermis, the dermis contains blood vessels, lymph vessels, nerves and collagen fibres in abundance. The main cell classes in the dermis are fibroblasts, mast cells and dermal dendritic cells. This layer is responsible for cellular and fluid exchanges between the skin and the blood and lymphatic networks. The subcutaneous fat tissue lies beneath the dermis, forming a thermal barrier, storing energy and providing a mechanical cushion for the rest of the body. Appendages such as sweat glands and hair follicles originate either from the subcutaneous fat layer or the dermis, and form important discontinuities in the skin structure.

The stratum corneum is the uppermost layer of the epidermis and is responsible for the barrier function of the skin (figure 1.1). The SC is located in the upper 15-20μm of the epidermis and consists of corneocytes, rigid desmosome-linked epithelial cells, embedded in a highly organised lamellar structure. The arrangement of this layer has been likened to "bricks and mortar", making it impermeable to molecules larger than 500Da in the absence of some intervention.

Although skin structure itself remains the same between individuals, it is important to note that the thickness of each layer described varies depending on body site, gender, age and ethnic origin (Lambert and Laurent 2008).

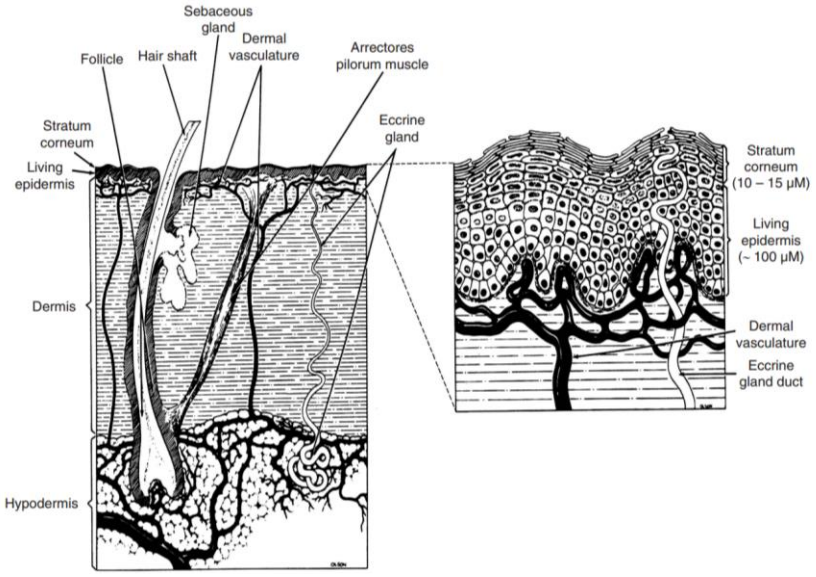

Figure 1.1: Major skin structures (Schuetz, Naik et al. 2005).

1.2.2 Skin as a site of immunisation

Human skin is an efficient barrier designed to keep our "insides in and the outsides out". More than just a physical barrier, the skin is an active immune organ. As a result of its network of lymphatic and blood vessels, the dermis contains most of the lymphocytes in the skin, as well as mast cells and tissue macrophages. Although the epidermis has no direct access to the blood or lymphatic circulation, it is equipped with immune-competent cells: Langerhans cells, the macrophage-like antigen-presenting cells of the epidermis; keratinocytes, epithelial cells with immune properties; dendritic epidermal T lymphocytes, resident cells that may serve as a primitive T-cell immune surveillance system; epidermotropic lymphocytes, migrants from vessels in the dermis; and melanocytes, epidermal pigment cells with immune properties (Bos and Kapsenberg 1993). These elements of the epidermis work in concert with dermal immune competent components to execute immune responses in the skin.

Langerhans cells are the major antigen presenting cells of the skin and play a key role as the peripheral component of the immune system. They are regularly spaced among keratinocytes making up 2-4% of

epidermal cells and their long dendritic processes intercalate between keratinocytes to form an "immunologic net" parallel to the skin surface (figure 1.2). Langerhans cells are characterised by the presence of a special type of intracytoplasmic 'tennis-racket-shaped' organelle called the Birbeck granule. Langerhans cells are one of a large family of class II major histocompatibility complex (MHC)-bearing dendritic cells, a set of cell surface molecules which bind to peptide fragments derived from pathogens and display them on the cell surface for recognition by the appropriate T-cells (Janeway, Travers et al. 2001). Langerhans cells are therefore critical to antigen processing and presentation to T-lymphocytes (Mishra, Dhote et al. 2013). Antigen-bearing Langerhans cells undergo phenotypic changes and migrate via the dermal lymphatic network to regional lymph nodes where they stimulate specific naïve or primed T lymphocytes to proliferate and differentiate.

The efficiency of Langerhans cells to function as antigen-presenting cells depends not only on the expression of cell surface class II MHC molecules, but also on membrane adhesion molecules. Cellular adhesion molecules allow direct physical contact between Langerhans cells and T cells, thus facilitating their interactions and T-cell activation. Cytokines such as interleukin-1 and tumour necrosis factor (TNF)α that are produced by keratinocytes may increase class II MHC and adhesion molecule expression on Langerhans cells, thus augmenting their efficiency as antigen-presenting cells.

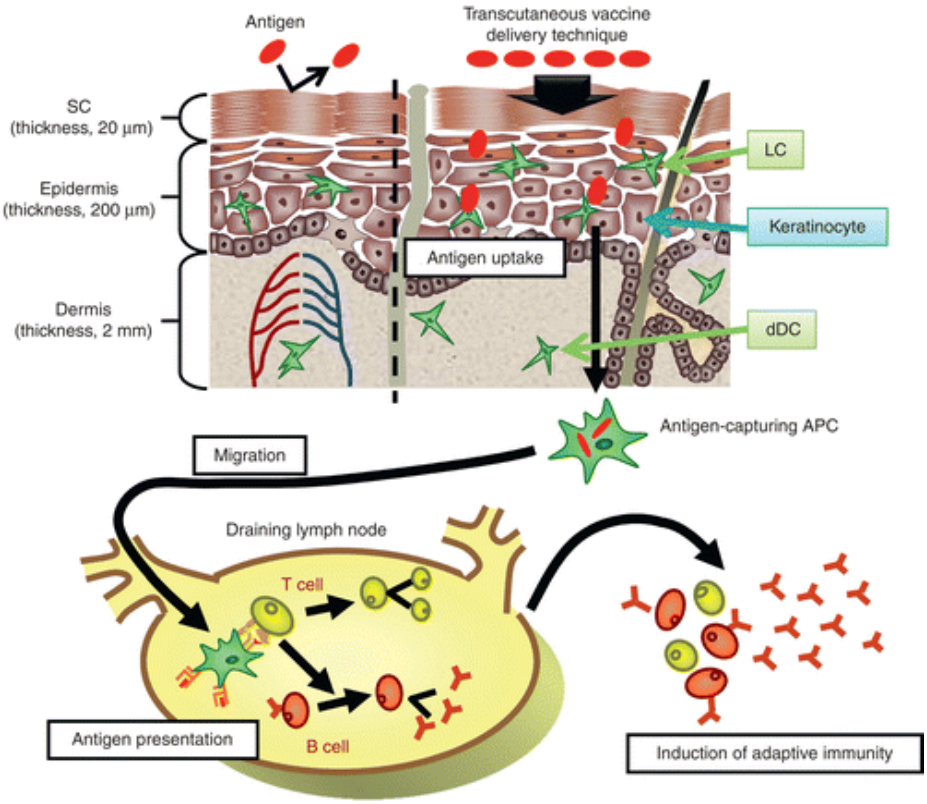

Figure 1.2: The induction mechanism of immune responses by a transcutaneous vaccine delivery technique (Hirobe, Okada et al. 2013). Langerhans cells are a form of antigen capturing APCs.

It is on the basis of these immune favourable anatomical features that skin has been the subject of research interest for transdermal vaccination.

1.2.3 Current state of the art in transdermal vaccine delivery

Historically, research in transdermal vaccine delivery has focussed on overcoming the SC. A number of methods have been implemented to increase SC permeability to vaccines. This section presents a literature survey of these methods and their progress to date.

Formulation optimisation

Formulation optimisation involves the use of agents to chemically alter or break down the ordered lipid structure of the SC to allow the passage of molecules through the skin. There is extensive literature on a number of penetration enhancers and their mechanisms of action (Williams and Barry 2004; Lane 2013) for reviews). Despite numerous studies conducted in the 1980's and 1990's(Marro, Delgado-Charro et al. 2001), research in this area has now slowed for two main reasons. Firstly, whereas low molecular weight therapeutics usually tolerate formulation with these aggressive chemicals, other protein drugs, especially vaccines, are less comfortable in their company. The second reason is safety. For most enhancers, activity is closely correlated to skin irritation, rendering the agents as clinically unacceptable (LASHMAR, HADGRAFT et al. 1989). Therefore, the consensus is that, because of the extremely low permeability coefficients of peptides and proteins, the magnitude of enhancement required to ensure delivery of pharmacologically acceptable concentrations is expected to be beyond the capability of chemical enhancers tolerated by the skin. Finally, one must question whether a modest increase in delivery due to a clinically acceptable quantity of chemical penetration enhancers is sufficient to warrant the additional regulatory issues associated to its widespread use. Compounds that have been investigated and used with some success include sulphoxides (e.g. Dimethylsulphoxide, DMSO), Azone ((1-dodecylazacycloheptan-2-one or laurocapram), pyrrolidones, fatty acids, alcohols (such as glycols), surfactants (such as sodium lauryl sulphate, SLS) and urea(Williams and Barry 2012). Future research is

directed at using low doses of chemical penetration enhancers synergistically with other techniques to enhance the permeability of the SC.

Minimally invasive techniques

(i) Microneedles

Based on the effectiveness of conventional injections, needles of micron dimensions can pierce the skin surface to create holes that are large enough for molecules to enter, but are small and shallow enough to avoid pain or significant damage. The concept of microneedles surfaced in the 1970's (Gerstel and Place 1976), but the technology to fabricate them only became available 20 years later. There are a number of different types of microneedle. The simplest form is made of metal that pierces the surface of the skin to increase permeability as a pre-treatment before a drug is applied. *In vitro* studies have demonstrated increases in permeability by orders of magnitude for small drugs, large macromolecules and nanoparticles after the application of microneedles (Henry, McAllister et al. 1998; McAllister, Allen et al. 2000). Animal experiments show similar results in compounds such as insulin (Martanto, Davis et al. 2004) and human studies report microneedles as painless when inserted into the skin of human subjects (Kaushik, Hord et al. 2001). Solid microneedles have been used for the transcutaneous delivery of diphtheria toxoid, but did not generate strong immune responses for influenza vaccine(Ding, Verbaan et al. 2009).

Solid microneedles can also be coated with a drug that is released when the needle is embedded into the skin. Coated microneedles have been used with a number of different types of influenza vaccines, as well as inactivated rotavirus (Moon, Wang et al. 2013) vaccine. The delivery of antigens for Hepatitis C (Gill, Söderholm et al. 2010) and ovalbumin (Matriano, Cormier et al. 2002) via this route has also been explored. Mice studies using inactivated influenza vaccine showed similar primary response and robust protective immunity after challenge compared to conventional intramuscular vaccination (Kim, Quan et

al. 2009). More recently, researchers have developed a solid microneedle device coated with dry live viral vectors called the Nanopatch (figure 1.3) and have shown the vectors to remain viable and immunogenic during formulation, drying and for 10 weeks of storage at 37°C (Pearson, McNeilly et al. 2013). However, the immune response that was generated was inferior to that of intradermal injection, and the authors hypothesised that this could be remedied by a higher dose of viral vectors on the Nanopatch in future studies.

The study of coated microneedles has recently moved toward developing arrays and vaccine formulations that eliminate the need for a cold chain for vaccine storage and transport. An i*n vivo* study recently compared both the immune response in mice between coated microneedle delivery vs. subcutaneous injection of inactivated measules virus, as well as the stability of the vaccine formulation itself. The measles virus was coated and dried onto metal microneedles with stability for 1 week at 37 °C while retaining at least 10% virus viability during storage. Coated microneedle vaccination produced antibody titers similar to vaccine delivered using a conventional subcutaneous injection. However, unlike subcutaneous injection, measles vaccination with a microneedle patch was rapid and simple to administer (Edens, Collins et al. 2013). Most recently, the development of a thermostable influenza immunisation microneedle patch that maintained antigen activity for up to 6 months at both room temperature and 40°C (when storedwith desiccant), offers further potential for cold chain elimination in vaccine storage and transport (Mistilis, Bommarius et al. 2014).

Another methodology involves the construction of microneedle arrays from biodegradable materials containing encapsulated drug. Upon application, the needles biodegrade and release the encapsulated drug into the body.

Arrays of hollow polymer microneedles can be used to flow drug solutions into the skin (McAllister, Wang et al. 2003) and have been used for vaccination against influenza, anthrax and other diseases in

human and animal subjects (Dean, Alarcon et al. 2005; Mikszta, Sullivan et al. 2005; Arnou, Icardi et al. 2009). A single hollow microneedle device was introduced into clinical practice in 2008 for intradermal influenza vaccination because skin vaccination was shown to provide superior immunogenicity in the elderly, who are at the highest risk of morbidity and mortality from seasonal influenza (Holland, Booy et al. 2008).

The use of microneedles offers advantages over non-invasive approaches by actively delivering vaccines into the skin in a rapid, reliable, and efficient manner. Compared to hypodermic needles, the use of microneedles reduces or eliminates pain, biohazardous sharps waste, and the need for specially trained medical personnel. Indeed, a recent study investigating the usability and patient acceptability of microneedle patches for self-vaccination against influenza showed that patients were able to correctly appl microneedle patches, and the use of the patches compared to subcutaneous injection increased the patient's intent to vaccinate from 44% to 65%. 64% of the participants intending vaccination would have rathered self-vaccination in this study (Norman, Arya et al. 2014). However, minimally invasive methods remain invasive and therefore have greater safety concerns and sterility requirements than non-invasive methods (Kim and Prausnitz 2011).

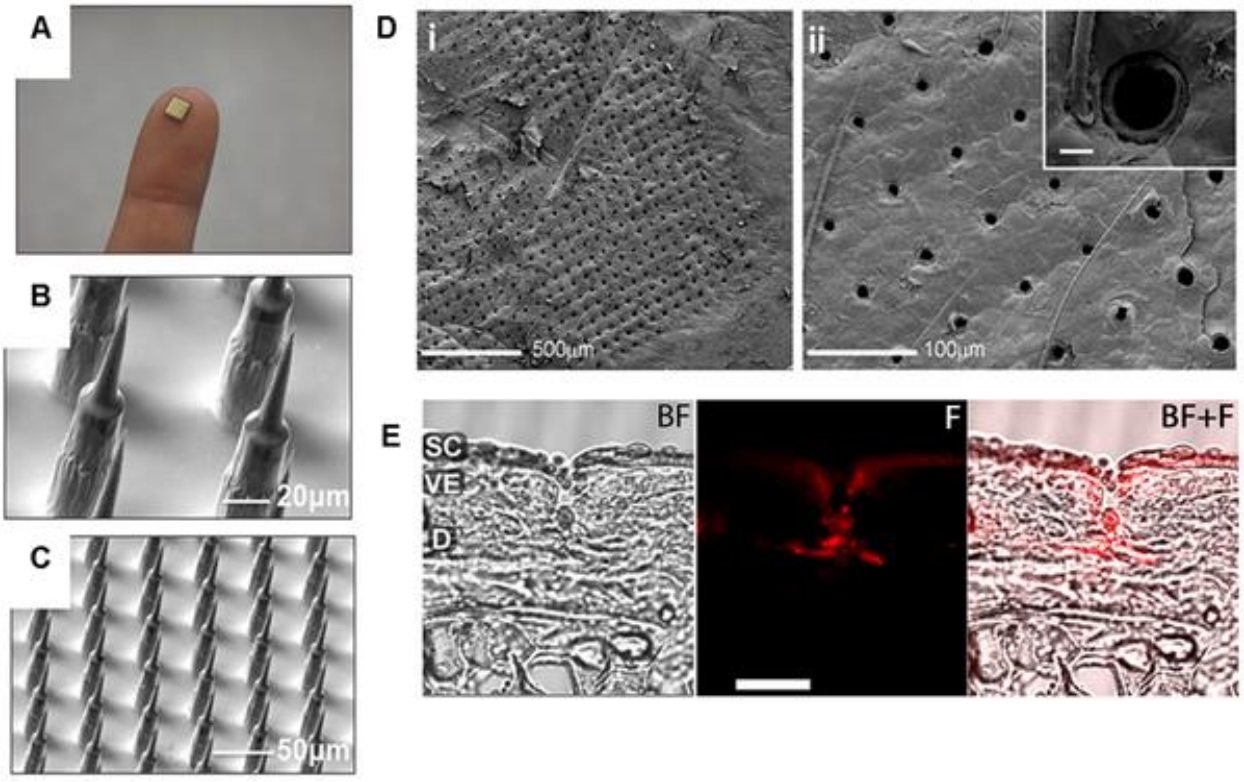

Figure 1.3: Imaging of skin penetration by Nanopatch microprojections. (A) The size of a single Nanopatch relative to a forefinger. (B+C) SEM images of microprojection morphology after dry-etch fabrication. (D) Representative cryo-SEM images of mouse ear skin surface following application of a single Nanopatch. D(i) far field view of the corner of the patched area, with micro-channel openings characteristic of microprojection penetration, adjacent to unbroken skin. D(ii) perforated area in higher magnification, with a single micro-channel next to a hair follicle inset. Scale bar inset = 10 µm. (E) Representative micrographs of ear tissue sections following delivery of Nanopatch coated with a fluorescent dye. BF: brightfield image, F: fluorescence image, BF+F: both brightfield and fluorescent images overlaid. SC = *stratum corneum*; VE = viable epidermis; D = dermis. Taken from (Pearson, McNeilly et al. 2013)

(ii) Liquid jet injectors

Liquid jet injections utilise a high-speed jet to puncture the skin and deliver drugs without the use of a needle. The basic design of liquid jet injectors comprises of a compressed gas or spring, drug-loaded compartment and a nozzle with orifice sizes typically ranging between 150 and 300 μm (Mitragotri 2013). Upon triggering the actuation mechanism, the power source pushes the piston which impacts the drug-loaded compartment, leading to a rapid pressure increase (Schramm and Mitragotri 2002). This forces the drug solution through the nozzle orifice as a liquid jet with velocities ranging between 100 and 200 m/s. Upon impact, the jet punctures the skin and delivers the liquid into deeper layers of skin and into subdermal tissues including fat and muscle.

The key advantages of jet injectors include the ability to use currently approved formulations, ability to work without electronics and power and provision of small portable devices. The first advantage is particularly significant since it greatly facilitates clinical adoption (Mitragotri 2013).

Liquid jet injectors can be broadly classified into two groups. Multi-use nozzle jet injectors (MUNJIs) and disposable cartridge jet injectors (DCJIs). Liquid jet injections for immunisations were first carried out using MUNJIs , which allowed repeated injections of vaccine from the same apparatus at a rate of up to 1,000 immunisations per hour. They were successfully used for vaccination against measles, smallpox, cholera and hepatitis B virus (HBV). The drawback of MUNJIs (that led to their discontinuation) however, has been the potential for subject-to-subject contamination, discovered through the spread of HBV. Splashes of small amounts of liquid, contaminated with blood or interstitial fluid, on the nozzle of the jet injector were blamed for the HBV spread(Mitragotri 2006). In light of the increased risk contamination, the World Health Organisation recommends that MUNJIs should not be used for immunisation until all safety issues have been resolved, although the Centers for Disease Control and Prevention state that MUNJIs can be used for mass immunisation only when the gains outweigh the risks of blood-borne

infections, such as in the case of pandemic influenza or bioterrorism attacks(Mitragotri 2006). To minimise the risk of contamination, protective and disposable covers for the nozzles have been developed, and studies have shown that there was no risk in a population of 22,714 participants (Dimache, Croitoru et al. 1997).

Although MUNJIs are no longer used for routine immunisations, DCJIs are used for both childhood and adult vaccination. However, there have been mixed reviews, and clinical acceptance is low despite successful products such as the PowderJect technology (Oxford, UK). Some studies report more pain compared to needles(Jackson, Austin et al. 2001), and jet injections have been associated with more frequent local site reactions (Matheï, Van Damme et al. 1997). Most importantly, concerns have been raised about 'splatter', namely the impact of the jet onto the skin creating airborne droplets that could lead to cross-infection.

(iii) Stratum corneum ablation

Some scientists have approached the problem of the SC by simply trying to remove it altogether. Radiofrequency and thermal ablation cause a local heating effect on the SC resulting in tissue ablation. This results in the formation of local micropathways through which a wide range of molecules can pass into the skin. The micropathways are reported as about 50-200 μm in width, and 30-50 μm in depth, indicating that the ablation process does not cause any damage to the deeper layers of the skin(Kalluri and Banga 2011). After ablation, skin is believed to repair and regenerate, although time frames for this healing process have not been reported. Laser ablation utilises rapid heating leading to the evaporation of water molecules to create the same effect.

This technique has been tested in a number of clinical studies and thermal ablation devices have experienced significant research and development in recent years (Mitragotri 2013). Altea Therapeutics (Atlanta, GA) developed a patented technology, the PassPort patch (Smith, Zhang et al. 2008), using

metallic filaments to locally ablate the SC over an small area. Preclinical data has reported the delivery of several protein molecules including parathyroid hormone, inferon-α and hepatitis B antigen (Bramson, Dayball et al. 2003).

Stratum corneum ablation has been widely explored to deliver drugs beyond the SC, but vaccines specifically are yet to be investigated. The high temperatures involved are believed to be more damaging to delicate vaccines than they are to the drugs currently studied. The other limiting factor to this technology is the cost. Patches such as the Passport system are expensive to produce and therefore are not yet as cost effective as needle and syringe systems for vaccine delivery. The use of lasers for ablations is also limited to niche applications within hospital settings due to the cost of obtaining and maintaining functional lasers.

Energy driven techniques

(i) Iontophoresis

Application of low amplitude (typically < 0.5mA/cm^2 of skin)(Schuetz, Naik et al. 2005) electric currents has been shown to enhance transdermal transport of drugs, particularly for charged molecules, using a phenomenon referred to as iontophoresis (Kalia, Naik et al. 2004). Iontophoresis has been successfully used for the transdermal delivery of various low molecular weight drugs including lidocaine (Spierings, Brevard et al. 2008) and dexamethasone as well as high molecular weight drugs including insulin (Langkjær, Brange et al. 1998) and luteinizing hormone-releasing hormone (Raiman, Koljonen et al. 2004). Iontophoretic delivery of lidocaine has been clinically approved for local anesthesia (Spierings, Brevard et al. 2008) and of pilocarpine for diagnosis of cystic fibrosis(Coury, Fogt et al. 1983).

The two main mechanisms of transport governing iontophoretic delivery are electromigration (for charged molecules) and electroosmosis (for neutral molecules)(Kalluri and Banga 2011).

Electromigration is the repulsion of the charged drug by an electrode with the same polarity as the predominant mechanism of transport. Transport enhancements induced by this mechanism scale with the charge to mass ratio; molecules with high charge to mass ratio exhibit greatest enhancement. Electroosmosis is the flow of solvent from anode to cathode via which water soluble molecules can also be transported into the skin. Due to these mechanisms of transport, it is possible to individualise delivery parameters for different molecules and their dosage over time by adjusting electrical parameters such as current and duration of application.

Application of iontophoresis has been generally found to be safe in humans (Mitragotri 2013). Typically, low amplitude generally causes no pain or irritation beyond mild erythema (Prausnitz, Mitragotri et al. 2004). The appealing feature of iontophoresis is the potential for a low-profile, user-friendly and disposable device for delivery of macromolecules. Iontophoresis is also able to provide temporal control of fluxes across the skin. This opens the pathway to an infusion-like wearable device that eliminates the use of needles.

The main limitation of this technique is the restriction on size limit to ~10-15kDa (Kalluri and Banga 2011). This is because it is simply a 'pushing' force that is introduced, as opposed to increasing the permeability of the SC itself, making this delivery technique better than diffusion, but still subject to size restriction. Furthermore, if the molecular size of the protein is close to this limit, it could aggregate within delivery channels, making delivery unsuccessful. Potential malfunction of the device itself and the possibility of dose dumping also need to be considered.

(ii) Sonophoresis

The use of ultrasound waves (frequencies of above 20kHz) to deliver drugs across the skin has a long history dating back to the middle of the 20th century. A broad spectrum of ultrasound frequencies (20kHz-16MHz) have been used to break down the SC and increase the permeability of skin – a

phenomenon termed sonophoresis. The mechanism of this effect is believed to be acoustic cavitation; a result of the interaction of the ultrasound wave with bubbles in the ultrasound field, which cause nano- and micron-sized disruptions in the lipid bilayer of the SC (Paliwal, Menon et al. 2006). For further detail in acoustic mechanisms, the reader is referred to section 2.3. Depending on the ultrasound parameters, structural changes can be limited to the superficial layers of the skin only, and repair after a period of time. Pre-treatment of skin with ultrasound prior to drug application, as opposed to concurrent drug and ultrasound application (when the drug is present in the coupling medium), is possible due to the fact that the skin remains highly permeabilised for a number of hours following ultrasound application(Mitragotri 2006) and has the advantage of avoiding exposure of the drug to potentially damaging ultrasound waves.

In the 1990's, low frequency (20-40kHz) ultrasound was shown to effectively deliver high molecular weight drugs including proteins and nucleotides (Mitragotri, Blankschtein et al. 1995). More recently, it has been used for the extraction of analytes from the skin for diagnostic purposes such as albumin, urea, lactate and dextran (Kost, Mitragotri et al. 2000; Mitragotri, Coleman et al. 2000), offering potential for use in diabetes for simultaneous continuous monitoring of blood glucose level and the delivery of insulin.

Several ultrasound devices are available for clinical use; the most common being a physiotherapy device that enhances delivery of steroids and other anti-inflammatory drugs into skin (Lavon and Kost 2004). Such devices typically operate at high frequencies (1–3 MHz) and have been commonly used for over five decades. A device operating at low-frequency has also been developed and approved for topical delivery of lidocaine (Choi and Kwak 2012).

While the literature on ultrasound-induced transdermal drug delivery is extensive, that on ultrasound-assisted transcutaneous immunisation is scarce and includes a few reports on ultrasound-assisted

vaccination in fish, for application in fish farming (Fernandez-Alonso, Rocha et al. 2001). One notable study, however, found that tetanus toxoid vaccine was successfully delivered to mice when ultrasound was used as an immunisation "adjuvant" to permeabilise the skin before the antigen was introduced(Tezel, Paliwal et al. 2005). Consequently, the effects of ultrasound duty cycle, SDS presence and its concentration in the coupling medium on immune responses in mice following transcutaneous immunisation with tetanus toxoid were also investigated (Dahlan, Alpar et al. 2009). This study showed anti-tetanus toxoid IgG and neutralising antibody titres that were above those required for protection against tetanus when skin was pretreated with ultrasound, even in the absence of chemical penetration enhancers. This indicated that SDS – a skin irritant – may not be required for low-frequency ultrasound-assisted transcutaneous immunisation. Furthermore, studies have shown that ultrasound resulted in slight LC activation and migration even in the absence of antigen. This was hypothesised to be caused by the disruption of the skin caused by ultrasound-induced cavitation at the surface, suggesting that the ultrasound was acting as an immunisation adjuvant, and was capable of eliciting a small, but detectable immune response alone (Tezel, Paliwal et al. 2005).

The disadvantages associated with ultrasound as a transdermal immunisation technique lie in the need for bulky ultrasound equipment, and its associated cost.

1.2.4 Current limitations to transdermal vaccine delivery

The skin is an important immunological site and, although it poses a formidable barrier, has the potential to be an ideal non-invasive vaccination site. The development of transdermal vaccine delivery systems involves balancing increased transdermal transport with patient safety and cost. The methods explored above have seen varied levels of success, with microneedles proving effective yet invasive, and chemical enhancers displaying insufficient permeability increases in doses compliant with clinical safety regulations to justify their use. Methods involving ultrasound and electric fields have more extensively

increased transdermal delivery for small drugs and macromolecules, but their ability to deliver drugs effectively is partially counterbalanced by their reliance on electronically controlled devices requiring an energy source. A suggested strategy for dealing with the limitations introduced by each of the individual techniques described is combination therapy – where two or more techniques are used synergistically. Studies have combined sonophoresis with chemical penetration enhancers and shown promising effects (Mitragotri, Ray et al. 2000) . These combination studies are not yet widespread and conclusive enough to translate into clinical use, so at present it appears that any one technique alone has not yet shown the ability to deliver therapeutics without the disadvantages mentioned above.

A common limitation between the techniques described in this section is that none are conducive to self-application by the patient. The use of chemical penetration enhancers cannot be released to patients because of the hazards associated with their incorrect use. Minimally invasive techniques also require some supervision. Stratum corneum ablation requires equipment that should only be operated by trained personnel, and although microneedles are more user-friendly, there is further study to be done before patch-like designs can be released to the public for use without medical supervision. Energy driven techniques all require the use and the buying power for complex equipment. These methods could be suited for a primary care environment, but the potential for self-application by the patient remains low.

As well as vaccine delivery method, vaccine formulation is also an important factor to consider. The vast majority, if not all, of the studies performed with any delivery method to date have taken advantage of the solubility of vaccines and used a liquid dosage form. This dosage form will be effective for as long as the liquid is contained, but for application to the skin it is often dropped on the skin. In a practical sense, the liquid would spread on the skin surface, perhaps coming to rest on areas of unpermeabilised skin. This results in inefficient use of the vaccine, a significant drawback when the cost of these complex

proteins is very high. The stability and shelf life of liquid antigen formulations is also quite low, and requires storage and transport infrastructure. Although vaccines can be reconstituted from powder form just before use, it would be preferable to remove this step altogether and formulate the vaccine in a stable dosage form that is deliverable as is by a delivery technique.

A key advantage of the use of needle and syringe for immunisation is the fact that dose is controlled, and the entire quantity of the vaccine is delivered to the site of action. This characteristic is not achievable by the transdermal methods listed above. Each method has an associated delivery efficiency, ranging from moderate to high in microneedles, but decreasing significantly in the case of iontophoresis or liquid jet injectors. This leads to two main issues. Firstly, there is wastage of antigen which can affect the cost associated to the treatment. Secondly, there is no form of dose control.

In conclusion, significant barriers to transdermal vaccine delivery continue to limit its widespread clinical use. A number of the issues given above are addressed in this thesis, which seeks to develop methods for promoting and monitoring cavitation to enhance transdermal vaccine delivery by ultrasound. It is hoped that through the work presented, and further research, that transdermal vaccination can, one day, realise its great promise.

References:

Ada, G. (2003). "Overview of vaccines." Methods Mol Med **87**: 1-17.

Arnou, R., G. Icardi, et al. (2009). "Intradermal influenza vaccine for older adults: A randomized controlled multicenter phase III study." Vaccine **27**(52): 7304-7312.

Bal, S. M., Z. Ding, et al. (2010). "Advances in transcutaneous vaccine delivery: do all ways lead to Rome?" J Control Release **148**(3): 266-282.

Biradar, D. D. and N. Sanghavi (2014). "Technologies in Transdermal Drug Delivery System: A Review." small **6**: 15.

Bos, J. D. and M. L. Kapsenberg (1993). "The skin immune system: progress in cutaneous biology." Immunology Today **14**(2): 75-78.

Bramson, J., K. Dayball, et al. (2003). "Enabling topical immunization via microporation: A novel method for pain-free and needle-free delivery of adenovirus-based vaccines." Gene therapy **10**(3): 251-260.

Choi, S. W. and Y. H. Kwak (2012). "The effect of SonoPrep® on EMLA® cream application for pain relief prior to intravenous cannulation." European journal of pediatrics **171**(6): 985-988.

Coury, A. J., E. J. Fogt, et al. (1983). "Development of a screening system for cystic fibrosis." Clinical Chemistry **29**(9): 1593-1597.

Dahlan, A., H. O. Alpar, et al. (2009). "Transcutaneous immunisation assisted by low-frequency ultrasound." International Journal of Pharmaceutics **368**(1–2): 123-128.

Dean, C. H., J. B. Alarcon, et al. (2005). "Cutaneous Delivery of a Live, Attenuated Chimeric Flavivirus Vaccines against Japanese Encephalitis (ChimeriVaxTM-JE) in Non-Human Primates." Human Vaccines **1**(3): 106-111.

Deshpande, S. and M. Wagh (2013). "Iontophoresis-An Approach for Transdermal Drug Delivery: A Review." Research Journal of Pharmaceutical Dosage Forms and Technology **5**(6): 361-370.

Dimache, G., M. Croitoru, et al. (1997). "A clinical, epidemiological and laboratory study on avoiding the risk of transmitting viral hepatitis during vaccinations with the Dermojet protected by an anticontaminant disposable device." Vaccine **15**(9): 1010-1013.

Ding, Z., F. J. Verbaan, et al. (2009). "Microneedle arrays for the transcutaneous immunization of diphtheria and influenza in BALB/c mice." Journal of Controlled Release **136**(1): 71-78.

Edens, C., M. L. Collins, et al. (2013). "Measles vaccination using a microneedle patch." Vaccine **31**(34): 3403-3409.

Fernandez-Alonso, M., A. Rocha, et al. (2001). "DNA vaccination by immersion and ultrasound to trout viral haemorrhagic septicaemia virus." Vaccine **19**(23-24): 3067-3075.

Gerstel, M. S. and V. A. Place (1976). Drug delivery device, Google Patents.

Gill, H. S., J. Söderholm, et al. (2010). "Cutaneous vaccination using microneedles coated with hepatitis C DNA vaccine." Gene therapy **17**(6): 811-814.

Henry, S., D. V. McAllister, et al. (1998). "Microfabricated microneedles: a novel approach to transdermal drug delivery." Journal of Pharmaceutical Sciences **87**(8): 922-925.

Hirobe, S., N. Okada, et al. (2013). "Transcutaneous vaccines-current and emerging strategies." Expert Opinion on Drug Delivery **10**(4): 485-498.

Holland, D., R. Booy, et al. (2008). "Intradermal Influenza Vaccine Administered Using a New Microinjection System Produces Superior Immunogenicity in Elderly Adults: A Randomized Controlled Trial." Journal of Infectious Diseases **198**(5): 650-658.

Indermun, S., R. Luttge, et al. (2014). "Current advances in the fabrication of microneedles for transdermal delivery." Journal of Controlled Release **185**: 130-138.

Jackson, L. A., G. Austin, et al. (2001). "Safety and immunogenicity of varying dosages of trivalent inactivated influenza vaccine administered by needle-free jet injectors." Vaccine **19**(32): 4703-4709.

Jacobson, R. M., A. Swan, et al. (2001). "Making vaccines more acceptable—methods to prevent and minimize pain and other common adverse events associated with vaccines." Vaccine **19**(17): 2418-2427.

Janeway, C. A., P. Travers, et al. (2001). Immunobiology: the immune system in health and disease, Churchill Livingstone.

Kalia, Y. N., A. Naik, et al. (2004). "Iontophoretic drug delivery." Adv Drug Deliv Rev **56**(5): 619-658.

Kalluri, H. and A. K. Banga (2011). "Transdermal delivery of proteins." Aaps Pharmscitech **12**(1): 431-441.

Kaushik, S., A. H. Hord, et al. (2001). "Lack of pain associated with microfabricated microneedles." Anesth Analg **92**(2): 502-504.

Kim, Y.-C., F.-S. Quan, et al. (2009). "Improved influenza vaccination in the skin using vaccine coated microneedles." Vaccine **27**(49): 6932-6938.

Kim, Y. C. and M. R. Prausnitz (2011). "Enabling skin vaccination using new delivery technologies." Drug Deliv Transl Res **1**(1): 7-12.

Kost, J., S. Mitragotri, et al. (2000). "Transdermal monitoring of glucose and other analytes using ultrasound." Nature Medicine **6**(3): 347-350.

Lambert, P. H. and P. E. Laurent (2008). "Intradermal vaccine delivery: Will new delivery systems transform vaccine administration?" Vaccine **26**(26): 3197-3208.

Lane, M. E. (2013). "Skin penetration enhancers." International Journal of Pharmaceutics **447**(1–2): 12-21.

Langkjær, L., J. Brange, et al. (1998). "Iontophoresis of monomeric insulin analogues in vitro: Effects of insulin charge and skin pretreatment." Journal of Controlled Release **51**(1): 47-56.

LASHMAR, U. T., J. HADGRAFT, et al. (1989). "Topical application of penetration enhancers to the skin of nude mice: a histopathological study." Journal of pharmacy and pharmacology **41**(2): 118-121.

Lavon, I. and J. Kost (2004). "Ultrasound and transdermal drug delivery." Drug Discovery Today **9**(15): 670-676.

Marro, D., M. B. Delgado-Charro, et al. (2001). Peptides and proteins - transdermal absorption. Encyclopaedia of Pharmaceutical Technology, 2nd ed. Vol. 2nd Edition. J. Swarbrick and J. C. Boylan. New York, Marcel Dekker**:** 2125-2140.

Martanto, W., S. P. Davis, et al. (2004). "Transdermal delivery of insulin using microneedles in vivo." Pharmaceutical research **21**(6): 947-952.

Matheï, C., P. Van Damme, et al. (1997). "Hepatitis B vaccine administration: comparison between jet-gun and syringe and needle." Vaccine **15**(4): 402-404.

Matriano, J. A., M. Cormier, et al. (2002). "Macroflux® microprojection array patch technology: a new and efficient approach for intracutaneous immunization." Pharmaceutical research **19**(1): 63-70.

McAllister, D. V., M. G. Allen, et al. (2000). "Microfabricated microneedles for gene and drug delivery." Annual Review of Biomedical Engineering **2**(1): 289-313.

McAllister, D. V., P. M. Wang, et al. (2003). "Microfabricated needles for transdermal delivery of macromolecules and nanoparticles: fabrication methods and transport studies." Proc Natl Acad Sci U S A **100**(24): 13755-13760.

Meier, T., G. Wasner, et al. (2003). "Efficacy of lidocaine patch 5% in the treatment of focal peripheral neuropathic pain syndromes: a randomized, double-blind, placebo-controlled study." Pain **106**(1–2): 151-158.

Mikszta, J. A., V. J. Sullivan, et al. (2005). "Protective Immunization against Inhalational Anthrax: A Comparison of Minimally Invasive Delivery Platforms." Journal of Infectious Diseases **191**(2): 278-288.

Mishra, D. K., V. Dhote, et al. (2013). "Transdermal immunization: biological framework and translational perspectives." Expert Opinion on Drug Delivery **10**(2): 183-200.

Mistilis, M. J., A. S. Bommarius, et al. (2014). "Development of a Thermostable Microneedle Patch for Influenza Vaccination." Journal of Pharmaceutical Sciences: n/a-n/a.

Mitragotri, S. (2006). "Current status and future prospects of needle-free liquid jet injectors." Nat Rev Drug Discov **5**(7): 543-548.

Mitragotri, S. (2013). "Devices for overcoming biological barriers: The use of physical forces to disrupt the barriers." Adv Drug Deliv Rev **65**(1): 100-103.

Mitragotri, S., D. Blankschtein, et al. (1995). "Ultrasound-Mediated Transdermal Protein Delivery." Science **269**(5225): 850-853.

Mitragotri, S., M. Coleman, et al. (2000). "Transdermal extraction of analytes using low-frequency ultrasound." Pharmaceutical research **17**(4): 466-470.

Mitragotri, S., D. Ray, et al. (2000). "Synergistic effect of low-frequency ultrasound and sodium lauryl sulfate on transdermal transport." J Pharm Sci **89**(7): 892-900.

Moolchan, E. T., M. L. Robinson, et al. (2005). "Safety and efficacy of the nicotine patch and gum for the treatment of adolescent tobacco addiction." Pediatrics **115**(4): e407-e414.

Moon, S., Y. Wang, et al. (2013). "Dose sparing and enhanced immunogenicity of inactivated rotavirus vaccine administered by skin vaccination using a microneedle patch." Vaccine **31**(34): 3396-3402.

Neutra, M. R. and P. A. Kozlowski (2006). "Mucosal vaccines: the promise and the challenge." Nature Reviews Immunology **6**(2): 148-158.

Norman, J. J., J. M. Arya, et al. (2014). "Microneedle patches: Usability and acceptability for self-vaccination against influenza." Vaccine **32**(16): 1856-1862.

Paliwal, S., G. K. Menon, et al. (2006). "Low-frequency sonophoresis: ultrastructural basis for stratum corneum permeability assessed using quantum dots." Journal of investigative dermatology **126**(5): 1095-1101.

Pearson, F. E., C. L. McNeilly, et al. (2013). "Dry-Coated Live Viral Vector Vaccines Delivered by Nanopatch Microprojections Retain Long-Term Thermostability and Induce Transgene-Specific T Cell Responses in Mice." PLoS One **8**(7): e67888.

Prausnitz, M. R., S. Mitragotri, et al. (2004). "Current status and future potential of transdermal drug delivery." Nat Rev Drug Discov **3**(2): 115-124.

Raiman, J., M. Koljonen, et al. (2004). "Delivery and stability of LHRH and Nafarelin in human skin: The effect of constant/pulsed iontophoresis." European Journal of Pharmaceutical Sciences **21**(2-3): 371-377.

Rajapaksa, T. E., K. M. Bennett, et al. (2010). "Intranasal M cell uptake of nanoparticles is independently influenced by targeting ligands and buffer ionic strength." Journal of Biological Chemistry **285**(31): 23739-23746.

Russell-Jones, G. J. (2000). "Oral vaccine delivery." Journal of Controlled Release **65**(1–2): 49-54.

Russell-Jones, G. J., H. Veitch, et al. (1999). "Lectin-mediated transport of nanoparticles across Caco-2 and OK cells." International Journal of Pharmaceutics **190**(2): 165-174.

Schramm, J. and S. Mitragotri (2002). "Transdermal drug delivery by jet injectors: Energetics of jet formation and penetration." Pharmaceutical research **19**(11): 1673-1679.

Schuetz, Y. B., A. Naik, et al. (2005). "Emerging strategies for the transdermal delivery of peptide and protein drugs."

Schuetz, Y. B., A. Naik, et al. (2005). "Transdermal iontophoretic delivery of triptorelin in vitro." Journal of Pharmaceutical Sciences **94**(10): 2175-2182.

Smith, A., J. Zhang, et al. (2008). "Gene expression analysis on sections of zebrafish regenerating fins reveals limitations in the whole-mount in situ hybridization method." Developmental Dynamics **237**(2): 417-425.

Spierings, E. L. H., J. A. Brevard, et al. (2008). "Two-minute skin anesthesia through ultrasound pretreatment and iontophoretic delivery of a topical anesthetic: A feasibility study." Pain Medicine **9**(1): 55-59.

Tezel, A., S. Paliwal, et al. (2005). "Low-frequency ultrasound as a transcutaneous immunization adjuvant." Vaccine **23**(29): 3800-3807.

Williams, A. C. and B. W. Barry (2004). "Penetration enhancers." Advanced drug delivery reviews **56**(5): 603-618.

Williams, A. C. and B. W. Barry (2012). "Penetration enhancers." Adv Drug Deliv Rev **64, Supplement**(0): 128-137.

Woodrow, K. A., K. M. Bennett, et al. (2012). "Mucosal Vaccine Design and Delivery." Annual Review of Biomedical Engineering **14**(1): 17-46.

2 Acoustic Principles in Ultrasound-Assisted Transdermal Vaccine Delivery

2.1 Acoustic waves

Sound is a longitudinal wave of alternating pressure perturbations about an equilibrium pressure, which causes local regions of compression or rarefaction when propagating though an elastic medium. These pressure perturbations are generated at a frequency *f* and propagate at the speed of sound, *c*.

2.1.1 Linear Propagation of Ultrasound

Ultrasound refers to sound at frequencies higher than those within the range of normal human hearing (20Hz to 20kHz). Like all acoustic waves, they obey the wave equation:

$$\frac{\partial^2 p(\mathbf{x},t)}{\partial t^2} = \mathrm{c}^2 \nabla^2 p(\mathbf{x},t) \tag{2.1}$$

where p is the pressure perturbation from ambient conditions, **x** is the three-dimensional position vector, t is time and c denotes the speed of sound, given by:

$$c^2 = \frac{1}{\kappa_0 \rho_0} \tag{2.1a}$$

where κ_0 and ρ_0 are the medium compressibility and density respectively. Compressibility is a measure of the relative volume change of a fluid or solid as a response to a stress change, expressed in an isentropic medium in units of Pa^{-1}.

In one dimension, the wave equation reduces to:

$$\frac{\partial^2 p(x,t)}{\partial t^2} = \frac{1}{c^2}\frac{\partial^2 p(x,t)}{\partial x^2} \tag{2.2}$$

where positive x now denotes the scalar distance in the direction of wave propagation.

The solution to the 1D linear wave equation for a sinusoidal source is a harmonic plane wave, periodic both in space and time, which propagates with both forward and backward travelling components, given by:

$$p(x,t) = p_0 e^{-i\omega(t\pm\frac{x}{c})} \tag{2.3}$$

where p_0 is the ambient pressure, ω is the angular frequency of the source, and x is the distance travelled along the axis of propagation.

Attenuation is an important feature of many media, and manifests itself as an exponential decrease in the amplitude of the wave as it travels through the medium. Although attenuation can arise from a combination of effects, in this work its dominant underlying mechanism is absorption and scattering by the microstructure of the tissue. Equation 2.3a can therefore be modified to include a frequency dependent attenuation term:

$$p(x,t) = p_0 e^{-i\omega(t\pm\frac{x}{c})} e^{-\propto(\omega)x} \tag{2.3a}$$

where ω is the angular frequency of the source, p the pressure, x is the distance travelled along the axis of propagation, and α(ω) is the attenuation coefficient of the material.

2.1.2 Non-Linear Propagation of Ultrasound

As the excitation amplitude increases, local fluctuations in pressure and density become more significant. For a plane wave, the phase speed is higher than the small-signal sound speed in regions of compression (positive acoustic pressure) and slower in regions of rarefactions (negative acoustic pressure). This leads to the gradual steeping of the initially sinusoidal waveforms, the effect increasing with amplitude, frequency and propagation distance (equation 2.4). After a sufficient propagation distance, a shockwave will form (Muir and Cartensen 1980; Hamilton and Blackstock 1998). A shockwave

is composed of the higher harmonics of the original periodic signal. In the frequency domain, this results in the appearance of harmonic components of the original fundamental frequency (Hill, Bamber et al. 2004)."

The distance required for the formation of a shockwave from a progressive plane wave with a sinusoidal waveform is:

$$\bar{x} = \frac{\rho c^3}{\beta \omega P_0} \qquad (2.4)$$

where β is the coefficient of non-linearity of the medium, and P_0 is the source pressure amplitude.

2.2 Ultrasound Transducers and Focal regions

Acoustic transducers are usually made from piezoelectric materials to either generate acoustic waves by converting electrical input energy into mechanical energy, or detect acoustic signals passively by performing the reverse conversion and using the mechanical energy from the wave itself to generate a voltage.

Transducers can either be unfocussed or focused. The geometry of a focused transducer is designed so that most of the energy from the active site is concentrated in a specific region located a certain distance away from the transducer. The focal zone of a focused transducer is usually defined as its -3dB region; the region where the beam power is no less than half of its maximum value. The transducers used in the research outlined in this thesis employ spherical focusing. For these transducers, the -3dB region is shaped as a prolate spheroid, more commonly referred to as a "grain of rice" shape (figure 2.1a).

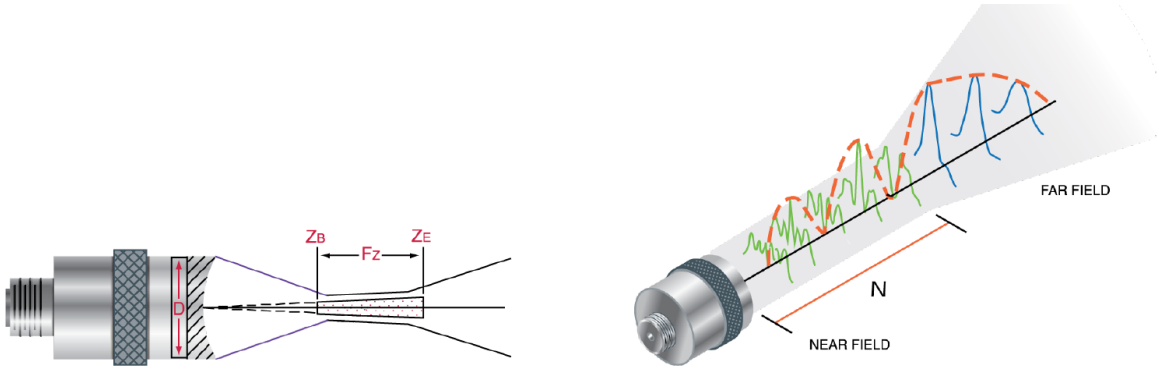

Figure 2.1: (a) The focal zone of a spherically focused transducer – element diameter, D and focal zone dimensions: Start, Z_B; length, F_Z; and end Z_E. (b) Near field and far field axial regions in a focused transducer, with transverse beam profiles also shown. *Reproduced from technical notes by Olympus NDT(NDT 2006)*

The beam profile of focused transducers can be examined in the axial direction (perpendicular to the radiating surface) as shown in figure 2.1b. In this direction, the beam profile can be separated into near field, and far-field regions; the latter is where the focal zone shown in figure 1.2a is located. In the far-field region, the beam amplitude generally increases up to the focal length and then gradually decays thereafter. The distance at which the far-field region begins in an unfocused transducer is given by:

$$N = \frac{D^2}{4\lambda} = \frac{D^2 f}{4c} \qquad (2.5)$$

where *D* is the diameter of the radiating element, *f* is the transducer frequency, λ is the wavelength and *c* is the speed of sound in the medium in which it will propagate.

Using this quantity, the length F_Z of the focal zone can be calculated using:

$$F_Z = \frac{4F^2}{2N + F} \qquad (2.6)$$

where *F,* the focal length, is the axial distance at which the beam amplitude is highest.

In a plane taken transversely through the focus (parallel to the transducer) the beam profile will be approximately Gaussian in shape, with the maximum value occurring along the axial axis (figure 2.1b). Present outside of the main focal region will be sidelobes, although they are not a major concern at the pressure amplitudes employed in this work. It can be shown that the -3dB beam diameter in a focused transducer is given by *mFλ/D* where *m* is a constant whose value depends on the distribution of energy across the transducer aperture. For spherically focused transducers, *m* is approximately 1.02. This gives a -3dB beam diameter of

$$BD_{-3dB} = \frac{1.02F\lambda}{D} = \frac{1.02Fc}{fD} \tag{2.7}$$

Using this value, the transverse area of the focal zone is given by the formula for a circle:

$$A_{focus} = \frac{\pi(BD_{-3dB})^2}{4} \tag{2.8}$$

while the focal volume can be calculated by utilizing the formula for a prolate spheroid:

$$V_{focus} = \frac{\pi(BD_{-3dB})^2 F_Z}{6} \tag{2.9}$$

In many applications, including the use of ultrasound in drug delivery, it is of interest to determine the acoustic power flux being generated by the transducer, i.e., the amount of acoustic power generated per unit area. This quantity is known as the acoustic intensity *(I)* and for a harmonic plane wave is proportional to the square of the pressure amplitude, *P* (equation 2.10).

$$I = \frac{P^2}{2\rho_0 c_0} \tag{2.10}$$

where ρ_0 is the density of the medium, and c_0 is the speed of sound in the medium.

However, the peak rarefactional pressure amplitude produced by a focused transducer varies in space according to the beam profile. The mechanical index (MI)(equation 2.11) characterizes the potential for acoustic cavitation at a given peak rarefactional pressure (in MPa) and ultrasound frequency (in MHz)

$$MI = \frac{PRFP}{\sqrt{f}} \qquad (2.11)$$

The current FDA limit for diagnostic ultrasound is 1.9 (FDA 2008).

2.3 Acoustic mechanisms of interaction with biological tissue

When ultrasound interacts with a medium such as biological tissue, a number of effects are observed. These effects are reviewed in this section, with a view to identification of the predominant mechanisms by which ultrasound-assisted transdermal vaccine delivery can occur.

2.3.1 Thermal effects

Thermal effects have been studied in great detail with respect to sonophoresis; absorption of ultrasound energy leads to viscous heating of the medium though which the wave travels. An increase in temperature can increase skin permeability and transport by i) increasing the kinetic energy and diffusivity of drug compounds, ii) dilating points of entry of the skin (e.g., hair follicles and sweat glands), iii) facilitating drug absorption in the skin, and iv) enhancing circulation of blood in the treated area in *in vivo* experiments) (Meidan, Walmsley et al. 1995). As well as beneficial effects however, prolonged and excessive heating can cause unwanted side effects such as burns and skin detachment.

Acoustic intensity is used to describe the rate at which sound energy flows through a unit area, and is expressed in units of watts per cm^2 (Equation 2.10). Intensity is important as it gives an indication of the heating effects of ultrasound, as thermal effects are directly proportional to the ultrasound intensity and duty cycle. Due to higher attenuation at higher ultrasound frequencies, heating effects increase

monotonically with increasing ultrasound frequency and total exposure time. Thermal tolerance of cells exposed to mild hyperthermia is generally well described by the Cumulative Equivalence Minutes (CEM) thermal dose model of Sapareto and Dewey (Sapareto and Dewey 1984), which suggests that there will be no measureable thermal damage to cells for exposures longer than 240 minutes at 43°C. However, this model has not been validated for either skin or fat cells which lie beneath the skin, and more importantly, does not predict the thermotolerance of drug or vaccine molecules. Significant heating (temperature increases of 5-7°C) caused by attenuation can be detrimental to nearby vaccine molecules (Sokhey, Gupta et al. 1988). Therefore low frequencies are preferred for transdermal applications to minimise thermal damage to the skin.

Reports have differed on the importance of heating as a mechanism of sonophoresis. Some studies have concluded that thermal effects do not play a role at higher frequency (1-16 MHz, spatially averaged intensity (SAi) 0.2-3.0W/cm^2) transdermal transport, as temperature in the donor solution was not observed to increase more than 1-2°C (Levy, Kost et al. 1989; Bommannan, Menon et al. 1992). However, a study of sonophoresis at a frequency of 150 kHz concluded that thermal effects may be a significant mechanism for the increased inflow of hydrophilic permeants (Ueda, Sugibayashi et al. 1995). Recent studies however, have paid more attention to minimising thermal effects because significant increase and sustained exposure to high temperatures can lead to harmful side effects (Boucaud, Montharu et al. 2001). Consequently, most current sonophoresis treatment protocols involve periodic replacement of the coupling medium, and ultrasound pulsing is common because it decreases thermal effects by allowing time for heat to dissipate (Meidan, Walmsley et al. 1995).

Thermal effects have been shown not to play a significant role in low frequency sonophoresis studies with short exposure times (Tang, Wang et al. 2002; Tezel, Sens et al. 2002; Alvarez-Roman, Merino et al.

2003; Polat, Figueroa et al. 2011). However, if the temperature is allowed to increase and is maintained for an extended time, thermal effects will play a role; Merino et al. demonstrated that during a 2-hour treatment using 20 kHz low frequency sonophoresis (SAi 4.5-15.0 W/cm^2 at a 10% duty cycle), thermal effects could explain up to 25% of the observed mannitol transport, with temperature increasing as much as 20°C during the treatment (Merino, Kalia et al. 2003).

It is worthy of note that if sonophoresis is caused purely by ultrasonic heating, then clearly the process is of no great therapeutic interest since the same effects could be observed using any applied heat source.

2.3.2 Mechanical effects

2.3.2.1 Acoustic Radiation

At high amplitudes of ultrasound, conditions of non-linear acoustics will typically prevail. In these conditions a transfer of momentum occurs from the ultrasound wave to the medium, generating a unidirectional force, also known as radiation force (Frenkel 2008). Radiation forces are proportional to the absorption coefficient of the medium and the rate of energy being applied, and inversely proportional to the speed of sound of the ultrasound wave in the medium (Wu and Nyborg 2006) (equation 2.11). If radiation forces are large enough and in a fluid medium, they will be capable of producing motion in the form of a steady flow, also known as acoustic streaming (Nyborg 2006).

In a medium such as soft tissue, in which the primary cause of attenuation is absorption and the contributions to attenuation from scattering can reasonably be neglected, the magnitude of the radiation force (F) created by a focused ultrasound field at a specific spatial location is dictated by the absorption (α), the speed of sound (c) in the tissue, and the local temporal average intensity (I) of the acoustic beam. Under those conditions, the magnitude of the radiation force (in the form of a body force) acting on the bulk fluid at a given spatial location is given by equation 2.12 (Nightingale 2011).

$$F = \frac{2\alpha I}{c} \quad (2.12)$$

Acoustic streaming causes the bulk fluid to move in the direction of the applied ultrasound field, which in the case of sonophoresis is towards the skin surface.

For molecules and particles which are much smaller than the wavelength, including smaller bubbles which do not experience significant buoyancy, there is no direct acoustic force acting on the particle itself, but entrainment by acoustic streaming (caused by a combination of scattering and absorption in the bulk medium) will cause them to move towards the surface of the skin. Furthermore, this bulk fluid movement causes rigorous mixing of the coupling medium, which can enhance transport in areas of the skin where cavitation microjets do not occur (Polat, Hart et al. 2011). Acoustic streaming can reduce ultrasound-induced heating through the increase in convective heat loss(Wu, Winkler et al. 1994), and can increase the mass transport of nanoparticles for improved transdermal delivery (Frenkel, Kimmel et al. 2000; Frenkel, Gurka et al. 2001).

A particle that is of a size comparable to the wavelength of the ultrasound wave will be subject to a direct radiation force, whereas there is no effect of this mechanism on molecules that are smaller than the wavelength of the ultrasound.

2.3.2.2 Acoustic cavitation and bubble interactions

Although all the mechanisms responsible for skin permeability enhancement and/or facilitation of molecular transport by sonophoresis are not fully understood, it is generally accepted that the main contributor is acoustic cavitation, particularly in the case of low frequency ultrasound (Tang, Wang et al. 2002; Tezel, Sens et al. 2002; Tezel and Mitragotri 2003). In the context of sonophoresis and ultrasound assisted transport, acoustic cavitation can be loosely defined as the process by which any of the

following occurs: i) small gas bubbles already present in a liquid pulsate or grow, ii) gas bubbles form in the bulk or on nuclei due to acoustic pressure variations (nucleation), or iii) the occurrence of any other type of growth, splitting, or interaction of gas bubbles due to acoustic pressure oscillations in solution (Margulis and Leib 1995).

Cavitation can be further divided into two types: stable and inertial (figure 2.2). Stable cavitation is the pulsation of cavitation bubbles over many acoustic pressure cycles without collapse(Coussios and Roy 2008). Inertial cavitation is the rapid and uncontrolled growth of cavitation bubbles over the negative part of a pressure cycle, followed by their collapse into smaller bubbles or to the formation of a microjet (Crum 1998). A microjet results from the asymmetry in bubble collapse pressure near an interface such as the skin. Depending on the properties of the interface, the bubble can either generate a jet towards or away from the interface, or collapse in an alternate shape (Fong, Klaseboer et al. 2006). The collapse of a cavitation bubble as a microjet directed towards the interface tends to occur near more rigid surfaces (Fong, Klaseboer et al. 2006) and, although the skin is not rigid but soft, this mechanism has been implicated in causing skin perturbation during ultrasound treatment (Polat, Hart et al. 2011). However, microstreaming from the inertial collapse of bubbles is also likely to play a dominant role.

The onset of inertial cavitation is often described in terms of the minimum acoustic pressure required to initiate this rapid and uncontrolled growth and collapse. This so-called inertial cavitation threshold is dependent on: the size and number distributions of any nucleation sites; the dissolved gas concentration; the acoustic parameters (primarily the frequency and amplitude); the viscoelastic properties of the host medium and the local temperature (Webb, Payne et al. 2011). Pinpointing this minimum pressure within a continuum of bubble behaviours is somewhat subjective, the three most commonly used criteria being:

- When the bubble expansion radius, R_{max} is equal to twice the initial radius (Flynn 1975).
- When the maximum collapse temperature, T_{max}, of the bubble reaches 5000K (Apfel and Holland 1991).
- When the bubble wall collapse speed exceeds the speed of sound in air (Church 2002).

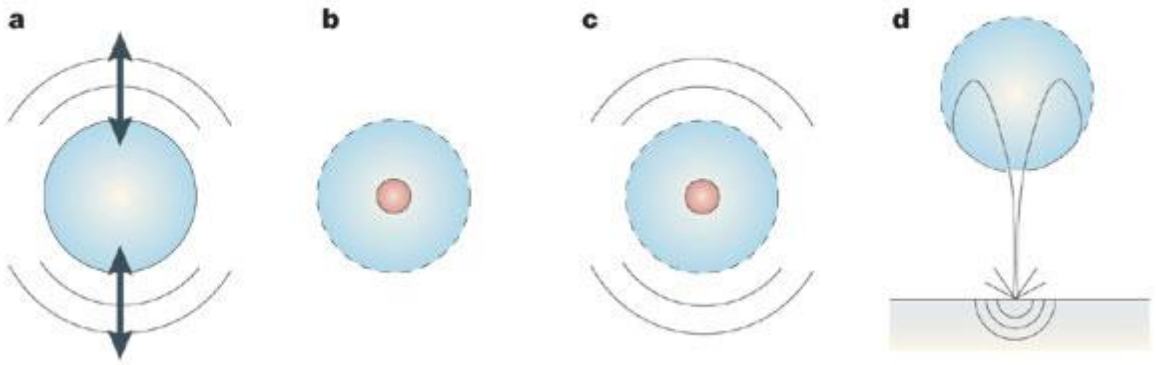

Figure 2.2: Bubble behaviour. a | Acoustic streaming: cavitation bubbles can oscillate around their resonant size and generate velocities that induce shear stresses on cells and tissues (implicated in gene and drug delivery into cells). b | Sonochemistry: sudden collapse of bubbles generates momentary high temperatures in the bubble core. The hot bubble can induce chemical changes in the surrounding medium, including free-radical generation (implicated in sonodynamic therapy). c | Shock waves: sudden collapse of cavitation bubbles leads to the formation of shock waves that are capable of disrupting the tissues and enhancing drug transport (implicated in sonophoresis and sonoporation). d | Liquid microjets: collapsing bubbles near a surface experience non-uniformities in their surroundings that results in the formation of high-velocity microjets. The microjet can penetrate into the tissue or generate secondary stress waves in the tissue (implicated in sonophoresis).

The maximum oscillation radius of cavitation bubbles exhibits an inverse relationship with the applied ultrasound frequency (Frenkel, Kimmel et al. 2000). The average size of cavitation bubbles in a given system will dictate where cavitation can occur. Larger bubbles cannot fit into the voids created in the skin, and therefore cavitation occurs predominantly in the coupling gel at lower frequencies. At higher frequencies, smaller bubbles present in skin voids are able to oscillate and increase skin permeability. For example, when sonophoresis is used to enhance skin permeability, if the resonant bubble radius is larger than the dimensions of the skin voids available for cavitation, it is unlikely that cavitation within the skin itself can play a significant role in permeability enhancement. Therefore, cavitation within the skin is more likely to occur with high frequency ultrasound, when the resonant bubble radius is on the order of microns or smaller.

Ueda et al. have shown through acoustic spectroscopy measurements, that the amount of inertial cavitation generated in the coupling medium between the ultrasound horn and the skin membrane increases with decreasing ultrasound frequency, in the range of 41 kHz-445 kHz (Ueda, Mutoh et al. 2009). This suggests that not only cavitation bubble size, but also the amount of inertial cavitation itself increases with decreasing ultrasound frequency, which has implications on the level of sonoporation that can be achieved at lower ultrasound frequencies, relative to higher ultrasound frequencies.

In addition to pulsating and growing in response to ultrasound, cavitation bubbles are also subject to radiation pressure and convective forces in an ultrasound field that can cause translational motion or interactions between bubbles (Polat, Hart et al. 2011). This translational motion arises from the coupling of bubble oscillations in an ultrasound field to the acoustic pressure gradient and is referred to as the primary Bjerknes force (Leighton, Walton et al. 1990). This phenomenon means smaller bubbles in the

coupling medium between the ultrasound transducer and the skin to move towards the surface of the skin.

The primary Bjerknes force causes bubbles that are smaller than the resonant bubble radius, at the applied frequency, to move up pressure gradients and larger bubbles to move down pressure gradients (Leighton, Walton et al. 1990). Therefore at lower frequencies, any small bubble produced in the coupling medium between the ultrasound transducer and the skin will tend to move towards the surface of the skin. Once in close proximity to the skin, its cavitation activity will then be effective to (i) enhance the permeability of the skin through the action of microjets, and (ii) transport molecules present in the coupling gel due to micropumping action.

The secondary Bjerknes force can cause the mutual attraction or repulsion of oscillating cavitation bubbles, and occurs as a result of the coupling of the sound field emitted by each oscillating bubble (Pelekasis, Gaki et al. 2004). It can also cause other, higher-order phenomena such as acoustic streamers (pairs of bubbles oscillating together) and cavitation bubble clouds (Polat, Hart et al. 2011). It is hypothesised that this is a major factor in the formation of localised transport regions (LTRs) which have been observed in a number of low frequency sonophoresis studies (Tezel, Sens et al. 2001; Kushner, Kim et al. 2007; Kushner, Blankschtein et al. 2008; Polat, Figueroa et al. 2011). Formation of bubble clouds could also contribute to increased transport of molecules if they are present near the skin surface.

The majority of studies have hypothesised that acoustic cavitation is the predominant mechanism in permeability enhancement and transport. Studies in the late 1980's hypothesised that cavitation could play a role in transdermal delivery with sonophoresis (Kost, Levy et al. 1986; Levy, Kost et al. 1989), and it was then shown that cavitation within the skin is a significant mechanism between 10MHz and 16MHz

(Bommannan, Menon et al. 1992). The most significant mechanistic study of sonophoresis alone concluded that cavitation plays the dominant role using therapeutic ultrasound at 1-3MHz (Mitragotri, Blankschtein et al. 1995). This study hypothesised that the oscillations of the cavitation bubbles induced disorder in the stratum corneum lipid bilayers, thereby also increasing transdermal transport. Microscopy-based findings in this study showed that cavitation occurred within the stratum corneum specifically at this higher frequency, and therefore the direct interaction of the oscillating bubbles resulted in increased skin permeability (Mitragotri, Blankschtein et al. 1995).

A number of investigations have tried to determine whether cavitation within the skin, or at the skin's surface is more effective in increasing transdermal permeability. Tang et al. demonstrated the importance of the location of cavitation in permeability enhancement in a series of experiments involving the selective suppression of cavitation inside and outside the skin at frequencies in the range of 20-100kHz (Tang, Wang et al. 2002). Results showed significant changes in porcine skin permeability when cavitation was present in the coupling medium, and it was concluded that cavitation outside the skin was the most important mechanism of skin permeability enhancement (Tang, Wang et al. 2002). To investigate whether stable or inertial cavitation plays a more significant role in skin permeability enhancement, Tang et al. and Tezel et al. independently measured the pressure amplitudes of subharmonic emissions (associated with stable cavitation) and broadband noise (associated with inertial cavitation) (Tang, Wang et al. 2002; Tezel, Sens et al. 2002). The findings showed that there was no relationship between the sub-harmonic emission recordings and skin permeability enhancement, but a strong correlation existed between the broadband noise and skin permeability enhancement. Studies further investigated the contribution of particular mechanisms (within inertial cavitation events) such as shockwaves and microjets to increases in skin permeability. It was concluded that the action of microjets

was more significant than that of shockwaves for skin permeability enhancement over a larger area in low frequency sonophoresis (Wolloch and Kost 2010).

Recent reports have shown that by combining US transducers operating at frequencies in the range of 20kHz – 3MHz, acoustic cavitation activity is enhanced compared to that of single ultrasound frequencies operating alone (Liu and Hsieh 2009; Hasanzadeh, Mokhtari-Dizaji et al. 2011). Consequently, a recent study has attempted to increase the efficacy of ultrasound for the rapid permeabilisation of skin through the simultaneous application of dual frequency high intensity ultrasound (Schoellhammer, Polat et al. 2012). This study utilized a novel setup (figure 2.3) where a high frequency (1 or 3MHz) transducer was used to nucleate bubbles and stream them close to the skin, and a low frequency (20,40 or 60kHz) transducer was used to trigger bubble collapse. Results showed a significant increase in cavitational activity when two frequencies were applied instead of just one, and ex vivo testing in porcine skin tissue indicated that the permeability and the resulting formation of LTRs are greatly enhanced when the dual frequency system was used. The combination of 20kHz/1MHz was shown to cause the greatest increases in permeability (Schoellhammer, Polat et al. 2012).

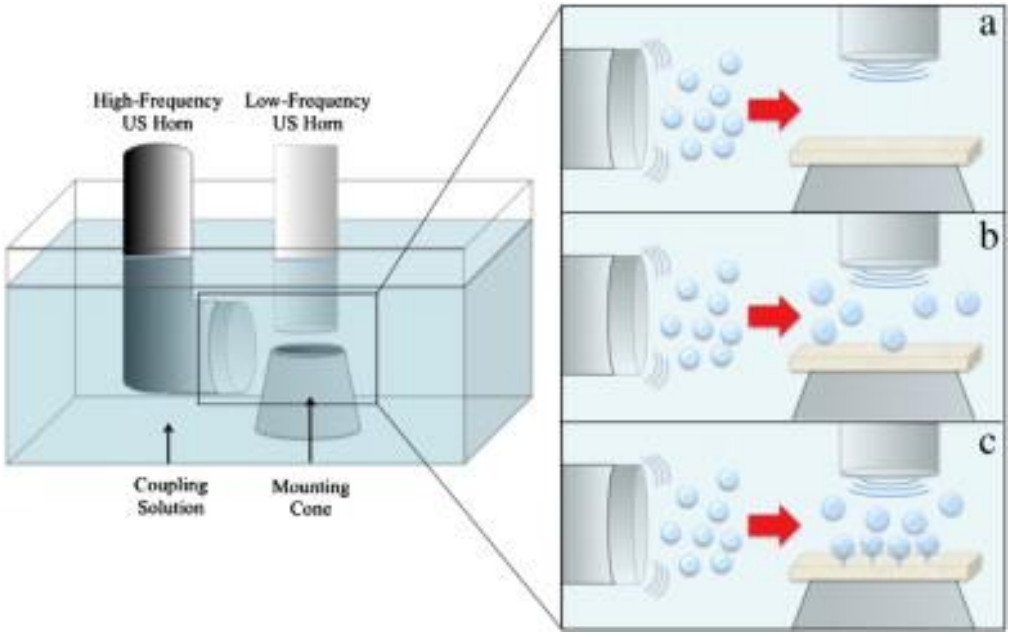

Figure 2.3: Schematic diagram of the setup used in Schoellhammer et al., showing the coupling solution bath and the mounting cone over which the skin is mounted. It is hypothesized that the high-frequency US horn nucleates small bubbles, which then stream below the low-frequency horn (a). The additional bubbles nucleated by the high-frequency horn grow by rectified diffusion under the influence of the low-frequency horn (b). Upon approaching the skin, the bubbles begin to oscillate non-linearly and collapse toward the skin surface (c) (Schoellhammer, Polat et al. 2012).

Studies that have looked into the permeabilisation of the skin have mostly assumed that if there are large holes in the stratum corneum, diffusion will be sufficient for transport of the drug molecules into the lower layers of the skin. Consequently, there have been few, if any, studies looking into transport alone.

2.3.2.3 Acoustic cavitation detection

Cavitation activity gives rise to a complex set of acoustic emissions that can be identified by interpreting their frequency content. As discussed previously, acoustic cavitation (particularly inertial cavitation) is a governing factor in transdermal delivery, and thus monitoring cavitation activity is important in enhancing and controlling delivery.

Passive cavitation detection (PCD) typically uses broadband ultrasound transducers of a centre frequency greater than the therapeutic frequency to record acoustic emissions from cavitation activity generated by a separate therapeutic transducer. In this manner, a low frequency transducer, appropriate for therapeutic applications, can be used to induce cavitation n, and a transducer of higher frequency can be used to listen to the resulting cavitation emissions (Leighton 1994). The higher frequency transducer has the advantages of better spatial resolution and improved frequency separation compared to the therapeutic transducer. This method has been employed in therapeutic applications, such as monitoring heat deposition non-invasively in cavitation enhanced thermal ablation (Coussios, Collin et al. 2007) and drug delivery (Arvanitis, Bazan-Peregrino et al. 2011).

The spectrum of any acoustic emissions is a set of discrete components superimposed onto background noise. The discrete component s are emissions at a nf_0/m frequency, f_0 being the fundamental. Harmonic, subharmonic or ultraharmonic emissions are distinguished by the different values in m and n. Decomposing the signal into various discrete components is very important when studying cavitation noise spectra, because each of the components is associated with one (or more) different bubble behaviours.

Harmonic emissions are the discrete components that occur at multiples of the fundamental frequency. The occurrence of harmonics of the exciting frequency (nf_o, n=2,3,4… and m=1) can be attributed to

scattering of a non-linear exciting waveform, due to the non-linearity of the medium. Additionally, harmonic emissions can be generated from non-linear bubble pulsations.

Subharmonic emissions (nf_o/m, n=1 and m= 2,3,4…) are generally representative of stable cavitation, but can also occur for inertially cavitating bubbles if a bubble continues to grow, skipping the contraction phase, resulting in oscillations at a period multiple to the fundamental (known as period doubling, tripling etc.). The exact mechanism for the generation of ultra-harmonic emissions (nf_o, n=2,3,4… and m= 2,3,4…) is not fully understood, however they have been attributed to propagation and scattering of subharmonic emissions through a non-linear medium (Zhang, Xi et al. 2009).

Finally, broadband emissions (an increase in the noise floor of the spectrum) are attributed to inertial cavitation activity. Upon bubble collapse, the bubble wall velocities approach the speed of sound causing shock wave formation and a rapid collapse. Such a signal is very short in the time domain, and very broad in the frequency domain. Hence, broadband noise emissions in the acoustic spectrum are uniquely attributed to inertial cavitation (Ilyichev, Koretz et al. 1989). High-pass filtering of the signal received by the PCD is often used a further method of rejecting harmonics of the fundamental frequency and improving detectability of broadband acoustic emissions.

Passive cavitation detection has the great advantage of allowing to record acoustic emissions during the HIFU exposure (real-time), which cannot be done with other methods of acoustic monitoring.

2.3.3 Biological effects

The vast number of effects of ultrasound in transdermal drug and vaccine delivery is attributed to mechanical interactions of the ultrasound wave with tissues. In contrast, less is known about the therapeutic potential of subtle, biological effects of ultrasound on cells and tissues. Most organisms exhibit innate ability to respond to various environmental insults so as to facilitate robust recovery and

minimal long term effects of the insult. In this context, ultrasound also exerts non-lethal trauma to the biological milieu and can incite a survival response (Paliwal and Mitragotri 2008). Studies have addressed biological responses of ultrasound on cells previously, but this has been in the context of understanding and developing safety standards for countering the possible harmful bio-effects of ultrasound exposure (Nyborg 2001). Therefore, very little is known about the beneficial bio-effects of ultrasound.

In the context of transdermal drug delivery, the most interesting bio-effect of ultrasound is the stimulation of an immune response. Ultrasound has been demonstrated as a potent physical adjuvant for transdermal immunisation. Specifically, a pre-exposure of ultrasound (20kHz, 2.4W/cm^2) followed by topical immunisation of tetanus toxoid resulted in strong systematic increase of specific IgG antibody titres in mice, which were comparable to those obtained from mice that had been more traditionally immunised by injection, though at much higher doses (Tezel, Paliwal et al. 2005). The mechanism for this has been suggested as the triggering of the skin's inflammatory response to deal by structural insult from the applied ultrasound.

2.4 Ultrasound Assisted Transdermal Vaccine Delivery

It is evident that the transdermal route for drug and vaccine administration is viable, but that some method of delivery enhancement, such as that offered by ultrasound, is required to deliver molecules larger than a certain size. Ultrasound-assisted transdermal delivery of drugs and vaccines is possible through two synergistic effects: (1) an increase in skin permeability, and (2) the transport of the drug and vaccine molecules themselves through the skin. A significant body of past work has investigated the mechanisms for permeability enhancement of the skin, and a subset of these studies assumes that diffusion subsequent to the permeability enhancement of the skin is responsible for transport (Mitragotri, Blankschtein et al. 1995). A number of these studies make the distinction between

permeability enhancement and molecular transport, and also hypothesise that ultrasound enhances transport but there is markedly less work in this area.

2.4.1 Current knowledge in ultrasound-assisted transdermal vaccine delivery

2.4.1.1 Modes of delivery and dosage media

All of the studies performed to date have utilised one of two skin treatment protocols. The pretreatment protocol involves exposing the skin to ultrasound immediately before, but not during, drug application. The simultaneous treatment protocol involves the application of the drug and ultrasound together.

The majority of studies have used the pretreatment protocol to show increased permeability of the skin after ultrasound exposure, and have attempted to demonstrate the mechanism by which this occurs. The pretreatment protocol has been more commonly used for three reasons: (i) the action of ultrasound on drugs or other chemical entities can cause degradation of molecules or other chemical reactions, resulting in loss of activity or formation of harmful intermediate compounds, (ii) clinically, the simultaneous protocol requires that patients wear an ultrasound device for the duration of the treatment, while pretreatment offers the advantage of simply wearing a patch after ultrasound exposure (Ogura, Paliwal et al. 2008), and (iii) it has been proposed that the use of ultrasound to increase skin permeability has been extensively explored, and skin permeability can be significantly increased so that drugs can be effectively delivered without the need for enhancement of transport (Mitragotri, Blankschtein et al. 1996)

This final reason is the subject of some debate. Enhancement of drug transport by convection is feasible in the simultaneous protocol (Polat, Hart et al. 2011), therefore this protocol is hypothesised to be the

more effective at delivering the maximum dose of the drug. Studies utilising this protocol have predominantly been performed with the use of a Franz Cell Chamber (figure 2.3), an *in vitro* skin permeation assay frequently used in formulation development. Sarheed et al., attempted the development of an optimized application protocol for transdermal delivery using both the pretreatment and simultaneous protocol (Sarheed and Abdul Rasool 2011). 20kHz ultrasound was applied to porcine skin and a donor compartment filled with a liquid coupling agent combined with caffeine for 5 min at a 10% pulsed duty cycle (SATA intensity 0.37W/cm^2) and drug flux was compared to when the drug was deposited on the skin after ultrasound exposure. It was found that the best regimen was simultaneous application of the drug and couplant, inducing a 3.88-fold increase in steady state caffeine flux. Importantly, there was no caffeine degradation found after simultaneous exposure. This study also hypothesized that the effectiveness of the simultaneous protocol was transport of the drug as well as permeabilisation due to ultrasound.

The main drawback associated with the use of the Franz cell is that the experimentation is performed with solutions. In a clinical situation this is not feasible, as an ultrasound coupling material is a gel, not a solution. Formulation of the vaccine with a gel that could also be used as an ultrasound couplant would increase system feasibility in a clinical setting.

Despite the advantages associated with the simultaneous protocol, experimentation when the drug is in a gel rather than in solution is scarce. A single study performed in 2007 tested the anesthetic effects of lidocaine hydrochloride gel using 0.5MHz and 1MHz ultrasound and concluded that the gel formulation was suitable for ultrasound enhanced transport, particularly at 0.5MHz (Kim, Jung et al. 2007). This demonstrated the potential of this delivery protocol.

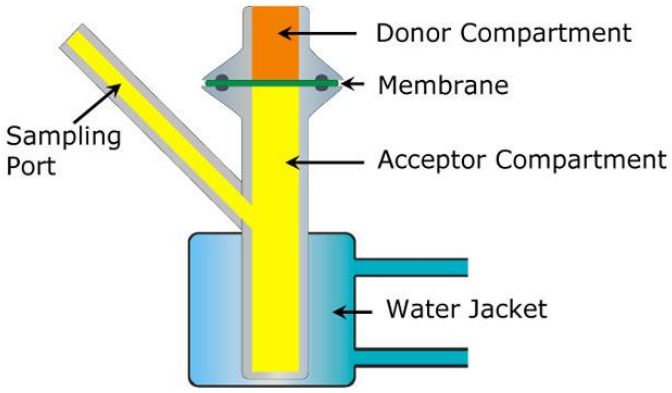

Figure 2.4: A Franz Cell Chamber: an in vitro skin permeation assay. The Franz Cell apparatus consists of two primary chambers separated by a membrane. Although animal skin can be used as the membrane, human skin is preferred. The test product is applied to the membrane via the top chamber. The bottom chamber contains fluid from which samples are taken at regular intervals for analysis. This testing determines the amount of active that has permeated the membrane at each time point. The solution in the donor compartment is subjected to ultrasound, and compared to a control without any ultrasound exposure to measure enhancement of transport.

2.4.1.2 Combination therapies

Recent studies have tested the effectiveness of combining low frequency sonophoresis with chemical penetration enhancers, such as sodium dodecyl sulphate (SDS) (Mitragotri, Blankschtein et al. 1996; Mitragotri, Ray et al. 2000; Kushner, Kim et al. 2007; Polat, Seto et al. 2011; Schoellhammer, Polat et al. 2012). This agent breaks down the lipid structure of the stratum corneum, allowing for increased permeability. In *in vitro* studies using pig skin, permeability to mannitol was increased 200-fold when SDS was included in the coupling medium, compared to a 8-fold increase for ultrasound alone

(Mitragotri, Ray et al. 2000). This study also showed that ultrasound enhanced SDS permeation into the skin and it has been suggested that ultrasound application increased SDS dispersion in the stratum corneum (as opposed to localisation in aggregates). Therefore ultrasound and chemical penetration enhancers such as SDS are believed to work synergistically to increase skin permeability. However, as mentioned in section 1.2.3, vaccines are less suited to formulation with these aggressive chemicals.

2.5 Gap in knowledge

Injection as a vaccine delivery platform has significant disadvantages that affect both the patient and the medical professional administering the vaccine. Transdermal delivery represents an alternative delivery route but is limited due to the low permeability of the skin. Ultrasound-induced sonophoresis has been demonstrated to cause skin permeability enhancement (Mitragotri, Blankschtein et al. 1995), and a review of the current literature shows that the use of ultrasound as a pre-treatment to the transdermal application of drugs has been widely explored (Polat, Hart et al. 2011). Additional evidence has shown that ultrasound application at the parameters widely used for sonophoresis cause no pain (Maruani, Boucaud et al. 2010). However, a major limitation in the use of sonophoresis is that subsequent to ultrasound pretreatment, passive diffusion-related mechanisms are relied upon for the transport of vaccine molecules into the skin, and there are no active mechanisms for transport subsequent to permeability increase. Simultaneous application of ultrasound has the potential to both enhance skin permeability and induce the active streaming of vaccine molecules into the skin. However, due to concerns regarding the stability of vaccine molecules to ultrasound, this method and the mechanisms of transport enhancement have not been fully explored. Therefore, the first part of this thesis explores ultrasound-induced mechanisms (during simultaneous vaccine and ultrasound application) for active molecular transport and the extent of delivery in a skin tissue mimicking material.

To date, researchers in this area have utilised vaccines for delivery in liquid formulations. Liquids are used for their ease of formulation and their low viscosity which offers little resistance to the formation of cavitational events in an ultrasound field. However, without a vessel for containment of the vaccine during delivery or a more efficient application process, this is not economically viable (due to the wastage of vaccine due to leakage) nor clinically feasible. An alternative dosage form is a gel, such as coupling gels already used for ultrasound coupling during diagnostic ultrasound treatments. Formulation of a vaccine within a gel represents a more clinically applicable dosage form, but ultrasound-induced transport mechanisms are dampened by the higher viscosity. To address this limitation of gel formulations, cavitation-inducing particles can be added to the gel formulation to generate cavitation, and therefore lower thresholds necessary for active transport mechanisms, as well as enhancing the effectiveness of the transport mechanisms themselves. Therefore, the work in this thesis addresses the formulation of a gel-based vaccine dosage form with acoustic properties conducive to active molecular transport. Additionally, the stability of the vaccine will be assessed within the dosage form before, during and after ultrasound exposure.

To the author's knowledge, there is currently no existing ultrasound-assisted gel-based transdermal vaccine delivery platform. Furthermore, there is little evidence to suggest that such a system has been tested either *ex* or *in vivo.* The final part of this thesis therefore details the efforts of the author to validate the complete ultrasound-assisted transdermal vaccine delivery platform in physiologically relevant scenarios.

In summary, the gaps in current knowledge that this thesis aims to address are:

1. Identify and exploit of ultrasound induced mechanisms for active molecular transport in a skin tissue mimicking material.

2. Formulate a gel-based vaccine dosage form with acoustic properties conducive to active molecular transport.
3. Assess the stability of the vaccine within the dosage form before, during and after ultrasound exposure.
4. Validate the ultrasound-assisted transdermal vaccination system *ex vivo* and *in vivo.*

References:

Alvarez-Roman, R., G. Merino, et al. (2003). "Skin permeability enhancement by low frequency sonophoresis: lipid extraction and transport pathways." J Pharm Sci **92**(6): 1138-1146.

Apfel, R. E. and C. K. Holland (1991). "Gauging the likelihood of cavitation from short-pulse, low-duty cycle diagnostic ultrasound." Ultrasound in medicine & biology **17**(2): 179-185.

Arvanitis, C. D., M. Bazan-Peregrino, et al. (2011). "Cavitation-enhanced extravasation for drug delivery." Ultrasound Med Biol **37**(11): 1838-1852.

Bommannan, D., G. K. Menon, et al. (1992). "Sonophoresis. II. Examination of the mechanism (s) of ultrasound-enhanced transdermal drug delivery." Pharmaceutical research **9**(8): 1043-1047.

Boucaud, A., J. Montharu, et al. (2001). "Clinical, histologic, and electron microscopy study of skin exposed to low-frequency ultrasound." Anat Rec **264**(1): 114-119.

Church, C. C. (2002). "Spontaneous homogeneous nucleation, inertial cavitation and the safety of diagnostic ultrasound." Ultrasound in medicine & biology **28**(10): 1349-1364.

Coussios, C. C., J. R. Collin, et al. (2007). Non-Invasive Monitoring and Control of Inertial Cavitation Dynamics during HIFU Exposure In Vitro. AIP Conference Proceedings.

Coussios, C. C. and R. A. Roy (2008). "Applications of acoustics and cavitation to noninvasive therapy and drug delivery." Annu. Rev. Fluid Mech. **40**: 395-420.

Crum, L. A. (1998). Sonochemistry and sonoluminescence, Springer.

FDA (2008). Guidance for Industry and FDA Staff - Information for Manufacturers Seeking Marketing Clearance of Diagnostic Ultrasound Systems and Transducers. D. o. R. Radiological Devices Branch, Abdominal, and Radiological Devices, Office of Device Evaluation. USA, US Food and Drug Administration.

Flynn, H. G. (1975). "Cavitation dynamics: II. Free pulsations and models for cavitation bubbles." The Journal of the Acoustical Society of America **58**(6): 1160-1170.

Fong, S. W., E. Klaseboer, et al. (2006). "Numerical analysis of a gas bubble near bio-materials in an ultrasound field." Ultrasound Med Biol **32**(6): 925-942.

Frenkel, V. (2008). "Ultrasound mediated delivery of drugs and genes to solid tumors." Adv Drug Deliv Rev **60**(10): 1193-1208.

Frenkel, V., R. Gurka, et al. (2001). "Preliminary investigations of ultrasound induced acoustic streaming using particle image velocimetry." Ultrasonics **39**(3): 153-156.

Frenkel, V., E. Kimmel, et al. (2000). "Ultrasound-facilitated transport of silver chloride (AgCl) particles in fish skin." Journal of Controlled Release **68**(2): 251-261.

Hamilton, M. F. and D. T. Blackstock (1998). Nonlinear acoustics, Academic press San Diego.

Hasanzadeh, H., M. Mokhtari-Dizaji, et al. (2011). "Enhancement and control of acoustic cavitation yield by low-level dual frequency sonication: a subharmonic analysis." Ultrasonics Sonochemistry **18**(1): 394-400.

Hill, C. R., J. C. Bamber, et al. (2004). Physical principles of medical ultrasonics, Wiley Online Library.

Ilyichev, V., V. Koretz, et al. (1989). "Spectral characteristics of acoustic cavitation." Ultrasonics **27**(6): 357-361.

Kim, T.-Y., D.-I. Jung, et al. (2007). "Anesthetic effects of lidocaine hydrochloride gel using low frequency ultrasound of 0.5 MHz." J Pharm Pharm Sci **10**(1): 1-8.

Kost, J., D. Levy, et al. (1986). Ultrasound effect on transdermal drug delivery. International Symposium Controlled Release.

Kushner, J., D. Blankschtein, et al. (2008). "Evaluation of hydrophilic permeant transport parameters in the localized and non-localized transport regions of skin treated simultaneously with low-frequency ultrasound and sodium lauryl sulfate." Journal of Pharmaceutical Sciences **97**(2): 906-918.

Kushner, J., D. Kim, et al. (2007). "Dual-channel two-photon microscopy study of transdermal transport in skin treated with low-frequency ultrasound and a chemical enhancer." Journal of investigative dermatology **127**(12): 2832-2846.

Leighton, T. (1994). The acoustic bubble, Access Online via Elsevier.

Leighton, T., A. Walton, et al. (1990). "Primary bjerknes forces." European Journal of Physics **11**(1): 47.

Levy, D., J. Kost, et al. (1989). "Effect of ultrasound on transdermal drug delivery to rats and guinea pigs." Journal of Clinical Investigation **83**(6): 2074.

Liu, H.-L. and C.-M. Hsieh (2009). "Single-transducer dual-frequency ultrasound generation to enhance acoustic cavitation." Ultrasonics Sonochemistry **16**(3): 431-438.

Margulis, M. i. a. A. e. and G. Leib (1995). Sonochemistry and cavitation, Gordon and Breach London.

Maruani, A., A. Boucaud, et al. (2010). "Low-frequency ultrasound sonophoresis to increase the efficiency of topical steroids: a pilot randomized study of humans." International Journal of Pharmaceutics **395**(1): 84-90.

Meidan, V., A. Walmsley, et al. (1995). "Phonophoresisis it a reality?" International Journal of Pharmaceutics **118**(2): 129-149.

Merino, G., Y. N. Kalia, et al. (2003). "Frequency and thermal effects on the enhancement of transdermal transport by sonophoresis." Journal of Controlled Release **88**(1): 85-94.

Mitragotri, S., D. Blankschtein, et al. (1995). "Ultrasound-Mediated Transdermal Protein Delivery." Science **269**(5225): 850-853.

Mitragotri, S., D. Blankschtein, et al. (1995). "Ultrasound-mediated transdermal protein delivery." Science **269**(5225): 850-853.

Mitragotri, S., D. Blankschtein, et al. (1996). "Transdermal drug delivery using low-frequency sonophoresis." Pharmaceutical research **13**(3): 411-420.

Mitragotri, S., D. Ray, et al. (2000). "Synergistic effect of low-frequency ultrasound and sodium lauryl sulfate on transdermal transport." Journal of Pharmaceutical Sciences **89**(7): 892-900.

Muir, T. and E. Cartensen (1980). "Prediction of nonlinear acoustic effects at biomedical frequencies and intensities." Ultrasound in medicine & biology **6**(4): 345-357.

NDT, O. (2006). Ultrasound Transducer Technical Notes. O. NDT.

Nightingale, K. (2011). "Acoustic radiation force impulse (ARFI) imaging: a review." Current medical imaging reviews **7**(4): 328.

Nyborg, W. L. (2001). "Biological effects of ultrasound: development of safety guidelines. Part II: general review." Ultrasound Med Biol **27**(3): 301-333.

Nyborg, W. L. (2006). "Ultrasound, contrast agents and biological cells; a simplified model for their interaction during in vitro experiments." Ultrasound Med Biol **32**(10): 1557-1568.

Ogura, M., S. Paliwal, et al. (2008). "Low-frequency sonophoresis: current status and future prospects." Adv Drug Deliv Rev **60**(10): 1218-1223.

Paliwal, S. and S. Mitragotri (2008). "Therapeutic opportunities in biological responses of ultrasound." Ultrasonics **48**(4): 271-278.

Pelekasis, N. A., A. Gaki, et al. (2004). "Secondary Bjerknes forces between two bubbles and the phenomenon of acoustic streamers." Journal of Fluid Mechanics **500**(1): 313-347.

Polat, B. E., P. L. Figueroa, et al. (2011). "Transport pathways and enhancement mechanisms within localized and non-localized transport regions in skin treated with low-frequency sonophoresis and sodium lauryl sulfate." Journal of Pharmaceutical Sciences **100**(2): 512-529.

Polat, B. E., D. Hart, et al. (2011). "Ultrasound-mediated transdermal drug delivery: mechanisms, scope, and emerging trends." J Control Release **152**(3): 330-348.

Polat, B. E., J. E. Seto, et al. (2011). "Application of the aqueous porous pathway model to quantify the effect of sodium lauryl sulfate on ultrasound-induced skin structural perturbation." J Pharm Sci **100**(4): 1387-1397.

Sarheed, O. and B. K. Abdul Rasool (2011). "Development of an optimised application protocol for sonophoretic transdermal delivery of a model hydrophilic drug." Open Biomed Eng J **5**: 14-24.

Schoellhammer, C. M., B. E. Polat, et al. (2012). "Rapid skin permeabilization by the simultaneous application of dual-frequency, high-intensity ultrasound." J Control Release **163**(2): 154-160.

Sokhey, J., C. K. Gupta, et al. (1988). "Stability of oral polio vaccine at different temperatures." Vaccine **6**(1): 12-13.

Tang, H., C. C. Wang, et al. (2002). "An investigation of the role of cavitation in low-frequency ultrasound-mediated transdermal drug transport." Pharm Res **19**(8): 1160-1169.

Tezel, A. and S. Mitragotri (2003). "Interactions of inertial cavitation bubbles with stratum corneum lipid bilayers during low-frequency sonophoresis." Biophysical journal **85**(6): 3502-3512.

Tezel, A., S. Paliwal, et al. (2005). "Low-frequency ultrasound as a transcutaneous immunization adjuvant." Vaccine **23**(29): 3800-3807.

Tezel, A., A. Sens, et al. (2002). "Investigations of the role of cavitation in low-frequency sonophoresis using acoustic spectroscopy." Journal of Pharmaceutical Sciences **91**(2): 444-453.

Tezel, A., A. Sens, et al. (2001). "Frequency dependence of sonophoresis." Pharmaceutical research **18**(12): 1694-1700.

Ueda, H., M. Mutoh, et al. (2009). "Acoustic cavitation as an enhancing mechanism of low-frequency sonophoresis for transdermal drug delivery." Biological and Pharmaceutical Bulletin **32**(5): 916-920.

Ueda, H., K. Sugibayashi, et al. (1995). "Skin penetration-enhancing effect of drugs by phonophoresis." Journal of Controlled Release **37**(3): 291-297.

Webb, I. R., S. J. Payne, et al. (2011). "The effect of temperature and viscoelasticity on cavitation dynamics during ultrasonic ablation." The Journal of the Acoustical Society of America **130**(5): 3458-3466.

Wolloch, L. and J. Kost (2010). "The importance of microjet vs shock wave formation in sonophoresis." Journal of Controlled Release **148**(2): 204-211.

Wu, J. and W. L. M. Nyborg (2006). Emerging therapeutic ultrasound, World Scientific.

Wu, J., A. J. Winkler, et al. (1994). "Effect of acoustic streaming on ultrasonic heating." Ultrasound Med Biol **20**(2): 195-201.

Zhang, D., X. Xi, et al. (2009). "A dual-frequency excitation technique for enhancing the sub-harmonic emission from encapsulated microbubbles." Physics in medicine and biology **54**(13): 4257.

3 Ultrasound Assisted Molecular Transport Mechanisms[1]

3.1 Introduction and proof of concept

As reviewed in chapter 1, non-invasive drug and vaccine delivery is garnering significant research interest due to the substantial risk associated with the delivery of drugs and vaccines via needle and syringe (Saia 2013). In response, a wide range of needle-free delivery techniques such as those explored in chapter 1 have been developed. Ultrasound has shown promise to improve safety, increase patient compliance (Mitragotri and Kost, 2001) and enable self-administration and sustained release (Mathias and Hussain 2010).

Our approach of this ultrasound-assisted system involved two key elements; firstly, the use of an ultrasound coupling gel as a vaccine dosage form, and secondly, the use of the simultaneous application of ultrasound and drug to the skin to enhance delivery. The use of a hydrogel has not been explored in depth before, as it is believed that a gel with high viscosity may hinder delivery (Meshali, Abdel-Aleem et al. 2010). Studies have avoided the simultaneous application of the drug and ultrasound because of the significant challenges of making a US stable drug formulation. Thus, ultrasonic mechanisms such as microstreaming and acoustic radiation force have not been exploited to increase the transdermal *transport* of the drug.

In order to verify that ultrasound-assisted active transport delivered a clinically relevant dose of drug transdermally, we developed a proof of concept that ultrasonic mechanisms such as cavitation and radiation force could be used to promote the active transport of molecules from a hydrogel to a skin tissue mimicking material (TMM) .

[1] The work reported in this chapter has been published in the journal publication "Bhatnagar S, Schiffter H, Coussios C-C 2014. Exploitation of Acoustic Cavitation-Induced Microstreaming to Enhance Molecular Transport. Journal of Pharmaceutical Sciences 103(6):1903-1912."

This proof of concept study is the first to examine the mechanism by which *molecular transport* (as opposed to increased permeability) is affected by ultrasound. As this work represents a mechanistic study, the TMM used was designed to replicate the pore size and structure of permeabilised skin through which molecular transport could occur. Issues of sample-to-sample variability from excised animal or human skin would prevent identification and optimisation of the underlying mechanism, therefore actual skin was not used. A layered agarose TMM was therefore used as a model for a donor layer, barrier membrane, and recipient layer to test the penetration of agents at a range of ultrasound parameters. In particular, the influence of agent molecular mass (over a 3 kDa to 2000 kDa range), US frequency (0.256 MHz or 1.1 MHz) and US pressure (over a 0 to 10 MPa range) on transport was characterised. After inertial cavitation thresholds of the TMM were determined, agents of four different molecular sizes were embedded within the TMM in the presence or absence of cavitation nuclei and US applied to achieve no cavitation or inertial cavitation. Following ultrasound exposure, samples were analysed to determine the concentration and penetration distance of molecular agent transported for each set of US parameters, to enable identification and optimisation of the key underlying mechanisms.

The work reported in this chapter therefore aims to quantitatively and mechanistically study *in-vitro* the optimal mechanism by which ultrasound-assisted active transport of a range of sizes of drug and vaccine molecules can be achieved.

3.2 Materials and Methods

A TMM was formulated, and cavitation events within this model during ultrasound exposure were monitored to determine its inertial cavitation threshold. Samples of the TMM were then exposed to different ultrasound frequencies and pressures, selected to be both below and above the cavitation threshold at each frequency. Cavitation activity was measured in all experimentation using a Passive Cavitation Detector (PCD). Post insonation, samples were quantitatively analysed using fluorescence microscopy to visualise different sized molecules to determine the amount and distance of model drug transported, with the aim of determination of the dominant mechanisms of transport of molecules within the gel. The effect of the addition of cavitation nuclei on transport was also investigated to determine their potential usefulness in enhancing transport.

3.2.1 *In vitro* Tissue Mimicking Material (TMM)

Agarose gel has been widely used as a TMM (Holt and Roy 2001). Building on previous studies, a concentration of 0.5% w/v was used to mimic both the ultrasound gel and the soft tissue delivery target. The structure and porosity of agarose gel at this concentration is close to that of soft tissues such as the skin (agar pore size range 0.5-50 µm (Pernodet, Maaloum et al. 1997), skin pore size 0.5-30 µm diameter (Aguilella, Kontturi et al. 1994)). Cylindrical samples of degassed 0.5% w/v agar (UltraPure Agarose 1000, Invitrogen, UK) were prepared by dissolving the powdered agar in distilled, deionised water and heating to 90°C until all the powder had dissolved. The agar was then degassed under vacuum at 50°C to remove any dissolved gas and pipetted while a warm liquid into cylindrical moulds (30 mm length x 10 mm cross sectional diameter). The size of the sample was defined by the size of the focus of the ultrasound beam, whilst allowing efficient use of fluorescently labelled dextrans. Four differently sized and labelled dextrans were incorporated into an additional layer of gel (200 µl agar/dextran/talc solution), which was applied over one cross sectional surface of the

previously gelled cylinder (figure 3.3): 3 kDa dextran labelled with Cascade Blue Dye (Molecular Probes D7132, Invitrogen, UK), 70 kDa dextran labelled with Cy5 dye (Dex0013-4, Nanocs, USA), 155 kDa dextran labelled with TRITC (T1287, Sigma-Aldrich UK) and 2000 kDa dextran labelled with FITC (FD20S, Sigma-Aldrich, UK). The concentrations of these dyes were selected for optimal fluorescence visualisation based on a calibration study outlined below. Final concentrations were selected as 80μg/ml for 3 kDa, 70 kDa and 2000 kDa molecules, and 160 μg/ml for 155 kDa molecules.

Dextran masses represented a range of molecular sizes corresponding to the sizes of the drugs and vaccines in clinical use. Dextran molecules were chosen for use because, although their charge and branching characteristics differ from many conventional drugs and vaccines, their size can be widely and accurately quantified, and they can easily be conjugated with fluorescent dyes. The fluorescent dyes were chosen in attempt to minimise overlap between excitation and emission spectra of different dyes.

The donor layer in this setup represented the ultrasound gel acting as a drug carrier and the acceptor layer of 0.5% agar was representative of underlying soft tissues. Both layers were gelled separately but within the same mould. The donor layer was applied 4 hours after the acceptor layer had been applied and placed in a 4°C fridge to gel. Samples were fit for use 4 hours after the donor layer had been applied and the sample refrigerated.

Fluorescence Visualisation study

In order to determine the optimal concentration of labelled dextran to use in this work, solutions of the dextrans at 4 different concentrations were gelled in agar and viewed under the fluorescence microscope at identical exposure conditions. Figure 3.1 shows concentrations that were selected for

use as they produced a signal of intensity clearly distinguishable from background noise, without saturating the detector at the exposure settings selected (figure 3.1)

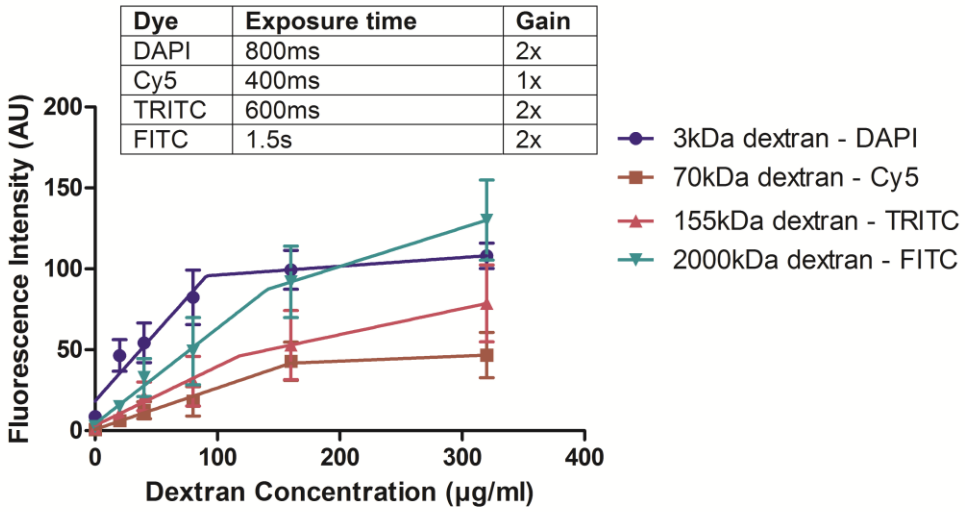

Figure 3.1. Intensity plot of increasing dextran concentrations with visualisation exposure settings.

Cavitation Nuclei

Cavitation nuclei (CN) are essentially rough surfaced particles that trap air bubbles on the surface, thereby providing an ample supply of bubbles where cavitation can occur(Gyongy and Coussios 2010). Talcum powder (86255, particle size -325 mesh [<44 µm] Fluka Analytical, UK) at a concentration of 0.25% w/v was added to the donor layer of 50% of the samples, in addition to the dextrans.

3.2.2 Ultrasound Sources

Two high intensity focussed ultrasound (HIFU) sources were utilised in this study. The axial and transverse pressure profiles of the foci of the 0.256MHz (Sonic Concepts 117D-01) and 1.1MHz (Sonic Concepts 102E-35) centre frequency piezoelectric transducers were measured by point-by-point scanning of areas around the ultrasound focus with a hydrophone (Onda SNO 1056, Onda Corp, CA, USA). Scans were performed in a tank of degassed deionised water and obtained axial (figure 3.2 (a)) and transverse (figure 3.2(b)) pressure profiles at the focus. Pressure output (peak to peak, and peak negative) at the ultrasound focus at a range of input voltages to each of the two transducers was also characterised (figure 3.2(c)).

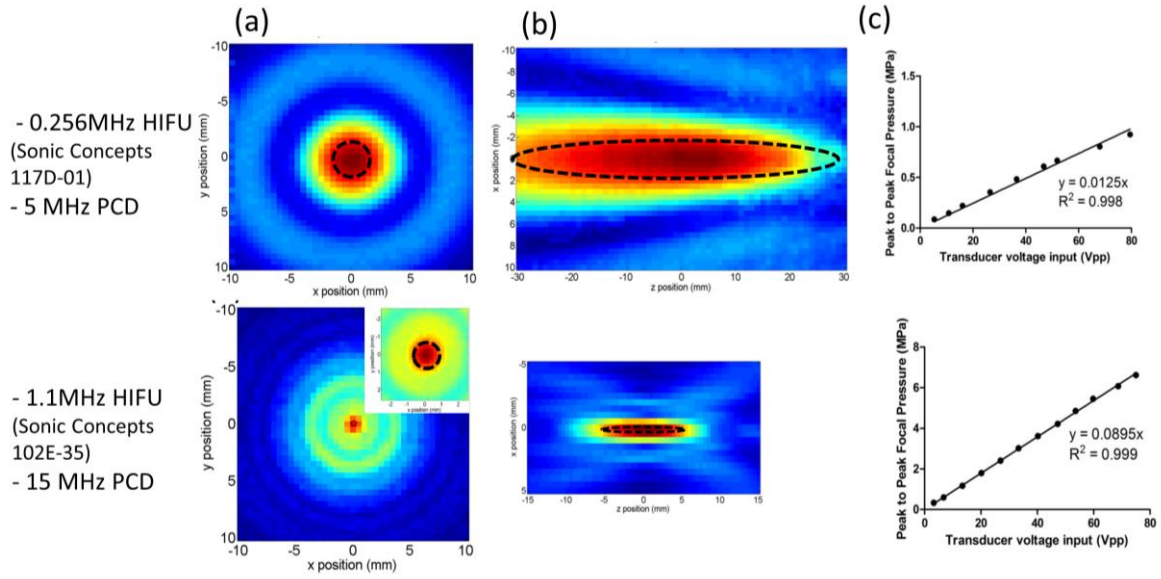

Figure 3.2: Normalised axial (a) and transverse (b) peak negative pressure profiles at the focus of the 0.256MHz (top) and 1.1MHz (bottom) transducers. Scans were performed with a pre-calibrated hydrophone (Onda SNO 1056, Onda Corp, CA, USA) (c) Peak to peak pressure output at the foci of the 0.256MHz and 1.1MHz transducers respectively for a range of voltage inputs. Black dotted lines represent focal regions of the passive cavitation detectors aligned confocally within each HIFU transducer. The focal volumes are ellipsoidal for all transducers.

3.2.3 Therapeutic Ultrasound Setup

The HIFU setup used to initiate cavitation in a hydrogel and drive molecular transport is shown in figure 3.3. A detailed description of the system has been provided elsewhere (Nandlall 2011). Briefly, the HIFU source was driven by a high power RF amplifier (Electronics and Innovation Model 1040L), with input signal provided by a function generator (Agilent 33220A). The amplifier output impedance was matched to the HIFU source via a matching network (Sonic Concepts H102 S/N 035 Rev E, and Sonic Concepts H117 S/N 001 Rev E). A 'low' frequency 0.256 MHz piezoelectric transducer is more effective at instigating cavitation events than at conferring acoustic radiation force. In contrast, a 'high' frequency 1.1 MHz piezoelectric transducer generates a larger acoustic radiation force. Each HIFU transducer had a central opening which could be fitted with a PCD, namely a single-element focused piezo-electric receiver used to detect acoustic emissions in the sample during ultrasound exposure, as previously described (Hockham, Coussios et al. 2010). A 5 MHz PCD (Panametrics, V309-SU, PZT element) was coupled with the 0.256MHz transducer and a 15 MHz PCD (Panametrics, V319-SU, PZT element) was coupled with the 1.1MHz transducer in order to ensure that the PCD centre frequency was 15-20 times greater than the main driving frequency. As a result, the detector was particularly sensitive to broadband emissions associated with inertial cavitation instead of harmonics of the fundamental driving frequency. The received signal was further high-pass filtered at 2MHz for the 5 MHz PCD and at 5MHz for the 15 MHz PCD, providing further isolation of the fundamental HIFU frequency and its harmonics, before being amplified using a dedicated amplifier (SR445a, Stanford Research Systems, Sunnyvale, CA) set to an amplification of 25 times, or 28 dB, and digitised using a 14-bit data acquisition (DAQ) card (PCI-5122, National Instruments, Austin, TX) operating at a sampling frequency of 100MHz. Samples were mounted (within their moulds with open ends) in a custom made sample holder at the focus of the ultrasound beam prior to insonation (figure 3.3).

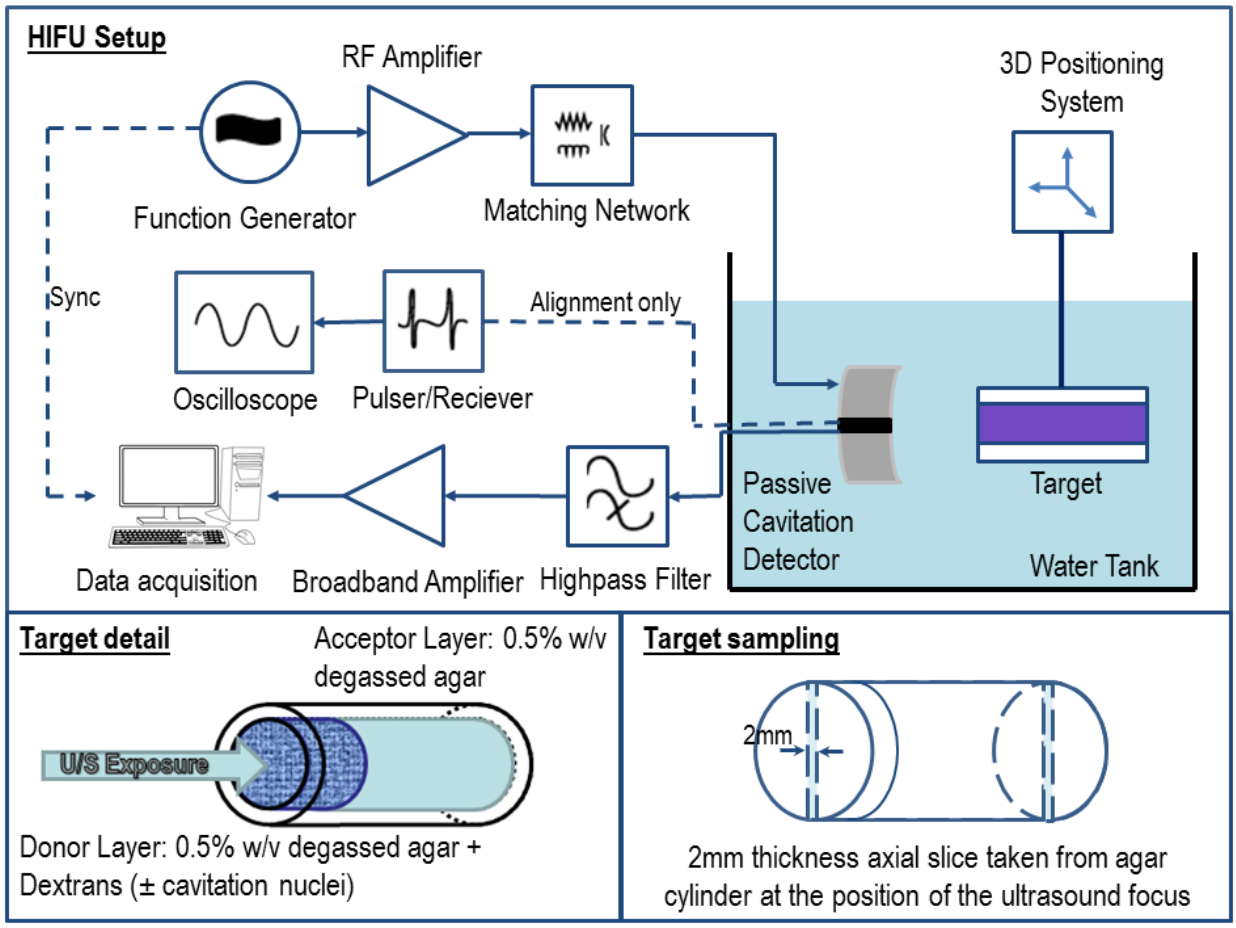

Figure 3.3: High Intensity Focussed Ultrasound (HIFU) setup used in this work. The driving signal for the HIFU transducer is generated by a computer-controlled function generator and a high-power RF amplifier, followed by a transducer-specific matching network to optimise power transfer. Meanwhile, acoustic emissions from the focus are measured using a passive detector aligned coaxially with the HIFU transducer. The signal from the passive detector transducer was conditioned using a high pass filter followed by a broadband amplifier before being recorded by the data acquisition unit. Also shown are an ultrasonic pulser/receiver and an oscilloscope, used to align the TMM with the transducers but were disconnected during exposures. Inset (left) shows further detail of the structure of the TMM devised for this study, and inset (right) shows the orientation of post-insonation sampling (Bhatnagar, Schiffter et al. 2014).

3.2.4 Selection of Ultrasound Exposure Parameters

Cavitation threshold determination

Cavitation is known to only occur above a certain peak rarefactional pressure amplitude at the focus, known as the inertial cavitation (IC) threshold. The IC threshold varies with frequency and sample composition, i.e., the presence of cavitation nuclei. The following process was repeated with each pair of HIFU and PCD transducers in order to determine the IC thresholds of the different types of TMM used in this study at each of the two ultrasound frequencies.

The PCD and HIFU transducers were first coaxially and confocally aligned, ensuring that the sensitive region of the PCD overlapped with the HIFU focus. Samples were then aligned with the focus of the transducers using the PCD transducer driven with a pulser-receiver (JSR Ultrasonics, DPR300 Pulser Reciever, Serial no: S/N DA0369) to monitor the position of the sample until its surface was at the focus. Identical samples were insonated with a single 10ms pulse of HIFU at 6 different peak rarefactional focal pressures (PRFP) in the range of 0-9MPa, and the PCD signal traces for the first 300μs of the pulse at each pressure recorded to quantify high energy emissions from the ultrasound focus – a direct result of cavitation activity. The traces were used to determine the presence of cavitation in the samples, and the variance of the received signal (used to quantify the presence and/or magnitude of an acoustic event) plotted against pressure to determine the pressure above which cavitation could reliably be assumed to occur. The cavitation threshold was determined as the pressure at which the variance of the acoustic signal showed an increase of at least 6 standard deviations above the baseline noise level. The results of this characterisation for all the types of samples used in this study are shown in figure 3.4.

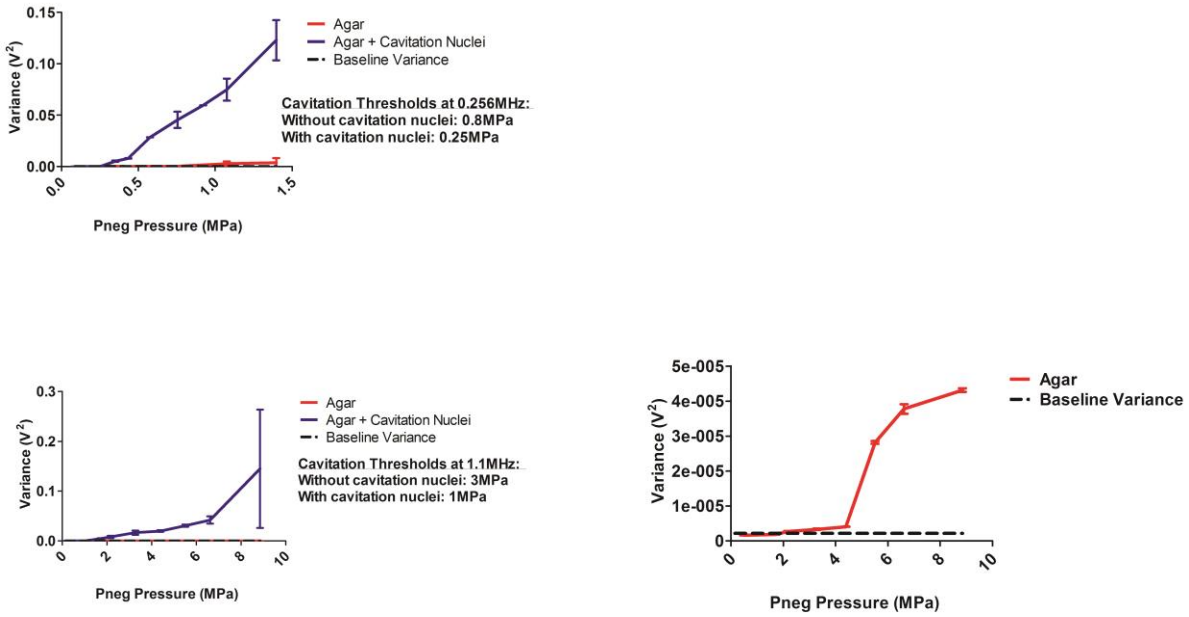

Figure 3.4: Cavitation thresholds of TMM at 0.256MHz (top) and 1.1MHz (bottom) in samples with (blue) and without (red) CN. Cavitation activity in samples without CN at 1.1MHz was extremely low, and is therefore shown on a separate graph (bottom right). Cavitation thresholds determined are given for each frequency.

The transport mechanism of the model drug was investigated by insonating samples at a number of different pressures at 0.256MHz and 1.1MHz. Comparisons were made between two different types of sample (with and without cavitation nuclei) at six different pressures selected.

Samples with and without cavitation nuclei were subjected to a 10% duty cycle (10 ms on, 90 ms off) for 100 cycles (total exposure time: 10 sec) at different focal pressures and frequencies shown in table 1, which gives reasons for their selection. A 10% duty cycle was chosen to minimise heating effects. Heating studies were carried out to determine the pressure amplitudes where the temperature rise became capable of tissue damage (<2°C rise) at the greatest pressure amplitude at both frequencies. At 256 kHz, a detectable temperature difference was not observed at a 10% duty cycle. In order to

demonstrate beyond doubt the absence of harmful heating effects, temperature changes were recorded at continuous wave (CW) exposure (figure 3.5). At 0.256 kHz, a temperature rise of less than 1°C was observed with continuous wave exposure at 1.4 MPa PRFP for 10 s, so a significant temperature rise at 10% DC was not anticipated. The continuous nature of the ultrasound is evident in the steady increase in the temperature as the exposure progresses (figure 3.5, left). At 1.1 MHz, temperature increases of 2°C were observed at the experimental parameters (10% duty cycle) at 5.5 MPa. The pulsatile nature of the ultrasound exposure is seen as rapid increases in temperature, followed by rapid decreases, leading to the sharp peaks in figure 3.5 (right).

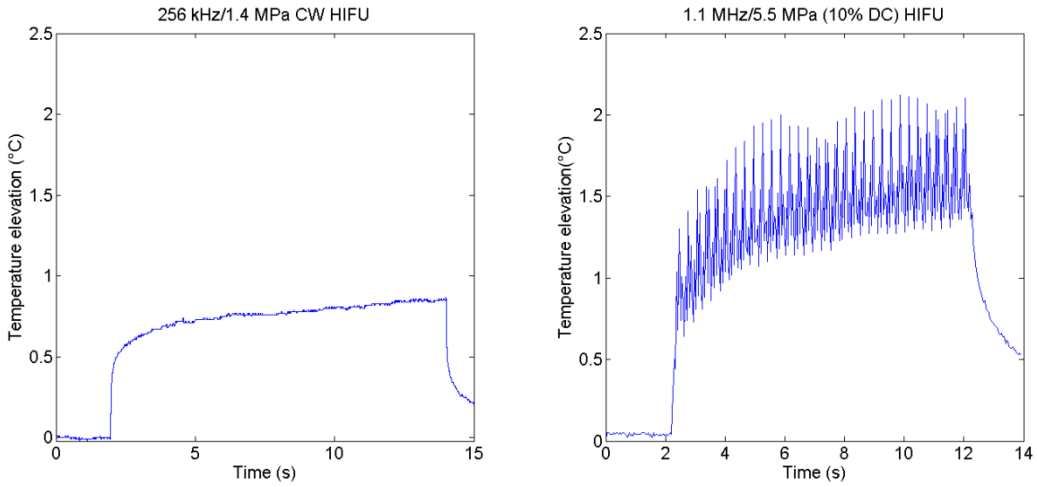

Figure 3.5: Representative heating curves for ultrasound exposure conditions. Heating on the order of 2 degrees Celsius was observed at at 1.1MHz for a peak rarefactional pressure of 5.5 MPz and a 10% duty cycle(right), whilst continuous exposure at 0.256 kHz for a pressure of 1.4 MPa yielded a temperature rise of less than 1 degree (left). HIFU exposure began 2 s after recording began, and ended 10 s later (at 12 s).

3.2.5 Determination of Cavitation Energy at Selected Exposure Parameters

During each 10ms pulse, voltage data from the PCD was recorded using the DAQ card. Due to computational memory restrictions at the sampling frequency used, only the first 200μs of the voltage signal received by the PCD was recorded. To verify that the start of the exposure was an appropriate sampling interval the variances of 200 μs segments over a single 10 ms trace were calculated. Results of this analysis are shown in figure 3.6 and demonstrate that the maximum levels of variation are consistently present at the start of the signal and that this level falls and forms a plateau after the first 1ms of exposure. In order to record this maximum level, the first 200 μs was chosen to be the sampling interval for the entirety of the work presented in this thesis. Post processing of the signal was performed using previously published methods (Hockham, Coussios et al. 2010). In short, the data was filtered to remove harmonics and subharmonics of the driving frequency to isolate signal that corresponded only to broadband frequency emissions, the hallmark of inertial cavitation activity. The variance of the filtered voltage trace was then calculated for each time-point where a measurement had taken place over the entire duration of the exposure, and the integral of the graph of variance of signal against time was used as a metric for acoustic power generated by cavitation at each different exposure condition (figure 3.9).

3.2.6 Quantification of Drug Delivery

Multiple fluorescent dyes were used simultaneously in order to ensure that all four sizes of molecules were subject to an identical ultrasound field. However, using fluorescent dyes in combination gives rise to a number of issues. Firstly, the possibility of each of the dyes interacting with each other increases, and this could affect their visualisation. Additionally, although care was taken to select dyes with distinct excitation and emission spectra, there could be some unintentional excitation or emission from dyes

that were not specifically being visualised at the time. To establish the impact of these issues, the dyes were visualised individually and in combination (in 0.5% agar) at the concentration of dextran in the donor layer (2 µg/ml). The results of this visualisation are shown in figure 3.12.

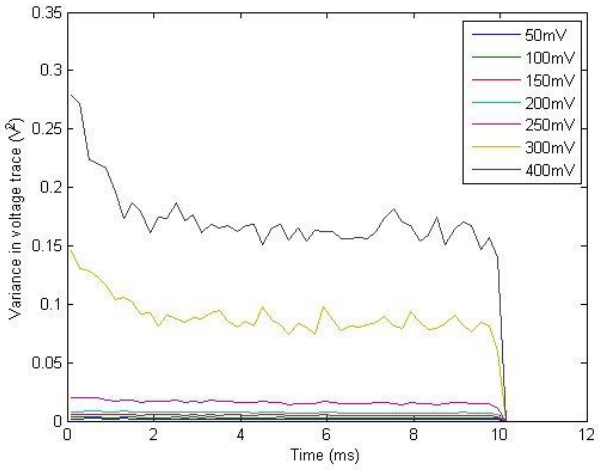

Figure 3.6: Variance values of 200µs segments during a 10ms pulse PCD data at variable HIFU transducer voltage inputs. Below the cavitation threshold, there is very little signal above the noise level, so variance of the voltage traces is low. Above the cavitation threshold, the variance of the segments is highest at the beginning of the exposure for the first 1ms, before plateauing at a constant level for the rest of the 10ms exposure.

Immediately after sonication, cylindrical samples were removed from the holder and their moulds, and an axial slice with 2 mm thickness was taken from the centre of the cylinder (figure 2 inset). Slices were viewed under a fluorescence microscope (Nikon Eclipse Ti) and images were taken in order to measure the ultrasound induced penetration depth of each of the four dextrans. Different exposure settings were used in order to allow optimised viewing of each dye, but were normalised to account for this. ImageJ software (National Institute of Health, Bethesda, MA) was used to detect and quantify any fluorescence imaged in the acceptor layer. The two metrics used to quantify delivery from these images were concentration and distance of transport.

Images were analysed as shown in figure 3.7. The concentration of drug transported was measured as the average intensity of the acceptor layer in the image, and this average intensity was converted to a dextran concentration using a calibration curve (figure 3.7a). For the measurement of peak transport distance, control images were thresholded to determine limiting values for the presence or absence of dextran, and the images taken of the post insonated samples were thresholded and peak transport distance was measured as the maximum depth (perpendicular to the donor layer) at which fluorescence was present.

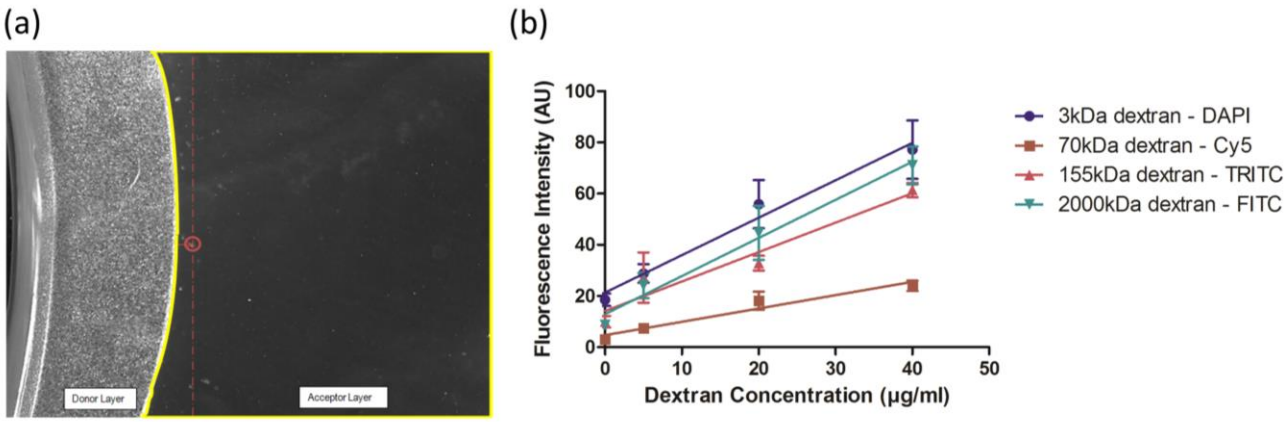

Figure 3.7: (a) Quantitative analysis methods: Concentration transported was calculated by obtaining the average pixel intensity in the acceptor layer (yellow) and converting back to dextran concentration using a calibration curve (b). Peak transport distance was obtained by identifying the furthest travelled fluorescent molecule and measuring the distance from the donor layer perpendicular to the direction of ultrasound exposure (red). Image (a) shows result of sample containing cavitation nuclei after insonation at 0.256 MHz and 1 MPa.

3.3 Results and Discussion

3.3.1 Fluorescence visualisation

Figure 3.9 demonstrates that the visualisation of Cy5 and FITC was unaffected by the other dyes present, as there is no significant difference in intensity when viewed individually or in combination. The intensity of Cascade Blue and TRITC dyes both decreased significantly when viewed in combination. In the case of the TRITC dye, there was seen to be some overlap between emission spectra of Cy5 and TRITC, with both emitting a red light when excited. Despite the response of Cy5 being unaffected by the TRITC, the converse was not the case. There are two possible reasons for this: (1) the TRITC dye could have been affected chemically by the presence of the other dyes, or (2) fluorescence emitted by the TRITC could have excited the Cy5 molecules, and the fluorescence emission from the Cy5 as a result of this could not be seen because the light was being filtered to pass only the light of the emission wavelength of TRITC. In either case, this would mean that the concentration of TRITC labelled dextran (155kDa) has been underestimated, and that actually more transport occurred than is shown. Reduced fluorescence emission of the Cascade Blue dye in combination could also have been a result of chemical interaction with the other dyes present, leading to the conclusion that the ultrasound enhanced transport observed in this study is an underestimate. In order to avoid underestimation of the absolute delivery amount in future studies, molecular marking strategies as quantum dots (Jaiswal and Simon 2004; Paliwal, Menon et al. 2006; Ryman-Rasmussen, Riviere et al. 2006; Maoquan, Qiang et al. 2007) or radiolabelling (Abernathy, Pou et al. 1995; Kushner, Blankschtein et al. 2007; Chen and Kristensen 2009) could be used instead of fluorescence.

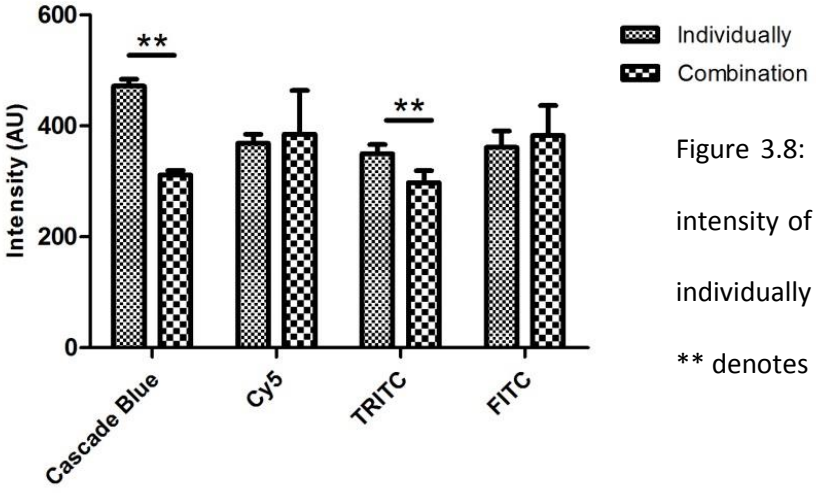

Figure 3.8: Differences in fluorescence intensity of each of the four dyes used individually vs. in combination (n=10) ** denotes p<0.01.

3.3.2 Acoustic Cavitation

Cavitation threshold determination is of great importance to ensure the utility and safety of ultrasound-assisted delivery. This varies with sample geometry, concentration and composition, and it is therefore necessary to accurately determine the IC threshold for each new system. Results for the cavitation threshold (figure 3.4) were in line with previous studies(Mylonopoulou, Bazán-Peregrino et al. 2013). Generally, overcoming the cavitation threshold required larger peak rarefactional focal pressures (PRFP) at 1.1MHz than at 0.256MHz. Similarly, a much higher PRFP was required at 1.1MHz to give comparable amounts of acoustic cavitation (as indicated by the variance of the voltage trace) as at 0.256MHz. The addition of cavitation nuclei lowered cavitation thresholds (and also cavitation activity above the threshold) at both frequencies (figure 3.4). Both inertial and stable cavitation activity levels increased in samples that incorporated cavitation nuclei.

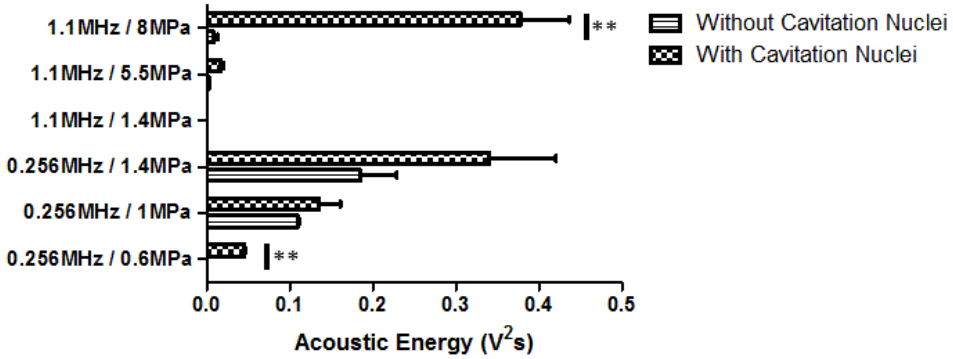

Figure 3.9. Levels of broadband acoustic emissions at each of the selected ultrasound exposure parameters in samples with and without CN. Stars denote significant difference (** = $p<0.01$, two tailed unpaired t-test))

Based on the cavitation thresholds (figure 3.4) acoustic exposure parameters in this mechanistic study were chosen to observe effects above and below the cavitation threshold at 0.256 MHz and 1.1 MHz, with acoustic radiation force expected to play a stronger role at the higher frequency. Levels of total broadband acoustic emissions over the entire 10s exposure are shown in figure 3.9 and are also in line with expected trends. Pressures of 8MPa and 5.5 MPa at 1.1 MHz frequency represented the attempt of the author to observe the effects of acoustic radiation force, but in a clinical context these pressures would cause unacceptable heating levels. Lower, more clinically acceptable pressures were seen to be below the IC threshold, indicating the reduced utility of this frequency for this application. Results at 0.256MHz confirmed the presence of high levels of inertial cavitation as pressure increased, and when cavitation nuclei were present. Additionally, the significant difference between broadband emissions at 0.6MPa shows the reduction in cavitation threshold in the presence of cavitation nuclei. Comparable levels of broadband emissions were observed at 1.1MHz/8MPa and 0.256 MHz/1.4 MPa, once again demonstrating the utility of the lower frequency.

3.3.3 Ultrasound Enhanced Bulk Transport – Concentration

In clinical use, a certain dosage of drug or vaccine is required to produce an effect, and the concentration penetration of a model drug molecule was used to simulate and measure this. The effects of ultrasound and cavitation generation on the transported concentration of dextrans of different molecular weights in the donor layer are shown in figure 3.10. The application of ultrasound significantly enhanced transport at all molecular sizes except 70 kDa (although there was an increase) at both frequencies tested, provided that ultrasound pressure exceeded the cavitation threshold for that type of sample (0.25/0.8 MPa at 0.256 MHz with/without cavitation nuclei respectively, and 1/3 MPa at 1.1 MHz with/without cavitation nuclei respectively). This enhancement was seen to be 20% -30% for 3 kDa and 2000kDa respectively when samples that incorporated cavitation nuclei were insonated at 0.256 MHz. It is hypothesised that the results for the 70kDa dextran are lower than the other molecular size classes due to the low signal to noise ratio associated with the visualisation of the Cy5 dye. As can be seen in figure 3.7(b), the calibration curve used to convert from fluorescence of Cy5 to dextran concentration was markedly lower than the other three molecular weight dextrans, with the signal intensity at 40µg (half the original concentration in the donor layer) at less than 30% of the signal seen with the other dyes. Due to low signal intensity therefore, it was difficult to detect changes in the Cy5, and therefore 70kDa dextran concentration, which could be a reason for what appears to be poor penetration in this study.

Once above the cavitation threshold, further increases in pressure yielded little additional benefit to transport. Acoustic radiation forces were not seen to have any significant effect. Results showed that at acoustic pressures conducive to acoustic radiation force (1.1 MHz above around 2-3 MPa) there was no further increase in concentration transport. It is highly likely that these effects are the result of prefocal cavitation due to the high pressure, which reduces the effective pressure at the donor/recipient layer

interface. This leads to the conclusion that pressures above 2-3 MPa at 1.1 MHz are unnecessary and did not enhance transport. Additionally, local heating effects at these pressures would prohibit the use of these ultrasound parameters in a clinical setting. For example, the local temperature increase at 1.1 MHz at 5 MPa was shown to be around 5°C in a separate study (figure 3.5).

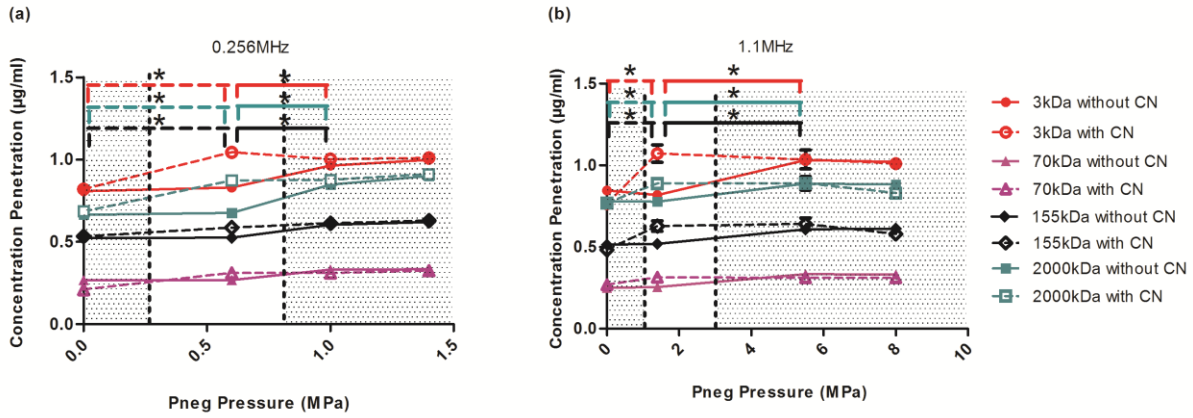

Figure 3.10: Enhancement caused in concentration transport as a result of the addition of cavitation nuclei at 0.256MHz (a) and 1.1MHz (b) at the range of pressures explored. Dotted vertical lines on each graph represent inertial cavitation thresholds with (left) and without (right) cavitation nuclei at each frequency, and the shaded areas represent pressures that are above or below both cavitation thresholds. Error bars represent 1 standard deviation. Stars denote significant increases in concentration penetration between adjacent ultrasound exposure conditions for dextrans of the same size (denoted by bar colour). Dotted significance bars denote that these differences were only present in the samples that contained cavitation nuclei at ultrasound exposure conditions that were below the cavitation threshold (0 MPa) vs. above the cavitation threshold (0.6 MPa at 0.256 MHz and 1.4 MPa at 1.1 MHz). Significant differences were determined by a one way ANOVA test between all adjacent points (*:$p<0.05$).

3.3.4 Ultrasound Enhanced Transport - Peak Penetration Distance

In order for vaccines to gain access to immune active Langerhans cells in the epidermis, they must be transported beyond the stratum corneum to the epidermis. Peak distance of transport was therefore chosen as a metric to indicate whether the molecules in this study would be transported to the required depth.

The enhancement in penetration distance as a result of ultrasound exposure and the addition of cavitation nuclei is shown in figure 3.11. Penetration depth of the 3 kDa dextran appeared unaffected by ultrasound exposure; therefore it is believed that the small size of this molecule facilitated diffusion into the pore structure of the gel. Transport of all the molecular sizes except 3kDa was found to be significantly enhanced by ultrasound both at 265 kHz and 1.1 MHz. However, at 265 kHz, modest acoustic pressures (<1.5 MPa) sufficed to increase the penetration distance from less than 1 mm without ultrasound to up to 4 mm in the presence of cavitation, whilst at 1.1 MHz increasing the penetration distance to beyond 3 mm required pressure amplitudes in excess of 5 MPa. As in the bulk transport results, the only significant increases in transport of the three larger molecular sizes was observed above the cavitation threshold for each type of sample. Looking across all molecular weights, it can be seen that increasing pressure only had a significant effect on penetration distance if the cavitation threshold was crossed. Beyond the cavitation threshold for any one medium and molecular size, further increases in pressure did not yield further increases in penetration distance. In other words, enhanced transport appears primarily mediated by the occurrence of the inertial cavitation events, rather than the violence of the collapses. This is possibly due to shielding, whereby the occurrence of a dense bubble cloud and violent collapses near the transducer precludes incident energy from enhancing the violence of cavitation events close to the recipient layer. Generally, enhancement in peak transport distance (figure 3.11) was much greater than in bulk transport enhancement (figure 3.10).

At both frequencies, cavitation nuclei were shown to reduce the cavitation threshold, facilitating deeper transport at lower pressures. The application of ultrasound above the cavitation threshold enhanced the distance of transport in all but 3 kDa molecular sizes, demonstrating the utility of cavitation nuclei in the pressure range between the cavitation thresholds of the two different types of sample. Harmful heating effects of ultrasound are greater at higher pressures, and with the addition of cavitation nuclei, transport is made possible at much lower pressures.

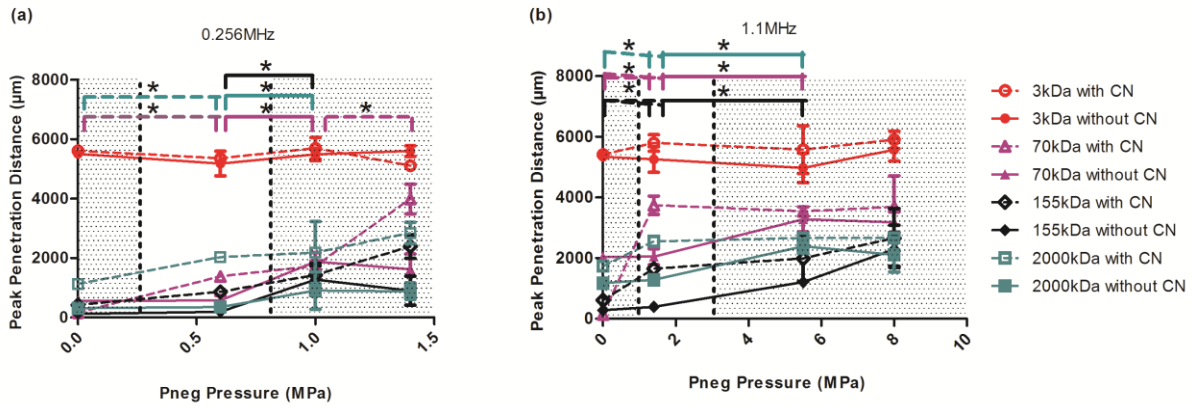

Figure 3.11: Enhancement caused in peak penetration distance as a result of the addition of cavitation nuclei at 0.256MHz (a) and 1.1MHz (b) at the range of pressures explored. Dotted vertical lines on each graph represent inertial cavitation thresholds with (left) and without (right) cavitation nuclei at each frequency, and the shaded areas represent pressures that are above or below both cavitation thresholds. Error bars represent 1 standard deviation. Stars denote significant increases in penetration depths between adjacent ultrasound exposure conditions for dextrans of the same size (denoted by bar colour). Dotted significance bars denote that these differences were only present in the samples that contained cavitation nuclei at ultrasound exposure conditions that were below the cavitation threshold (0 MPa) vs. above the cavitation threshold (0.6 MPa at 0.256 MHz and 1.4 MPa at 1.1 MHz). Significant differences were determined by a one way ANOVA test between all adjacent points (*:$p<0.05$).

An additional effect observed in the enhancement of peak transport distance only was the indication of optimal molecular sizes for US facilitated transport with and without cavitation nuclei. Figure 3.12 shows the maximum enhancement observed for each molecular size when compared to the control. The dependence of the observed enhancement as a function of molecular weight is most probably due to the size of the dextran molecules relative to the pore size of the agar, reported as 50-500 nm in the literature. At a size of less than 1 nm, we hypothesize that the 3kDa dextran diffuses more or less freely through the gel whether ultrasound is present or not. Conversely, with a size in the region of 450 nm, the 2000 kDa dextran will struggle to cross the mesh even when actuated by cavitation-induced microstreaming. However, with a size on the order of 50 nm, the 70 kDa dextran is best placed to benefit most from ultrasound-mediated convective transport. US-facilitated delivery methods can therefore be optimised depending on the size of the molecule that is to be delivered.

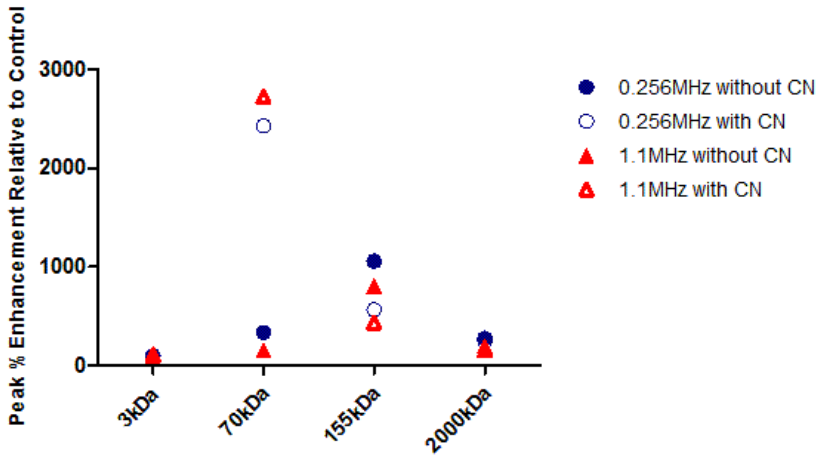

Figure 3.12: Enhancement of peak penetration distance relative to the control.

For these reasons, 0.256 MHz is suggested for use in ultrasound-assisted delivery applications, such as transdermal delivery. At this lower frequency, inertial cavitation can be instigated at lower pressures with minimal risk of heating. Additionally, due to the larger focus at the lower frequency (as shown in figure 3.2), a larger surface area can be treated at the same time.

3.3.5 Overall Observations and Sources of Error

Concentration penetration and peak transport distance were effective metrics for illustrating the differences in transport at different ultrasound settings and mechanisms. Clinically, concentration penetration correlates most closely with dose, and penetration depth is of importance when the delivery molecule has a known target at a known depth in the skin. In the case of vaccines, for example, delivery dose is required to be above a given threshold dose at a particular depth (to target the Langerhans cells in the epidermis). For drugs that are targeted to the bloodstream, a certain dose (with stringent upper and lower limits) would be required to penetrate all the way to the dermis, representative of a much more demanding application. Measurement of both penetration dose and depth gives useful information for both of these scenarios. Overall, it was seen that ultrasound at pressures above the cavitation threshold increases transport at all frequencies, leading to the conclusion that the presence of inertial cavitation activity was the predominant factor in enhanced transport. However, other mechanisms such as acoustic radiation and streaming, and maybe mild heating due to the application of the ultrasound, also played a minor role. Enhancement levels were seen to be much lower in terms of concentration than in terms of peak penetration distance.

Statistically significant increases in concentration transport were between 0.2 and 0.5 μg/ml in the samples. Although modest when placed in a clinical context, it was not the objective of this work to deliver clinically relevant quantities, but merely to show that ultrasound can be used to facilitate molecular transport. Molecular transport was only one half of the hypothesized delivery mechanism, and inertial cavitation-induced permeability increases (which were not assessed in this chapter) were also hypothesised to contribute to a further increase in concentration transport.

Exposure of samples to the same pressure amplitude (1.4 MPa) at different frequencies showed similar amounts of transport occurring in samples both with and without cavitation nuclei. When translating this result to clinical use, it is useful to consider heating effects, which decrease with frequency. On this basis, as the amount of transport is very similar, it would be of greater benefit to consider use of the lower frequency to maximise transport and minimise heating. Additionally, the transverse beam cross-section (which typically scales with the wavelength) will be about 4 times larger at 0.256 kHz than at 1.1 MHz for the same physical transducer size, enabling transport to occur over a larger area of tissue (figure 3.2).

It was observed that the addition of cavitation nuclei was of benefit in two ways: (1) lowering the cavitation threshold to allow enhanced transport, therefore giving a larger range of pressures at which transport could be enhanced, and (2) in the peak transport distance results, the addition of cavitation nuclei was also shown to increase transport distance of larger molecules at 0.256 MHz, although this effect was not seen in the concentration permeation results.

When placed in the context of ultrasound-assisted transdermal vaccine delivery, this work gives credence to the simultaneous application protocol. Ultrasound assisted transport in the TMM was significantly enhanced compared to diffusion in molecules of comparable sizes to vaccine molecules (70 kDa and above), with penetration distances on the order of mm which places the deepest particles in the epidermis and dermis with access to the systemic circulation. Enhancement in the delivery concentration, which corresponds most closely with dose, was 0.2 to 0.5 µg/ml, which is a small increase in terms of drug/vaccine dose. However, it is hypothesised that this can be improved with the permeability increases present in the skin upon exposure to inertial cavitation. However, it is important to demonstrate the capability of vaccine formulations to withstand high acoustic pressure without losing

their therapeutic potential. This loss of therapeutic potential is hypothesised to take place via two mechanisms: (i) excessive and prolonged heating, or (ii) mechanical damage on a molecular level due to acoustic cavitation mechanisms.

As mentioned previously, ultrasonic heating was measured for the exposure conditions utilised in this study, and temperature rises were not found to exceed 2°C in the 10s exposure period. This is thought to be due to the low duty cycle, allowing for local cooling during exposure. Vaccine formulations are designed to withstand temperature fluctuations this small (Chen and Kristensen 2009). Mechanical effects due to acoustic cavitation mechanisms are more difficult to quantify. However, a single study exists that demonstrates the capacity of tetanus toxoid vaccine to retain therapeutic potential despite exposure to acoustic cavitation (Tezel, Paliwal et al. 2005). Additionally, acoustic cavitation has been used to enhance the delivery and therapeutic efficiency of an oncolytic virus *in vitro* (Bazan-Peregrino, Arvanitis et al. 2012). Therefore, there exists sufficient literature in the field to assert that exposure to ultrasound is unlikely to affect the therapeutic potential of a vaccine.

3.4 Summary

We have demonstrated the potential of ultrasound to actively transport and enhance the penetration distance of molecules of size 70kDa or greater though a gel based TMM. It was found that in the absence of cavitation activity, there was little or no transport enhancement. Inertial cavitation, characterised by broadband acoustic emissions was therefore identified as the most significant mechanism in mediating transport. Other mechanisms, such as acoustic radiation force and small levels of heating (<2°C) were found to have little impact on transport.

The addition of talc as a source of cavitation nuclei to the donor layer makes a negligible difference to the amount of model drug transported or to the peak transport distance, but was seen to effectively lower the cavitation threshold, allowing enhanced transport at a lower acoustic pressure. Given the dominant role played by inertial cavitation and that significant levels of cavitation activity are more readily reached for lower pressures at lower frequencies, 256 kHz was shown to be better suited to drug and vaccine transport and delivery than 1.1MHz, Additionally, the lower frequency facilitates exposure of a larger cross-sectional area of tissue. Use of even lower frequencies, such as 20 kHz, would also be possible, however due to the much longer wavelength and lower attenuation, could lead to problems with controlling and suppressing cavitation activity in subcutaneous fat and muscle. For these reasons, 256 kHz became the frequency of choice for all other experimental work presented in this dissertation.

Addendum

Subsequent work in ex vivo porcine skin demonstrated that although a 10 s exposure period at the settings used in this study was sufficient to enable transport of molecules into an agarose hydrogel, it was not long enough to ultrasonically permeabilise skin to a level where enhanced transport was of benefit. This is hypothesised to be a result of the presence of a biological barrier, the stratum corneum, which required energy over a longer period of time to permeabilise, as opposed to the gel-gel interface used in the work presented in this chapter. Consequently, the work done in the remainder of this thesis (unless otherwise stated) was done with an ultrasonic exposure period of 90 s, not 10 s.

References

Abernathy, V. J., N. A. Pou, et al. (1995). "Noninvasive measures of radiolabeled dextran transport in in situ rabbit lung." Journal of Nuclear Medicine **36**: 1436-1436.

Aguilella, V., K. Kontturi, et al. (1994). "Estimation of the pore size and charge density in human cadaver skin." Journal of Controlled Release **32**(3): 249-257.

Bazan-Peregrino, M., C. D. Arvanitis, et al. (2012). "Ultrasound-induced cavitation enhances the delivery and therapeutic efficacy of an oncolytic virus in an in vitro model." Journal of Controlled Release **157**(2): 235-242.

Bhatnagar, S., H. Schiffter, et al. (2014). "Exploitation of Acoustic Cavitation-Induced Microstreaming to Enhance Molecular Transport." Journal of Pharmaceutical Sciences **103**(6): 1903-1912.

Chen, D. and D. Kristensen (2009). "Opportunities and challenges of developing thermostable vaccines." Expert Review of Vaccines **8**(5): 547-557.

Gyongy, M. and C. C. Coussios (2010). "Passive spatial mapping of inertial cavitation during HIFU exposure." Biomedical Engineering, IEEE Transactions on **57**(1): 48-56.

Hockham, N., C. C. Coussios, et al. (2010). "A real-time controller for sustaining thermally relevant acoustic cavitation during ultrasound therapy." Ultrasonics, Ferroelectrics and Frequency Control, IEEE Transactions on Biomedical Engineering **57**(12): 2685-2694.

Holt, R. G. and R. A. Roy (2001). "Measurements of bubble-enhanced heating from focused, MHz-frequency ultrasound in a tissue-mimicking material." Ultrasound in medicine & biology **27**(10): 1399-1412.

Jaiswal, J. K. and S. M. Simon (2004). "Potentials and pitfalls of fluorescent quantum dots for biological imaging." Trends Cell Biol **14**(9): 497-504.

Kushner, J. t., D. Blankschtein, et al. (2007). "Evaluation of the porosity, the tortuosity, and the hindrance factor for the transdermal delivery of hydrophilic permeants in the context of the aqueous pore pathway hypothesis using dual-radiolabeled permeability experiments." J Pharm Sci **96**(12): 3263-3282.

Maoquan, C., W. Qiang, et al. (2007). "In vitro and in vivo transdermal delivery capacity of quantum dots through mouse skin." Nanotechnology **18**(45): 455103.

Mathias, N. R. and M. A. Hussain (2010). "Non-invasive systemic drug delivery: Developability considerations for alternate routes of administration." J Pharm Sci **99**(1): 1-20.

Meshali, M., H. Abdel-Aleem, et al. (2010). "Effect of gel composition and phonophoresis on the transdermal delivery of ibuprofen: In vitro and in vivo evaluation." Pharmaceutical Development and Technology **16**(2): 93-101.

Mitragotri, S. and J. Kost (2001). "Transdermal delivery of heparin and low-molecular weight heparin using low-frequency ultrasound." Pharm Res **18**(8): 1151-1156.

Mylonopoulou, E., M. Bazán-Peregrino, et al. (2013). "A non-exothermic cell-embedding tissue-mimicking material for studies of ultrasound-induced hyperthermia and drug release." International Journal of Hyperthermia **29**(2): 133-144.

Nandlall, S. D. (2011). Monitoring Cell and Tissue Damage During Ablation by High-Intensity Focussed Ultrasound. Department of Engineering Science. Oxford, UK, St Anne's College, University of Oxford.

Paliwal, S., G. K. Menon, et al. (2006). "Low-frequency sonophoresis: ultrastructural basis for stratum corneum permeability assessed using quantum dots." J Invest Dermatol **126**(5): 1095-1101.

Pernodet, N., M. Maaloum, et al. (1997). "Pore size of agarose gels by atomic force microscopy." Electrophoresis **18**(1): 55-58.

Ryman-Rasmussen, J. P., J. E. Riviere, et al. (2006). "Penetration of intact skin by quantum dots with diverse physicochemical properties." Toxicological Sciences **91**(1): 159-165.

Saia, M. H., F. Sharman, J. Abiteboul, D. Campins, M. Burkowitz, J. Choe, Y. Kavanagh, S. (2013). "Needlestick Injuries: Incidence and Cost in the United States, United Kingdom, Germany, France, Italy, and Spain." Biomedicine International **1**(1): 41-49.

Tezel, A., S. Paliwal, et al. (2005). "Low-frequency ultrasound as a transcutaneous immunization adjuvant." Vaccine **23**(29): 3800-3807.

4. A Cavitation-Promoting Vaccine-Embedding Gel Formulation

An ultrasound-assisted transdermal vaccine delivery system is generally a combination of two distinct elements: (1) a dosage form that contains the vaccine in a formulation from which it can be transdermally delivered, and (2) an ultrasound source that facilitates increased skin permeability and enhances vaccine transport from the dosage form into the skin. Chapter 3 addressed the ultrasound source and successfully demonstrated that ultrasound induced inertial cavitation is able to enhance the transport of molecules of size similar to vaccine molecules through a tissue mimicking hydrogel. Existing literature in the field has also shown the capacity of inertial cavitation to increase the permeability of the skin (Mitragotri and Kost 2000; Mitragotri and Kost 2004; Mitragotri 2005; Tezel, Paliwal et al. 2005; Paliwal, Menon et al. 2006). This chapter therefore addresses the vaccine dosage form.

A fundamental requirement of a vaccine dosage form is that it contains and maintains the vaccine in its native form without alteration in structure or function. Aside from the functional need to keep the vaccine in an active form, clinical regulatory approval for a vaccine/drug dosage form is contingent upon provision of evidence of maintained stability and function over periods of months. Protein damage or denaturation can potentially occur at one or multiple levels of the protein structure (figure 4.1). The primary level of protein structure is the sequence of amino acid residues that form a polypeptide chain. The way that the polypeptide chains are organised into regular structures, such as α-helices and β-pleated sheets held together by hydrogen bonds, is described as the secondary structure of the protein. Tertiary structure describes the way that the whole chain (including the secondary structures) folds to form the protein molecule's 3-dimensional shape. Some complex proteins are composed of multiple polypeptide units, each with their own tertiary structures. Quaternary structure is the way that these units fit together to form an entire molecule. Disruption to any level of a protein's structure can affect its overall function and stability.

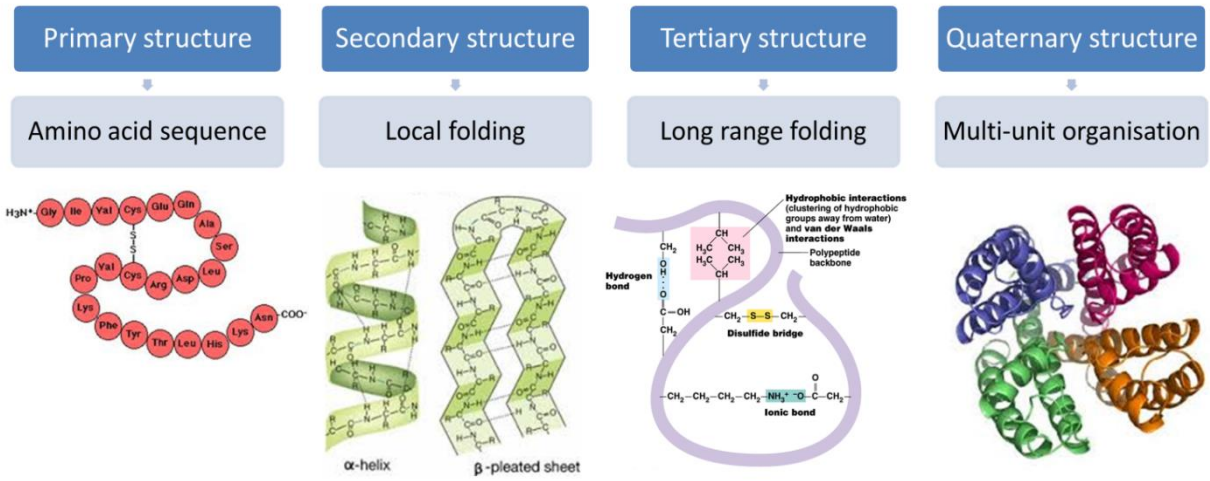

Figure 4.1: Levels of protein structure. Images taken from (Kimball 2006; Excellence 2007)

The addition of ultrasound exposure to the system introduces a further set of requirements. Not only must the vaccine remain structurally and functionally unchanged within the dosage form itself, but the vaccine molecules must also be protected from any mechanical and thermal forces present as a result of ultrasound exposure. Compression, rarefaction and shearing of the local environment of the vaccine molecules represent the mechanical forces that threaten the bonds within the protein structure. A review article investigating the range of forces required to rupture *single molecule* interactions found that these forces range between 10-1000 pico newtons (10^{-12} N) over an area the size of a few nanometres (Weisel, Shuman et al. 2003) – producing a force on the order of 0.001 Pa. Shear stress induced in the surrounding medium from oscillating bubbles has been suggested as on the order of 0.003 Pa (Collis, Manasseh et al. 2010), therefore the threat posed by these forces is worthy of consideration in a large population of bubbles, but unlikely to do large amounts of damage. Heating from attenuation of the ultrasound wave within the formulation could also cause damage particularly delicate proteins and reduce their potency, with some strains of Influenza vaccines affected in less than an hour above 40°C (Clarke and ter Haar 1997; Kristensen 2008). Therefore, significant temperature rises in the transdermal delivery system cannot be tolerated. Additionally, the properties of the dosage form must not hinder the transport mechanisms exploited

by using ultrasound. High viscosity, for example, is capable of rendering micro streaming mechanisms ineffective for transport (Wu and Nyborg 2008).

In addition to the minimum requirements of the dosage form, the effective delivery of the vaccine can be enhanced by tailoring the carrier's properties to suit an environment where ultrasound is present. As existing literature and previous work presented in chapter 3 has shown, inertial cavitation-related mechanisms are largely responsible for increased transport and increases in skin permeability. Therefore, a dosage medium that is conducive to the instigation and sustainability of acoustic cavitation is beneficial for this application, which as previously shown, is achieved with cavitation nuclei. If seeding the dosage medium with cavitation nuclei reduces the ultrasound pressure needed to instigate cavitation, the detrimental effects of applying high pressures may be circumvented. The cavitation nuclei would of course need to be (1) stable in the gel formulation, (2) promote a sustained cavitation enhancing response, and (3) be immunologically inactive, so as not to interfere with the immune response from the vaccine.

Previous research in the field of transdermal vaccine delivery has utilised a liquid vaccine dosage form (Tezel, Paliwal et al. 2005), either applied immediately after pre-treatment with ultrasound or within a couplant applied with an ultrasonic probe. Liquid dosage forms are easy to formulate and have good ultrasound coupling properties. Low viscosity in liquids also allows for the complete exploitation of inertial cavitation related phenomena (such as micro-streaming and micro jetting) to increase skin permeability.

As discussed in chapter 3, hydrogels have not been widely used for ultrasound assisted transdermal drug delivery due to the belief that increased viscosity will hinder delivery. However, the advantage of using hydrogels is that their use is more suited to a clinical environment. Gel can be applied to the skin to form a sustainable coupling layer (as is already used in prenatal ultrasound scans), without the need for a 'holder' to prevent liquid simply flowing off an uneven surface or being rapidly absorbed into non-target areas or layers of skin. Ultrasound coupling gel is already approved and

established within a clinical setting, therefore a logical progression is the addition of a vaccine candidate to this gel allowing ultrasound assisted transport into the skin. For this reason, only clinically approved coupling gels have been used for this study. Seeding of gels with cavitation nuclei to increase inertial cavitation activity at lower acoustic pressures is also proposed to overcome the increased viscosity of a gel formulation. No previous work has utilised such an approach, perhaps because the microbubble formulations which could act as an alternative to the nuclei described here do not provide the required stability or duration of response. There is therefore a need for alternative nuclei which meet the requirements above. Described in this work is the formulation and testing of a suitable cavitation nuclei candidate.

The work presented in this chapter therefore addresses the selection of a suitable gel dosage formulation and the assessment of vaccine stability both in the native gel and subsequent to ultrasound exposure. Three different clinically approved formulations of the same polyacrylamide gel, with varying viscosities, were first acoustically characterised in the presence and absence of cavitation nuclei to determine their native inertial cavitation thresholds. Native inertial cavitation thresholds were defined as the peak negative acoustic pressure at which the broadband energy emissions from the focal volume exceeded 6 standard deviations from the baseline variance level. Acoustic cavitation activity at previously optimised ultrasound parameters was also compared between the formulations, as previous work has shown that high levels of inertial cavitation facilitate greater skin permeability enhancement (Mitragotri and Kost 2000) and transport into the skin.

As well as the characterisation of the acoustically optimal formulation for ultrasound assisted delivery of a vaccine into the skin, a chemical comparison must also be performed, for the formulation is of limited use if the vaccine is denatured within it. Additionally, provision of evidence that a vaccine is and remains stable in a dosage form is a vital requirement for clinical approval. Therefore, this section addresses the structural stability of two model vaccine molecules, bovine

serum albumin (BSA) and ovalbumin (OVA) in the gel formulations, with a view to investigating whether these formulations fulfil the requirements of a transdermal gel dosage form. Each protein was assessed within each gel to ensure that the formulation of the protein with the gel did not affect the protein structure. Analyses that were capable of identifying changes in multiple levels of protein structure were utilised. Protein-laden gels were then exposed to ultrasound at the previously optimised ultrasound parameters to identify any damage caused as a direct result of ultrasound exposure.

BSA and OVA were chosen on the basis that they are well characterised globular protein molecules of similar size to conventionally used vaccines. Furthermore, OVA is one of the major allergens in in hen egg white, therefore is capable of eliciting an immune response and has been widely used as a vaccine analogue for delivery studies (Wang, Tan et al. 2014). It is of note that the function and immunogenicity of BSA and OVA was not tested in this chapter, and is addressed later in *in vivo* studies presented in chapter 6.

Initially, BSA was embedded in all three gel formulations in the absence of cavitation nuclei. The structure of BSA within the gels was assessed prior to ultrasound exposure to determine the effect, if any, on formulation within the gel. Structural reassessment took place subsequent to ultrasound exposure to investigate the extent of any ultrasound induced protein damage. Consequent to this work, and on the basis of later *ex vivo* delivery experiments performed using porcine skin, a second vaccine candidate, OVA, was subjected to the same analysis, albeit at slightly different ultrasound parameters, explained below in section 4.1.2.2.

4.1. Materials and Methods

4.1.1.Gel formulations and the characterisation of their acoustic properties.

Three different polyacrylamide gels of differing viscosities were used in this work. Gel recipes are given in appendix A, and were taken directly from the German Pharmacopeia. All three formulations

were similar in composition to conventionally used ultrasound gel, and clinically approved for applications such as moisturising gels, creams and hand and face lotions (Lubrizol-Corporation 2008). The gel formulations were first characterised to assess their native acoustic properties in the absence of cavitation nuclei and thereby determine whether there was a need for cavitation nuclei to enhance inertial cavitation activity. As the gels were made in an open air environment, there was likely to be some gas entrained within them. It was of interest to investigate whether this gas was sufficient to instigate and maintain inertial cavitation at clinically acceptable ultrasound parameters. In addition, it is important to know whether the native gas content is consistent throughout the gel. Therefore, we identified the acoustic effects of the native gas content in each gel because this directly affects variability in acoustic properties. In an effort to minimise variability and ensure testing in a reproducible gel formulation, degassing of the gel was implemented. Both inter and intra batch variations were investigated to test the consistency of acoustic properties in different samples of gel, which directly affect acoustic results and influence the robustness and repeatability of future data. Finally, the variation in acoustic properties in the gels with storage time was also investigated because this greatly impacted the constraints on storage of the gel when translated to clinical use.

Following assessment of the native gel properties, their acoustic properties in the presence of cavitation nuclei were assessed. It was evident from the work presented in chapter 3 that gel properties can be favourably modified through the introduction of cavitation nuclei. Cavitation nuclei introduce gaseous pockets to the medium, facilitating cavitation at lower pressures because gas exists within the medium; it does not have to be drawn out of solution by the negative pressure of the acoustic wave. Therefore, the gel formulations were characterised with cavitation nuclei to identify a gel formulation with the lowest cavitation threshold and the most consistent acoustic behaviour.

4.1.1.1. Gel preparation

Gels were made in house according to the recipe outlined in appendix A, obtained from the German Pharmacopeia (Formulary 2002). Briefly, dried polymer (polyacrylamide) powder was re-suspended in polyethylene glycol, and cross-linked by adding a 0.5% w/v solution of Trizma base to form 0.5% polyacrylamide gels. The polymers are hereafter referred to as formulations 1, 2 and 3, and their main structural and chemical properties are given in table 4.1 below.

Table 4.1: Structural and chemical properties of gel formulations.

Formulation	Polymer chain length	Viscosity* (Pa.s)	pH (±SD)**	Gel Concentration (%)
1	40,000	3.5	7.18±0.04	0.5
2	50,000	4.1	7.35±0.05	0.5
3	55,000	5.5	7.37±0.08	0.5

*Dynamic viscosity at shear rate 50 s^{-1} at 20°C

**n=3, measured with SevenEasy Benchtop pH probe, Mettler Toledo, UK).

To determine the significance of gel degassing, 100 mL batches of gel formulation 1 were produced according to the recipe outlined in appendix A. Gel was centrifuged (Sorvall Legend X1R centrifuge, Thermo Scientific, UK) at 4000 rpm for 4 minutes and 50 mL of gel was removed for acoustic testing without degassing and placed in custom made sample holders (figure 4.2), taking care to minimise the presence of visible bubbles. The remaining 50 mL of gel was degassed by placing it under a vacuum (-1 bar) for 3 hours, before transferring the gel to the holders and performing the acoustic characterisation as described in section 4.1.1.2 below.

In order to assess the variability of gels within the same production batch, 100 mL of each gel formulation was produced and degassed for 3 hours before being split up into 30 mL samples and acoustically characterised individually, as described below. To assess inter-batch variation, this process was repeated with three different batches of each of the three gel formulations.

Furthermore, the acoustic properties of freshly prepared gel was compared to gels that were approximately 8 weeks old to test the stability of acoustic response after extended time in storage.

4.1.1.2. Ultrasound exposure parameters for gel characterisation

The methodology employed in characterising acoustic energy emissions from a focal volume within each gel formulation was identical to that described in section 3.2.4. Briefly, 20g of degassed gel (with or without CN) was placed at the focus of the 0.256 kHz ultrasound source and insonated for a single 10ms pulse in the holder shown in figure 4.2. PCD traces were recorded and analysed as previously described to give an indication of cavitation activity in the samples at varying pressures. Each gel formulation was also characterised in the presence of each type of cavitation nuclei. Additionally, the total level of broadband acoustic emissions over an entire 90s exposure time in each different gel formulation were investigated. Total exposure time was changed from Chapter 3 from 10s to 90s on the basis of later *ex vivo* work (presented in chapter 5).

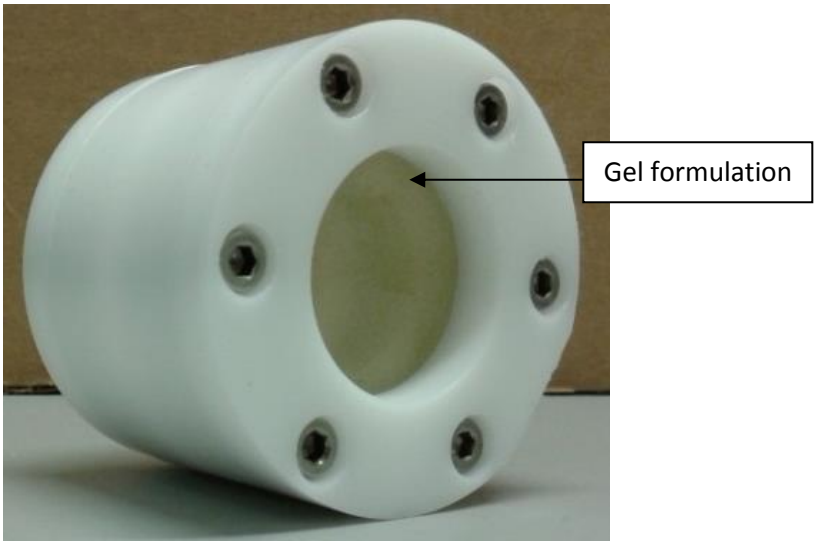

Figure 4.2: Phantom holder used for the acoustic characterisation of the three candidate gel formulations

4.1.1.3. Cavitation nuclei

Two types of cavitation nuclei were utilised in this study. Talc was used as micron-sized cavitation nuclei, as described in section 3.2.1. Talc was added to each of the three gel formulations at a concentration of 0.5% w/v. The second was a novel type of nanosized cavitation nuclei developed within BUBBL at the University of Oxford. Nanocups (NCs) are nano-sized cavitation nuclei composed of a copolymer of hydroxyethylmethyl methacrylate (HEMA) and methyl methacrylate (MMA) formed around and linked to a poly(styrene-co-divinylbenzene) (PS:DVB) copolymer core (10:1:6 v/v/v ratio of MMA:HEMA:DVB formed around a 300nm diameter PS bead). The hypothesized reaction mechanism is shown in figure 4.3a. Following the reaction to form the nanocups, the reaction solution was centrifuged 3 times for 45 min at 25,000 x g to remove unreacted polymer. Dynamic light scattering was used to verify nanocup final diameter as around 460nm (figure 4.3c). After formation and centrifugation, the nanocups were air-dried and re-dispersed in Millipure water with vigorous stirring. It is hypothesized that the cup shape entraps air during the drying process, and traps a single nano-bubble on the surface. The nano-bubbles then inertially cavitate when placed in an ultrasound field. It is hypothesized that partial encapsulation of the nanobubble by the nanocup enables adequate stabilization against dissolution, whilst facilitating unconstrained growth of the bubble during the peak rarefactional half-cycle. NCs were added to each of the three degassed gel candidates at a concentration of $5x10^9$ particles/g of gel.

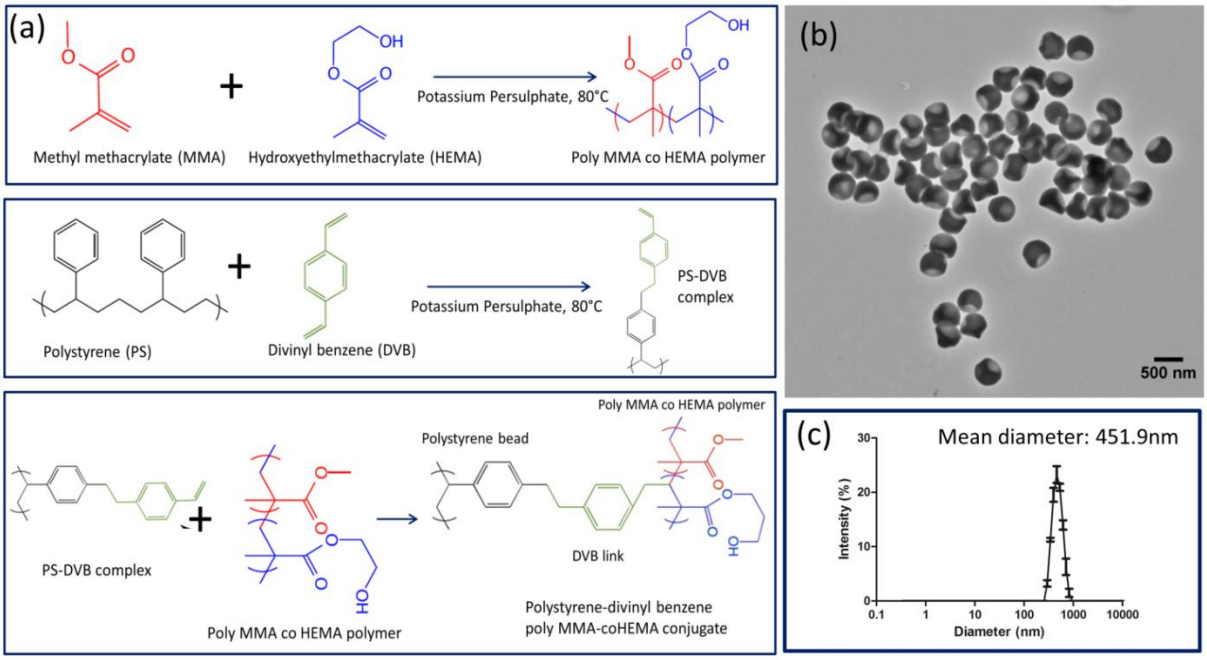

Figure 4.3: Nanocup characterisation. (a) Chemical reaction used to produce nanocups (b) TEM image of nano-sized cavitation nuclei. Reproduced with permission from Kwan et al., (2015, in review) and (c) size distribution data as measured by dynamic light scattering.

4.1.2. Vaccine Stability – Bovine Serum Albumin and Ovalbumin

4.1.2.1. Modifications to Therapeutic Ultrasound Setup – BSA

The setup described in chapter 3.2.4 was utilised to expose BSA (at concentration 10 mg/mL in the gel formulation) to ultrasound within all three gel formulations without cavitation nuclei. Briefly, 12 mL of gel was placed in the holder shown in figure 4.2, mounted in a water tank at the focus of the ultrasound beam and subjected to a 10% duty cycle (10 ms on, 90 ms off) for 100 cycles (total exposure time: 10 sec) at 1 MPa (peak negative) pressure and 0.256 MHz frequency. There were three experimental groups within each gel formulation; (1) pre ultrasound exposure, which looked at the integrity of the protein in the gel immediately after formulation, (2) post ultrasound exposure, to identify any changes caused as a result of insonation, and (3) heat denatured protein to provide an

example of denatured protein characteristics. Protein was heat denatured by placing the protein laden gel formulation in a water bath at 95°C for 10 minutes.

4.1.2.2. Modifications to Therapeutic Ultrasound Setup – Ovalbumin (OVA)

On the basis of later ex vivo studies in porcine skin, the ultrasound exposure time was increased from 10 s to 90 s (chapter 5.2). Only formulation 3 was tested. Additionally, cavitation nuclei candidates were added to the gels in order to test the stability of ovalbumin to the mechanical forces present during cavitation nuclei-enhanced inertial cavitation activity. All other parameters and analyses were identical to the BSA stability investigation.

4.1.2.3. Protein Analyses

The following techniques were used to identify any structural changes in protein structure due to formulation, ultrasound exposure or heat treatment.

Intrinsic fluorescence spectroscopy

Intrinsic fluorescence spectroscopy (Luminescence Spectrometer LS 50B, Perkin Elmer, USA) was used to compare the tertiary structure of the protein before and after US exposure. Native BSA and OVA both contain the fluorescent residue tryptophan, and therefore changes in fluorescence emission of this residue were used to identify changes in tertiary protein structure. Prior to testing, samples of gel were diluted to a concentration of 5mg/mL and filtered with a 280nm syringe filter. Emission spectra were obtained for the diluted samples between 300-400nm at an excitation wavelength of 295nm. Fluorescence intensity at 340nm was converted to protein concentration using pre-prepared calibration curves and used to compare BSA and OVA concentrations in pre and post exposure gel.

Sodium dodecyl sulphate polyacrylamide gel electrophoresis (SDS PAGE)

Sodium dodecyl sulphate polyacrylamide gel electrophoresis (SDS PAGE) was used to identify protein aggregates formed due to US exposure. Protein-laden gel samples from before and after ultrasound exposure and denaturation were mixed with loading buffer (no dilution) and heated for 5 minutes at 95°C. They were then subjected to SDS-PAGE on a 4-20% gradient polyacrylamide gel in 25 mMTris-glycine, pH 8.0 using standard procedures (constant voltage at 160 V; OVA: 0.5 µg protein/lane, BSA: 0.416 µg protein/lane). Gels were stained with Comassie Brilliant Blue stain (Brilliant Blue R-250, Cat no B 7920, Sigma Aldrich, UK).

Particle sizing

The formation of solid aggregates is a sign of protein denaturation, therefore particle sizing by dynamic light scattering was used to size the particles and identify any aggregates formed as a result of formulation or ultrasound exposure. Samples were diluted down to a testing concentration of 5mg/mL and filtered with a 280 nm pore size syringe filter (to remove cavitation nuclei and denatured, aggregated protein) prior to measurement pre and post ultrasound exposure. (Zetasizer Nano ZS, laser wavelength 633 nm; Malvern Instruments, UK).

4.2. Results and Discussion

4.2.1. Gel Characterisation

Inertial cavitation is the predominant mechanism of ultrasound enhanced transdermal permeability and transport(Bhatnagar, Schiffter et al. 2014). Because it is a threshold phenomenon that varies with medium and frequency, it is vital to accurately determine the acoustic pressure above which it will occur. For this reason, a full characterisation of each of the three gels was performed. All of the characterisations assessed changes in levels of high energy acoustic emissions originating from the focal volume of the ultrasound beam at a variety of acoustic pressures. High energy acoustic emissions originate from bubble activity, and therefore are a direct indicator of cavitation at the focus.

4.2.1.1. Degassed gel vs. Native gel

Variations in the native gas content were examined to determine whether native gas content was (1) consistent within the entire batch of gel, and (2) sufficient to allow the onset of a significant amount of inertial cavitation at clinically acceptable pressures regardless of the presence of cavitation nuclei. In the case of significantly variable native gas content, degassing the gels facilitates removal of a high proportion of the entrapped gas. Removal of a significant amount of native gas equalises the gas content, allowing gels with reproducible properties to be tested. Figure 4.4(a) shows the results of this investigation in gel formulation 1. The cavitation threshold of non-degassed gel was less distinct than the degassed gel samples, lying between 0.6 and 1.2 MPa. Degassed gel had a more distinct cavitation threshold of approximately 1.2 MPa, and this was also more consistent between gel samples within the same batch. The higher cavitation threshold in the degassed gel was due to the decrease in gas entrained in the gel that was available for cavitation nucleation. Therefore, degassing a gel formulation resulted in a slightly higher cavitation threshold, but, importantly, more consistent acoustic properties. As a result, all gels used in the work presented in this thesis were degassed under vacuum as previously described for a minimum for 4 hours.

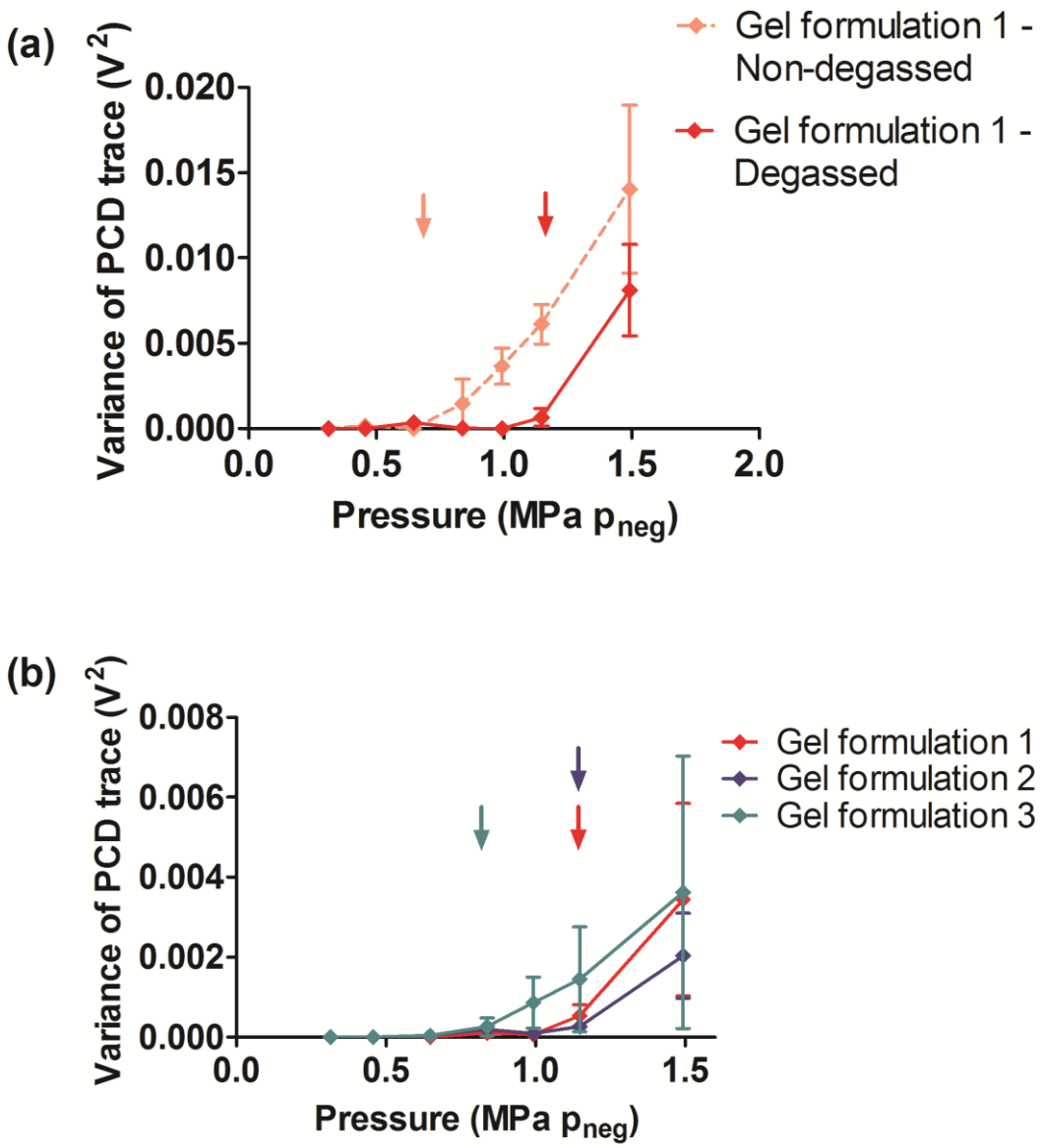

Figure 4.4: Variability in acoustic energy emissions at a range of pressures (a) for non-degassed formulation 1 vs degassed formulation 1 and (b) within the same batch of each of the three different gel formulations. Polymer chain length is the key distinguishing feature between the three formulations. Coloured arrows represent the cavitation thresholds for each group. (n=3). Error bars show 1 standard deviation on both (a) and (b).

4.2.1.2. Variability within gel batches

Acoustic energy emissions within different batches of each gel formulation are shown in figure 4.4(b). Each of the gel formulations exhibit distinct cavitation thresholds, with the lowest at 0.8 MPa in formulation 3, and formulations 1 and 2 at 1 and 1.2 MPa respectively. Error bars indicate the variability in acoustic energy emissions, which increase with acoustic pressure. Variability is due to the stochastic nature of cavitation; in the presence of ultrasound it is difficult to predict how many bubbles in a given volume will cavitate and how much energy is released. Formulation 3 displays the greatest variability in acoustic emissions, and this is thought to be due to its increased viscosity. The degassing process is impeded by high viscosity gel as stirring of the medium is hindered and reduces the diffusion of gas out of the gel. Therefore, the degassing process is less effective at removing the entrapped air.

Variability in cavitation activity above the cavitation threshold is further highlighted by comparing the y axes on figures 4.4 (a) and (b), where a comparison of the acoustic energy emissions in degassed formulation 1 at a pressure of 1.5 MPa shows a 2.5-fold difference, despite displaying the same cavitation threshold. At low pressures where cavitation is not yet present, all three of the gel formulations display consistent properties.

4.2.1.3. Inter-batch variability

A gel formulation with consistent properties between batches is vital for valid comparison of results. For this reason, inter-batch variability was investigated for each of the three gel formulations. Figure 4.5 shows the average acoustic emissions from each gel formulation between three separately prepared batches. All of the formulations showed consistent properties below the cavitation threshold, due to the absence of cavitation. All three gels displayed a constant cavitation threshold with very little difference between batches. The cavitation thresholds of the gels were 0.8MPa, for formulation 3, and 1.2 MPa for both formulations 1 and 2. At 1.5 MPa, formulations 1 and 2

displayed a high variability in the acoustic energy emissions due to sufficient acoustic energy for inertial cavitation combined with the stochastic nature of the phenomenon. Despite less consistent properties (mainly above the cavitation threshold) formulation 3 displayed the highest energy acoustic emissions.

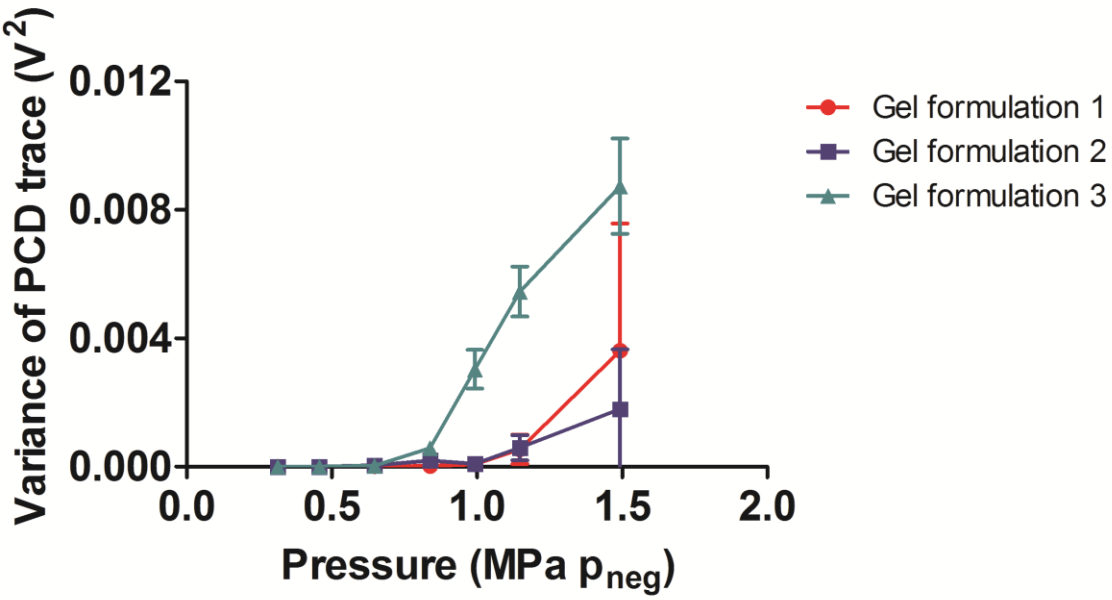

Figure 4.5: Influence of gel properties on acoustic cavitation signal. Gels were placed at the focus of a 256 kHz ultrasound transducer and insonated for 10ms. Passive cavitation detection was used to quantify and compare levels of cavitation (indicated by the variance of the PCD trace) at variable pressures in each of the gels in the first 200 µs of the 10 ms pulse. Three samples from of three batches of each gel were averaged for this analysis. (n=3), error bars show standard deviation.

4.2.1.4. Changes in acoustic properties over time

The final investigation in this section considered the stability of each gel's acoustic properties over time (figure 4.6). Gels were stored at room temperature in a sealed air-tight centrifuge tube post centrifugation and degassing for up to 73 days. Results show that despite efforts to keep the gel out of contact with air, the gels themselves did re-gas, as indicated by highly variable acoustic properties. This indicated that either a better method of storage would have to be devised to keep

the air out of the gel, or freshly-made gel is required for experimentation. The latter was implemented for all of the work presented in this thesis. In a clinical context, this means that the acoustic properties of the gel itself have a low “shelf life” so manufacture of a storage vessel or dosage form would have to be carefully designed to limit regassing. It is also of note to mention that an acoustic characterisation of gel formulation 3 at 73 days was attempted, but abandoned after large numbers of visible bubbles were consistently found in the holder, despite degassing and centrifugation efforts.

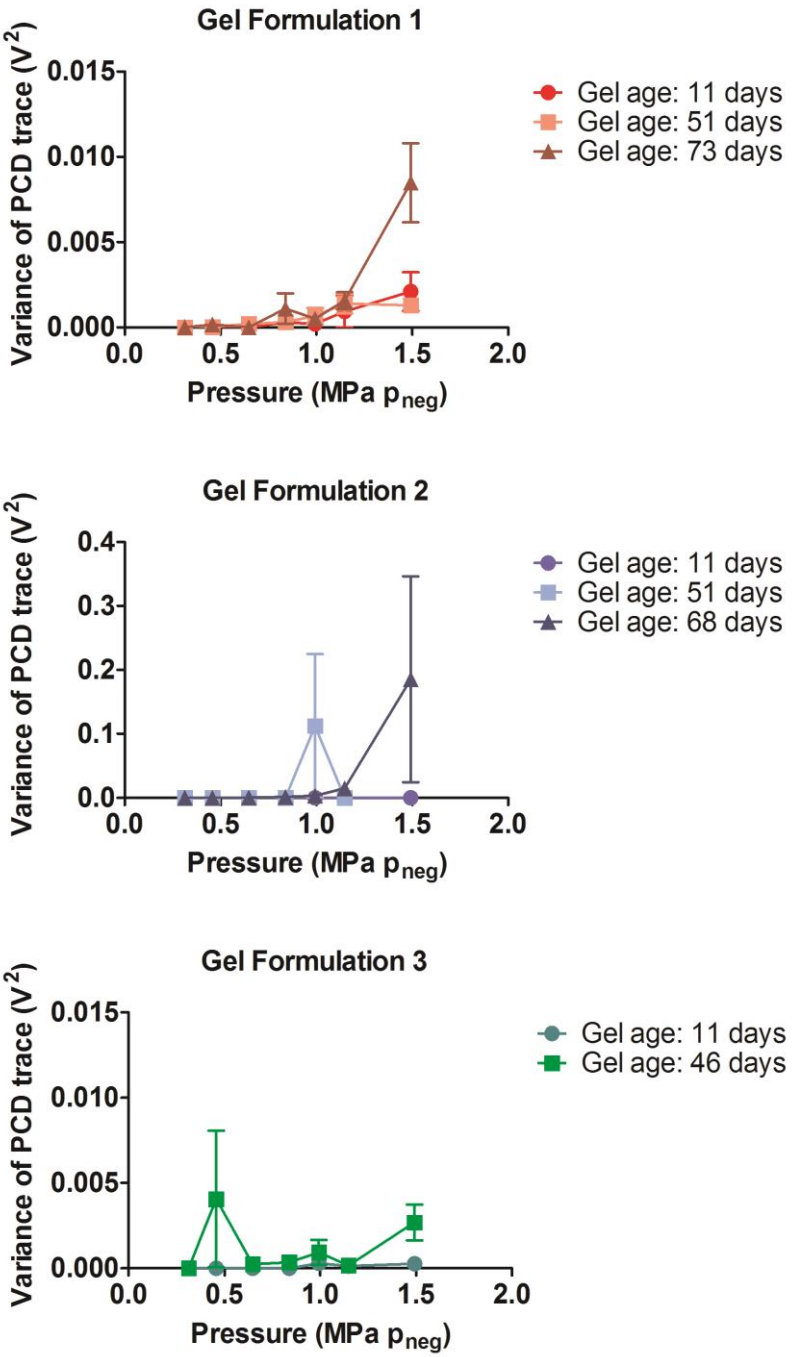

Figure 4.6: Acoustic properties of the three gel formulations after variable storage times. Gels were placed in sealed centrifuge tubes and stored at room temperature for up to 73 days before being exposed to a 10 ms ultrasound pulse as described in detail in methods. Cavitation was detected using a passive cavitation detector as described in section 4.1.1.2. (n=3), standard deviations shown.

4.2.1.5. Effect of cavitation nuclei

The selection of a suitable gel for this application is of paramount importance. Acoustic properties conducive to the production of inertial cavitation were required because inertial cavitation activity was shown in Chapter 3 to be the predominant mechanism in enabling ultrasound assisted transport of vaccine particles. Cavitation nuclei assist in both the instigation of inertial cavitation at lower acoustic pressures, and increase the duration of inertial cavitation in a gel. Figure 4.7(a) shows inertial cavitation activity in each gel formulation at a range of pressures from 0-1.4 MPa peak negative. The addition of nano-sized cavitation nuclei reduced the cavitation threshold (0.45 MPa) to less than half of the pressure required to induce inertial cavitation in the gel when it contained micron-sized nuclei (talc) (1 MPa), which had a significantly lower cavitation threshold than the gel with no cavitation inducing nuclei at all (1.5 MPa). Decreases in cavitation thresholds in the presence of cavitation nuclei are due to the presence of ready nucleation sites for cavitation. Above the cavitation threshold, all of the gel formulations that contained nanocups showed more than double the level of cavitation than those with talc or nothing at all. This is thought to be due to the "potential cavitation density" in a given area of the gel. Many more nano-sized nuclei, each with their own nucleation site, are able to pack into the focal volume of the US than micron-sized nuclei, cavitate and therefore produce higher energy emissions. There was little difference between the different gel formulations when they had been seeded with the same type of cavitation nuclei, indicating that differences in viscosity did not affect the acoustic properties significantly ($p>0.05$) and the predominant source of cavitation was the nuclei themselves.

Figure 4.7(b) shows the total level of acoustic emissions produced during the 90 s therapeutic exposure period from each different formulation. It is of particular note that these results are displayed on a logarithmic axis, and that the response recorded from gel that contained NCs was at least 3 orders of magnitude above the response from gel alone. Talc was also shown to be conducive to production of high levels of cavitation, but the nanocup response was once again one to two orders of magnitude higher than the talc response (formulations 2 and 3 with talc vs formulations 2

and 3 with NCs respectively, $p<0.001$). Furthermore, this figure illustrates that formulation 3 was able to instigate a significant amount of cavitation with relatively little variability in total acoustic energy emissions between different exposures. Consistency in acoustic energy emissions is desirable because the extent of acoustic activity at these settings is then more predictable.

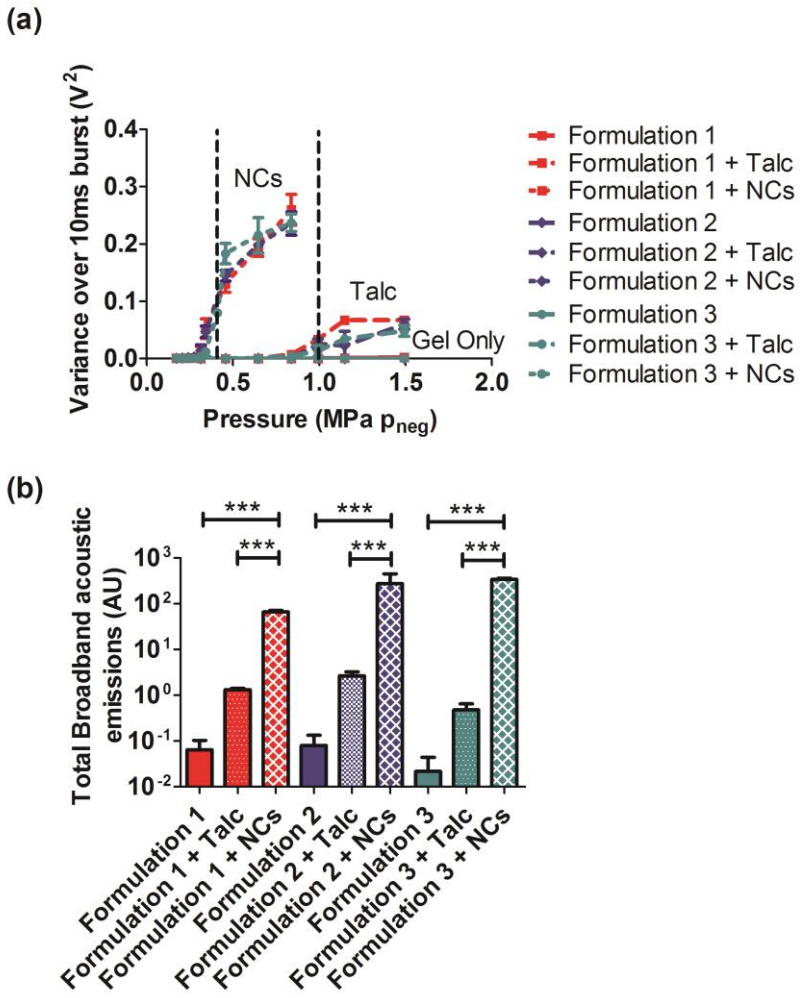

Figure 4.7: (a) Cavitation activity in the different gel formulations during a single 10 ms burst of ultrasound. Degassed gel was doped with previously stated concentrations of talc or nanocups and the gel then exposed to ultrasound, measurement of cavitation response was performed as described in methods and materials. Dotted vertical lines illustrate the cavitation thresholds of gels with talc (1.0 MPa) and gels with nanocups (0.45 MPa). (b) Total broadband emissions over the complete 90 s exposure in the different gel formulations (PRFP: 1 MPa, PRF 10 Hz, 10% DC)

The nanocups were able to generate inertial cavitation better than talc because of the increased number of nucleation sites available in a given insonated volume, compared to micron sized particles like talc. Additionally, it is hypothesised that air in the nanocup has the capability to be nucleated repeatedly, or little by little, over many ultrasound cycles, allowing more cavitation events to be sustained over a longer period of time. Although the gas volume of the air in the nanocups cannot be quantified using current technologies, it can be modelled as around $3mm^3$/ml of solution (assuming the maximum amount of air is trapped in each cup and that the crevice is half the diameter and depth of the hemispherical cup). Without knowledge of the talc morphology (which varies with each talc particle) it is not possible to calculate the gas volume in a volume of talc suspension for comparison.

In addition to using nanocups and talc as cavitation nuclei, microbubbles were also briefly explored for this application. DSPC PEG-40 stearate microbubbles (2-10 μm) filled with sulphur hexafluoride gas were produced by sonication at 22.5 kHz and injected into gel formulation 3 as a bolus in solution at a concentration of $5.5x10^6$ bubbles/mL. The bubble concentration was simply the concentration of the bubbles as they were produced because information regarding a maximum acoustic response was sought. The suitability of bubbles for this application was questioned at this stage, because it was difficult to (1) distribute the bubbles evenly in the gel, and (2) stop the bubbles dissolving in the gel over time, not least because of their buoyancy. Nonetheless, bubbles were injected into the gel within the phantom holder at the ultrasound focus and insonated at the previously specified ultrasound exposure conditions for 90 s. Figure 4.8 compares the magnitude and duration of the frequency components of the acoustic emissions received at the PCD over a 90 s (900 pulse) exposure with gel alone, DSPC PEG-40 microbubbles, talc and NCs.

Figure 4.8 further reinforces the superiority of NCs to produce a sustained inertial cavitation response. In the spectrograms shown, broadband emissions are represented by vertical lines

spanning multiple frequencies. The response seen with microbubbles was very similar to gel alone but with a much stronger harmonic component (bright horizontal lines), indicative of bubble expansion and shrinkage with the acoustic wave, also termed stable cavitation. Both the gel alone and microbubble emissions showed that cavitation nuclei present were depleted within the first 10-20 pulses at the ultrasound parameters used. Microbubbles therefore, would only be suitable cavitation nuclei for applications with very short (on the order of seconds) exposure times. Talc was able to sustain inertial cavitation for a longer duration of up to 80seconds, but bursts were sporadic and gradually decreased in broadband power. These results additionally demonstrate the propensity of NCs to instigate only inertial cavitation, as there is only a broadband response, such emissions are believed to be more useful in trying to achieve delivery reliant on inertial cavitation. over an exposure time on the order of 90s.

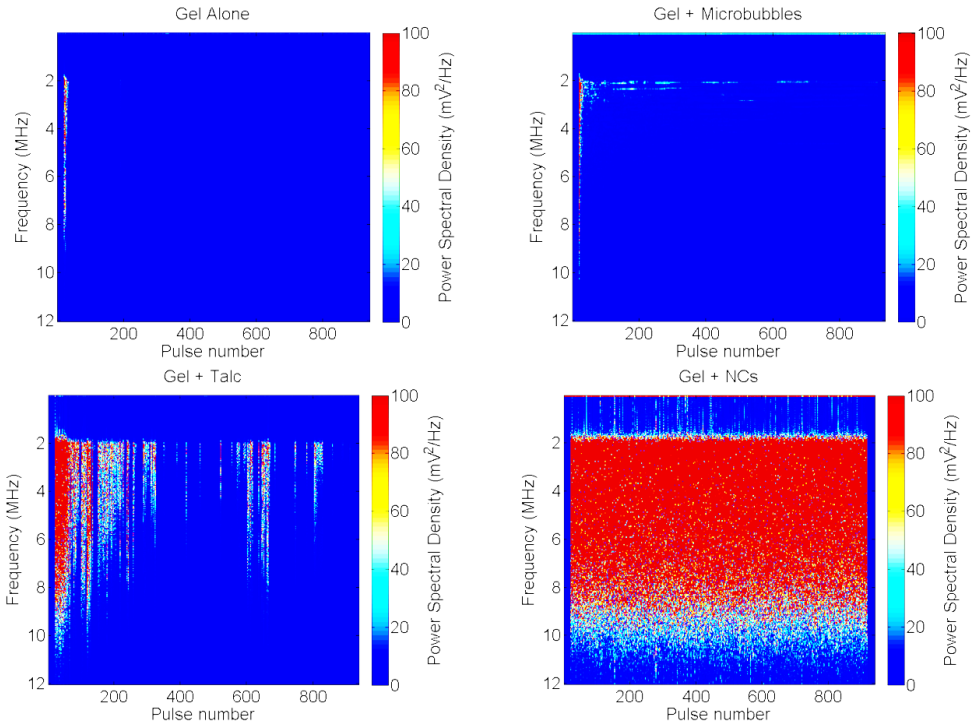

Figure 4.8: Spectrograms showing the power spectral density of acoustic emissions received for each of 900 consecutive 0.256 MHz ultrasound pulses (2560 cycles at 10 Hz), for different cavitation nuclei within the gel. Acoustic emissions were high-pass filtered at 2 MHz. The total exposure duration was 90 s.

4.2.2.Vaccine Stability

The protein analytics described in this chapter aimed to identify changes in protein structure as a result of gel formulation and ultrasound exposure/cavitation. Results for each experimental group were compared both with established results in literature and each other across the three analyses described.

4.2.2.1. Intrinsic fluorescence spectroscopy assessment

As described previously, intrinsic fluorescence spectroscopy gives the capability to identify changes in the tertiary structure of a protein. The fluorescence of a folded protein, such as BSA and OVA, is a mixture of the fluorescence from individual aromatic amino acids. Most of the intrinsic fluorescence emissions of a folded protein are due to the excitation of tryptophan amino acids, with some emissions due to tyrosine and phenylalanine. Typically, tryptophan has a wavelength of maximum absorption of 280 nm and an emission peak ranging from 300 to 350 nm depending in the polarity of the local environment. However, with fluorescence excitation at 295 nm, the tryptophan emission spectrum is dominant over the weaker tyrosine and phenylalanine fluorescence (Vivian and Callis 2001). Tryptophan fluorescence is strongly influenced by the proximity of other residues so changes in its fluorescence (or the fluorescence of the molecule overall) can be used to detect changes in the arrangement of amino acids around the tryptophan residues. These changes are caused by alterations in the protein's tertiary structure. Additionally, because fluorescence intensity is directly proportional to the number of tryptophan amino acids, intrinsic fluorescence spectroscopy has the capability to assess changes in protein concentration.

The intrinsic fluorescence spectra of BSA (excitation wavelength 295nm) for each gel formulation and each condition are shown in figure 4.9(a)-(c). Due to the fact that the three gel formulations are made of the same material, there is no significant ($p<0.05$) difference in the spectra in different formulations prior to ultrasound exposure. This indicates that the individual formulations do not chemically alter the tertiary structure or fluorescence of BSA. There is substantial overlap between

pre ultrasound exposure (ie. BSA in gel formulation) spectra and post ultrasound spectra within each formulation, indicating that these samples were near identical and that there had been no structural changes as a direct result of ultrasound exposure. Additionally, the significant overlap indicated a constant protein concentration in the pre and post ultrasound samples.

Spectra for the heated samples displayed key characteristics of a denatured protein. Firstly, a large peak at the excitation wavelength (around 1000 AU at 295 nm) indicates the presence of large (>100 nm) aggregate particles in the test solution, as these scatter the excitation light without changes in the wavelength. Secondly, filtering of the sample before analysis to remove aggregates led to the reduction of protein in the sample. Consequently, the intensity of the signal in the range 300-350 nm decreased significantly (3-fold decrease, $p<0.05$).

Figure 4.9(d) displays a summary of these results. Due to the noise in the signal, curves were fit to the each set of data values and the peak emission intensity in the range of 300-350 nm used to identify the average protein concentration for that type of sample. Significant differences ($p<0.05$) in BSA concentration exist between the denatured group and the other groups in all gel formulations tested.

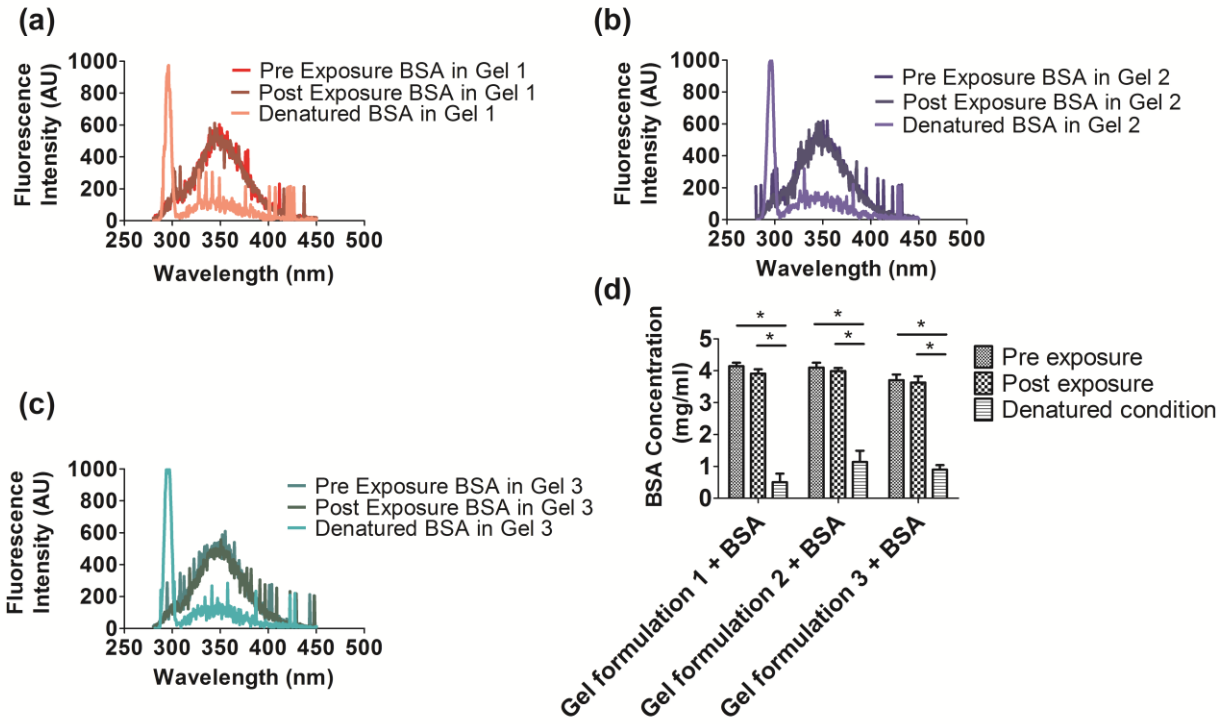

Figure 4.9: (a)-(c) Emission spectra of BSA at excitation wavelength 295 nm for each treatment within the three different gel formulations. Intrinsic fluorescence spectroscopy spectra are shown as the average of three identical runs. (d) average concentrations of BSA present in the different experimental groups. * denotes significant difference with $p<0.05$, ** denotes $p<0.01$, n=3.

Fluorescence spectra for OVA are shown in Figure 4.10. This investigation aimed to determine whether the presence of cavitation nuclei, and the enhanced levels of inertial cavitation that results, caused disruption to protein structure. Damage may be a result of both mechanical and thermal changes, and enhanced because of the increased presence of cavitation. OVA stability was examined in gel formulation 3. Modified ultrasound parameters (exposure time increased to 90 sec from 10 sec) were used, because they had been shown to cause permeability enhancement in porcine skin in later *ex vivo* studies. Aside from this, data collection and analysis methods were identical to that used in the BSA investigation.

In the absence of cavitation nuclei (figure 4.10(a)), OVA spectra in pre and post exposure gel showed no significant difference ($p<0.05$). The previous investigation with BSA had demonstrated protein stability in formulation 3, and OVA gave the same result. Following exposure to heat, OVA, like BSA, denatured, displaying a drop in protein concentration due to the removal of aggregates. The removal of nano-sized aggregates from the heat denatured sample via filtering was more effective in this case compared to the BSA experiments, as demonstrated by the markedly smaller peak at the excitation wavelength (295 nm) caused by scattering (50-150 AU compared to 1000 AU in the BSA experiments).

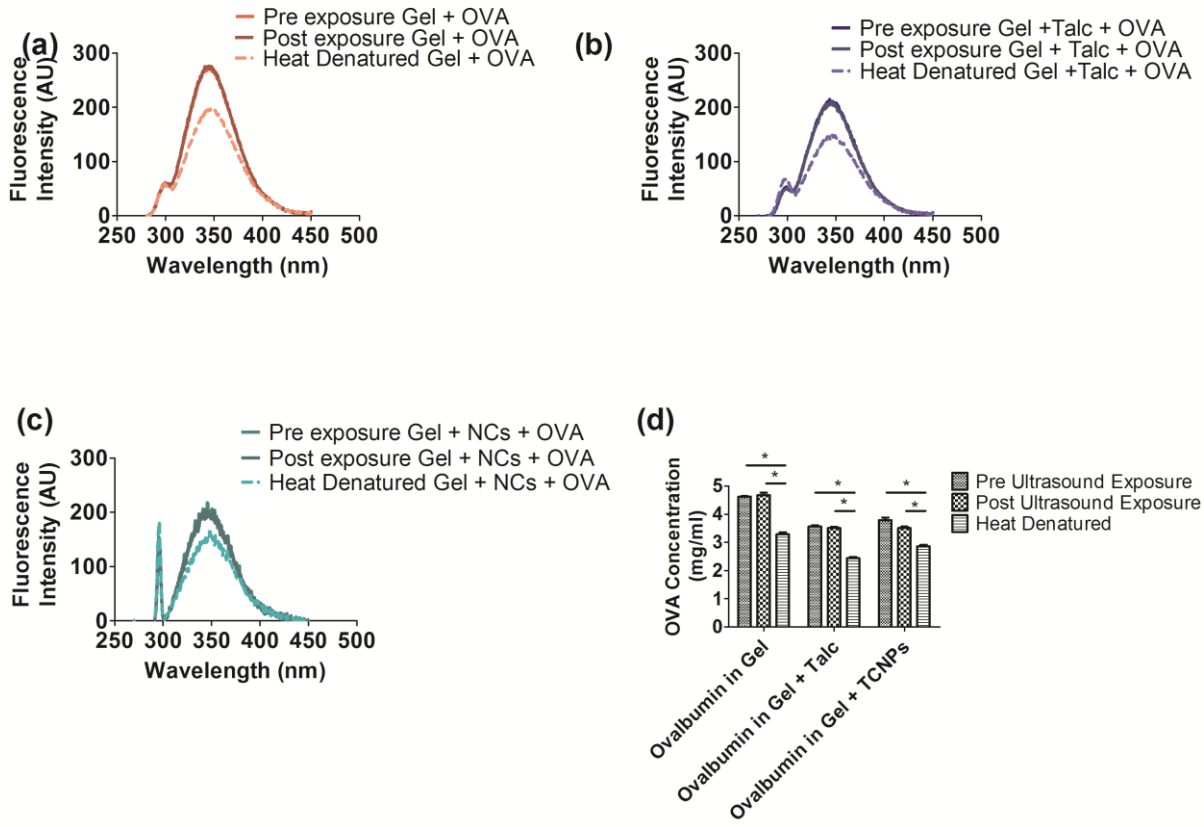

Figure 4.10: (a)-(c) Emission spectra of OVA at excitation wavelength 295 nm for each treatment within the three different formulations. Intrinsic fluorescence spectroscopy spectra are the average of three identical runs. (d) average peak emission intensity between 300 and 350nm. * denotes significant difference with $p<0.05$, ** denotes $p<0.01$, n=3.

The addition of talc as a source of cavitation nuclei showed, once again, very little difference in pre and post US exposure spectra (figure 4.10(b)). Of interest however, is that the overall protein concentration (which is directly proportional to the fluorescence intensity) decreased compared to the OVA in gel without any cavitation nuclei (figure 4.10(a)). Decrease in protein concentration is thought to be due to the protein molecules associating with the talc particles when the two are mixed in the gel. As this analytical technique is suited to dissolved samples, all of the gels were filtered prior to examination to remove the talc particles in the gel. During this process however, any protein associated with the talc was probably also removed resulting in a drop in concentration. The protein that did remain in the gel showed no structural damage as a result of ultrasound exposure. It is important to note that a drop in concentration of protein in the presence of cavitation nuclei is not of great concern. In clinical use, there will be no filtering of the gel, therefore any associated protein will remain at the treatment site and be carried into the skin to trigger an effect. Compared to ultrasound / cavitation treated samples heat denatured OVA displayed an increased peak at 295 nm, and a significantly decreased OVA concentration, both consistent with the characteristics of a structurally damaged protein.

Once again, there was no evidence of any changes in the emission spectra of OVA as a direct result of ultrasound exposure in the presence of NCs (figure 4.10(c)). Formulation with NCs also showed a decrease in concentration, and this was most likely due to the association of OVA with the NCs (NC zeta potential: -40 mV) (Kwan, Coviello et al. 2015)**.** In the heat denatured samples there was a much higher scattering peak at 295 nm (180 AU), indicating that the filtration process (filter pore size 280 nm) had not been as effective at removing solid aggregates as with the talc. Alternatively, smaller protein aggregates had formed in these samples and were able to pass through the filter undetected. Size of aggregates was also assessed and will be described later in the next section.

Figure 4.10(d) once again gives a quantitative summary of these results. Decreasing peak emission intensity indicates the association of the protein molecules to the cavitation nuclei. Significant

differences can also be observed between denatured protein samples and the other two groups, and there is no evidence in this data that the tertiary structure of BSA or OVA is affected by ultrasound exposure or cavitation induction.

4.2.2.2. Dynamic light scattering

Dynamic light scattering is essentially used to measure the hydrodynamic radius of a range of molecules and particles on the nano-scale. Time dependant fluctuations in laser light are measured by a fast photon counter, and are directly related to the rate of diffusion of the molecule through the solvent. The rate of diffusion is also directly related to the hydrodynamic radius of the particle.

In the context of this study, dynamic light scattering was used to identify the presence of sub-micron protein aggregates formed in the gel due to either ultrasound exposure or heat denaturation. Table 4.2 shows the sizes of (a) BSA and (b) OVA before and after ultrasound, and after denaturation.

Table 4.2: Hydrodynamic diameters of BSA and OVA at each experimental condition tested. n=3 for each group. ** denotes significant difference to the pre exposure samples for that experimental group ($p<0.01$). Measurements acquired using a ZetaSizer Nano, data shown as intensity analysis of 18 sub-runs with a polydispersity index of 0.153.

	Hydrodynamic radius [mean ± SD] (nm)					
	Gel 1 + BSA	Gel 2+ BSA	Gel 3 + BSA	Gel 3 + OVA	Gel 3 + Talc + OVA	Gel 3 + NCs + OVA
Pre exposure	7.02 ± 0.20	6.62 ± 0.80	7.47 ± 0.28	6.30 ± 0.09	9.17 ± 1.27	7.08 ± 1.40
Post exposure	6.97 ± 0.66	6.57 ± 0.06	7.58 ± 0.24	5.88 ± 0.20	8.16 ± 1.69	7.57 ± 1.53
Heat denatured	75.39±2.41**	101.10±2.35**	81.59±0.66**	62.65±5.24**	154.26±6.46**	78.36±9.86**

The reported hydrodynamic diameter of native BSA is quoted in the literature as 7 nm (Axelsson 1978) and native OVA as 7.96 nm (García de la Torre, Huertas et al. 2000). Values for pre and post

exposure correlate closely with these values indicating that neither the formulation of the protein with the gel nor ultrasound exposure/cavitation causes significant amounts of aggregation. In contrast, the protein in heat denatured samples were all significantly larger (approx. 10-fold, $p<0.01$) than the pre ultrasound exposure samples, indicating significant aggregation. It is of note that filter pore size was chosen to isolate the protein from both nano and micron sized cavitation nuclei as well as gel matrix material, so that clear conclusions about the protein alone could be made. Because the samples were filtered with a 280nm pore size filter, it was possible to detect sub-micron aggregates. Pre and post ultrasound exposure samples passed freely through the filter. Both proteins showed aggregates of similar size, which was expected as they are comparable in stability. This result further reinforces the conclusion that these proteins are stable to ultrasound.

4.2.2.3. Sodium dodecyl sulphate polyacrylamide gel electrophoresis (SDS PAGE)

SDS PAGE is a robust analytical technique that is widely used to separate biological molecules according to their electrophoretic mobility. An electrical gradient is placed across a porous polyacrylamide gel, and component molecules move through the gel at different rates according to the length, conformation and charge of the molecular components. Band intensity is directly proportional to protein component concentration. As concentrations had been quantified using fluorescence spectroscopy and comparisons were required as opposed to absolute values, a calibration curve was not undertaken for this study. Many proteins (including BSA and OVA) have distinct and widely established band patterns. Changes in the length, conformation and charge of the molecules can therefore be identified through comparison of banding patterns in the gel.

SDS PAGE analysis of BSA structure in the different gel formulations is shown in figure 4.11. BSA was examined within each gel formulation pre and post ultrasound exposure, as well as following heat denaturation. In all three gel formulations, banding patterns were identical in pre ultrasound and post ultrasound exposure samples (figure 4.11, lanes 3 & 4, 7 & 8, and 11 & 12). The banding patterns in these lanes show an intense band at around 66.5kDa, which is the molecular weight of

native BSA (Weber and Osborn 1969). Fainter protein bands can be seen between 100 kDa and 250 kDa and at around 60 kDa, which are stabilisers and preservatives used and retained during the BSA purification and production process. Because the intensity of these bands is not significant in relation to the much more intense band around 66.5 kDa, this is not of huge concern. A comparison of pre and post ultrasound exposure band position and intensity shows no significant difference ($p<0.05$), indicating that BSA did not undergo denaturation as a direct result of ultrasound exposure.

There were substantial differences, however, in the banding patterns in the heat denatured samples (lanes 5, 9 and 13), which can be defined by two key characteristics. Firstly, the significantly reduced intensity of the protein band at 66 kDa, and secondly the appearance of intense protein staining at the bottom of the wells where the samples were placed at the beginning of the experiment (figure 4.11, red arrowheads). Both of these effects can be explained by the denaturation of the protein and formation of aggregates. Upon aggregation, the protein molecules became too large (>250 kDa) to pass into the gel and stayed in the well where they were stained. Also due to aggregation, the concentration of viable, un-aggregated protein reduced significantly, leading to a reduction in intensity of the band at 66 kDa.

It is worth nothing that this was the only investigation that was performed with no gel filtration. Therefore, small amounts of cavitation nuclei were present in all samples, but because only proteins are stained by the Coomassie Blue stain these cannot be detected. These results demonstrated that BSA is stable to ultrasound, but not heating, within all three candidate gel formulations.

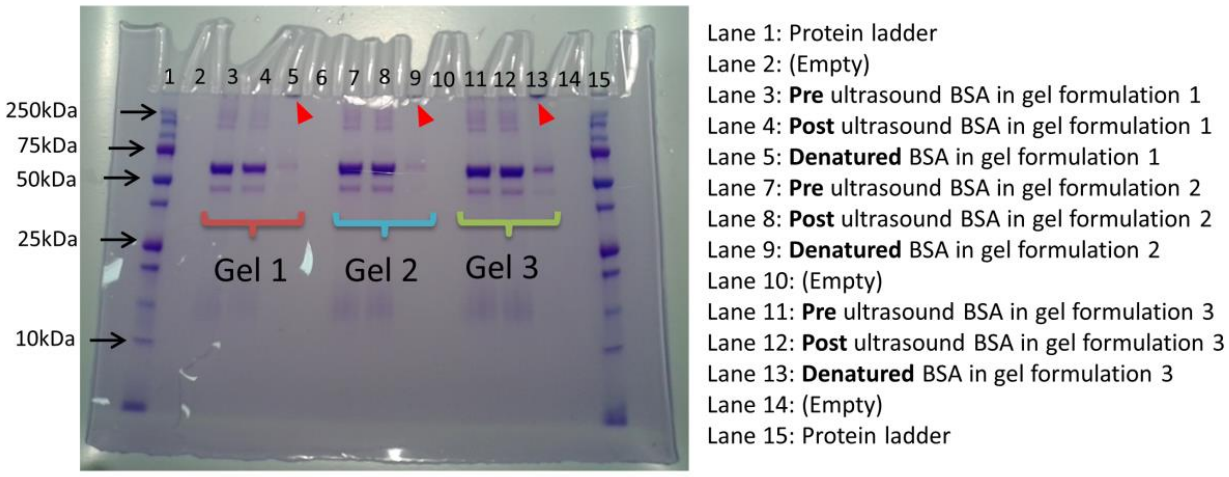

Figure 4.11: SDS PAGE analysis of BSA structure in the different gel formulations.

The effect of the presence of cavitation nuclei-enhanced cavitation activity on OVA stability is shown is figure 4.12. OVA has a much cleaner isolation process than BSA, therefore there were no visible bands other than at 45 kDa (its native molecular weight)(Weber and Osborn 1969) in all of the pre exposure samples. There were no significant differences in OVA banding between pre ultrasound exposure and post ultrasound exposure samples (lanes 3 & 4, 7 & 8, and 11 & 12), indicating that ultrasound exposure in either the presence of absence of cavitation nuclei does not damage or denature the OVA molecules, nor alter their concentration. In the heat denatured samples (lanes 5, 9 and 13) the two markers previously described indicated the presence of aggregates. OVA aggregates formed were smaller than those formed in heated BSA, and were able to pass into the gel. As a result of aggregation, concentration of native protein at 45 kDa was also markedly reduced in the heated samples.

Through the separation of BSA and OVA into their component proteins in denatured and native form, SDS PAGE analysis was able to demonstrate that the structure of BSA within all three gel formulations was not altered as a direct result of ultrasound exposure. Furthermore, the addition of cavitation nuclei before ultrasound exposure still did not alter the structure of OVA from the native state. This indicates that the formulation of a vaccine in a gel seeded with NCs may provide superior acoustic properties with no detriment to the structure of the vaccine molecule.

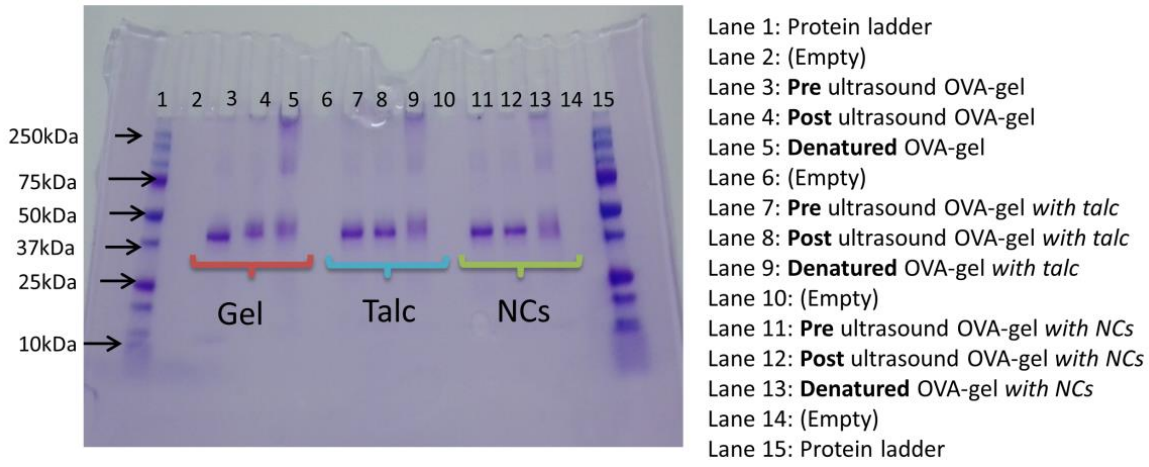

Figure 4.12: SDS PAGE analysis of OVA structure in gel formulation 3 with the different cavitation nuclei

4.3 Summary

The work presented in this chapter represents the efforts of the author to select a suitable combination coupling gel and dosage medium for an ultrasound assisted transdermal vaccine delivery system.

Acoustic characterisation of the native gel formulations has provided valuable information regarding their stability to short and long term storage. Firstly, it was demonstrated that the gels entrap gas from the environment as they are manufactured. As the amount of entrapped gas is variable, and directly affects acoustic properties, a degassing step during gel preparation is necessary to maintain consistent acoustic properties. At the frequency used in this study (256 kHz) cavitation thresholds are consistent, and lie between 0.8 and 1.2 MPa for all three gel formulations. When applied to the skin surface at 256 kHz, ultrasound at these pressures does not undergo significant attenuation, and therefore there is very little heating, as demonstrated in chapter 3 of this thesis. Acoustic pressures of 0.8-1.2 MPa could therefore be deployed clinically. Above the cavitation threshold, the energy levels of acoustic emissions varied widely. This issue is of limited importance – previous work in chapter 3 has shown that molecular transport mechanisms are affected by the presence or absence

of inertial cavitation, and increasing the acoustic pressure beyond the cavitation threshold has limited effects on the transport achieved. Looking into the formulations individually, formulations 1 and 2 displayed very similar properties. Formulation 3 displayed a lower cavitation threshold and higher energy acoustic emissions (indicative of higher amounts of inertial cavitation activity) for any given pressure, although the acoustic energy emissions were more variable than formulations 1 and 2. Finally, the work presented in this section showed that gel properties are not stable over time. This issue will need to be addressed packaging of the gel is designed for clinical use.

The addition of cavitation nuclei to a medium has been implemented to enhance its capability for inertial cavitation. The cavitation nuclei doped gels in this study were examined and compared to identify a gel formulation with the ability to instigate inertial cavitation with the highest acoustic energy emissions at the lowest pressure. The ability to instigate cavitation at low pressures means that power requirements decrease and there is less concern about heating effects caused by high intensity US exposure for prolonged periods of time. The results presented in this section showed an increased inertial cavitation response in the presence of cavitation nuclei. Notably, broadband emissions from inertial cavitation at the ultrasound focus over an entire 90s exposure were at least 3 orders of magnitude and significantly ($p<0.001$) higher when NCs were present than without (figure 4.7). Of the two cavitation nuclei candidates (NCs and talc), broadband emissions in the presence of NCs were at least 2 orders of magnitude higher ($p<0.001$) than when micron-sized talc was used.

For as long as co-formulation of these cavitation nuclei with vaccines does not adversely affect the activity of the vaccine, NCs are therefore a highly desirable addition to the coupling/dosage form. Furthermore, these results demonstrate the superior ability of NCs to instigate and *sustain* inertial cavitation activity in gel throughout exposure durations on the order of several minutes. Gel formulation 3 seeded with NCs displayed the highest and least variable amount of inertial cavitation activity at the acoustic parameters optimised in Chapter 3 (figure 4.7(b)) and was therefore was selected for this application and all subsequent work in this thesis.

Following the acoustic characterisation results, vaccine stability within the different gel formulations was investigated, and three separate analyses demonstrated that BSA and OVA are stable to ultrasound exposure at the optimised exposure parameters within all of the gel formulations, with and without cavitation nuclei. Interestingly, the proteins were not stable in the gel when subject to heating, indicating that the protein remains viable in a mechanical ultrasound regime as opposed to a thermal one. For this reason, the acoustically superior NCs were formulated within gel formulation 3, and deemed the most suited to this application and used in further studies. BSA and OVA were chosen to represent model vaccine as they are of comparable size and structure to other proteins used as vaccines. Additionally, their structures are well characterised in the literature, and there are widespread and validated protocols to detect molecular denaturation. Finally, OVA is also capable of generating an immune response *in vivo,* so was believed to be an effective and economical candidate with which to proceed with *in vivo* verification of immune response. It is acknowledged however, that BSA and OVA are within a relatively stable class of proteins compared to other vaccines (such as live attenuated vaccines) and this protocol will need to be repeated independently with all the vaccine candidates considered for use in this system.

The formulation chosen has optimal acoustic characteristics and provides an appropriate chemical environment for the vaccine embedded in the gel. It is important to note that the *function* of the vaccine has not been compared before and after ultrasound exposure, an issue which is addressed in chapter 6, where *in vivo* delivery studies are performed to test for immune response.

Consequent to the formulation of a suitable dosage form, and determination of optimal ultrasound parameters for ultrasound-assisted transport, the remaining work in this thesis aims to test the system as a whole, both *ex vivo* and *in vivo*.

References:

Axelsson, I. (1978). "Characterization of proteins and other macromolecules by agarose gel chromatography." Journal of Chromatography A **152**(1): 21-32.

Bhatnagar, S., H. Schiffter, et al. (2014). "Exploitation of Acoustic Cavitation-Induced Microstreaming to Enhance Molecular Transport." Journal of Pharmaceutical Sciences **103**(6): 1903-1912.

Clarke, R. L. and G. R. ter Haar (1997). "Temperature rise recorded during lesion formation by high-intensity focused ultrasound." Ultrasound in medicine & biology **23**(2): 299-306.

Collis, J., R. Manasseh, et al. (2010). "Cavitation microstreaming and stress fields created by microbubbles." Ultrasonics **50**(2): 273-279.

Excellence, A. B. f. C. o. T. (2007). "Proteins." Retrieved 28 December, 2014, from http://www.abcte.org/files/previews/biology/index.html.

Formulary, N. R. (2002). Ultrasound Gel. German Pharmaceutical Codex. Germany**:** 1-6.

García de la Torre, J., M. L. Huertas, et al. (2000). "Calculation of Hydrodynamic Properties of Globular Proteins from Their Atomic-Level Structure." Biophysical Journal **78**(2): 719-730.

Kimball, J. (2006, 24 March 2006). "Primary Structure." Retrieved 28/12, 2014, from http://users.rcn.com/jkimball.ma.ultranet/BiologyPages/P/PrimaryStructure.html.

Kristensen, D. (2008). Summary of Stability Data for Licenced Vaccines. P. V. a. P. T. Group. WA, USA.

Kwan, J. J., C. M. Coviello, et al. (2015). "Ultrasound-responsive gas-stablizing nanocups for tumor mapping and enhancement of drug delivery." ACS Nano **In submission**.

Lubrizol-Corporation (2008) Product Specifications - Carbopol 980 Polymer. **2015**, 1

Mitragotri, S. (2005). "Healing sound: the use of ultrasound in drug delivery and other therapeutic applications." Nat Rev Drug Discov **4**(3): 255-260.

Mitragotri, S. and J. Kost (2000). "Low-Frequency Sonophoresis: A Noninvasive Method of Drug Delivery and Diagnostics." Biotechnology progress **16**(3): 488-492.

Mitragotri, S. and J. Kost (2004). "Low-frequency sonophoresis: A review." Advanced Drug Delivery Reviews **56**(5): 589-601.

Paliwal, S., G. K. Menon, et al. (2006). "Low-frequency sonophoresis: ultrastructural basis for stratum corneum permeability assessed using quantum dots." J Invest Dermatol **126**(5): 1095-1101.

Tezel, A., S. Paliwal, et al. (2005). "Low-frequency ultrasound as a transcutaneous immunization adjuvant." Vaccine **23**(29): 3800-3807.

Vivian, J. T. and P. R. Callis (2001). "Mechanisms of Tryptophan Fluorescence Shifts in Proteins." Biophysical Journal **80**(5): 2093-2109.

Wang, Q., M. T. Tan, et al. (2014). "Time course study of the antigen-specific immune response to a PLGA microparticle vaccine formulation." Biomaterials **35**(29): 8385-8393.

Weber, K. and M. Osborn (1969). "The Reliability of Molecular Weight Determinations by Dodecyl Sulfate-Polyacrylamide Gel Electrophoresis." Journal of Biological Chemistry **244**(16): 4406-4412.

Weisel, J. W., H. Shuman, et al. (2003). "Protein–protein unbinding induced by force: single-molecule studies." Current opinion in structural biology **13**(2): 227-235.

Wu, J. and W. L. Nyborg (2008). "Ultrasound, cavitation bubbles and their interaction with cells." Advanced Drug Delivery Reviews **60**(10): 1103-1116.

5 *Cavitation-Enhanced* Vaccine Delivery in Porcine Skin *Ex Vivo*

Previous chapters of this thesis have (1) optimised ultrasound parameters for ultrasound assisted molecular transport through a gel and (2) formulated and characterised the optimal vaccine loaded coupling gel. In this chapter, we verify the successful delivery of a vaccine into the epidermal layer of actual skin as opposed to a tissue mimicking material. Skin varies widely in structure and composition not only between different individuals (Waller and Maibach 2005), but also within the same individual at different sites and positions (Waller and Maibach 2005). These dissimilarities result in variation (between doses and subjects) of the environment through which the vaccine molecules are expected to traverse. Additionally, inhomogeneities in skin structure cause unexpected distortions in the ultrasound field further affecting delivery that is dependant on a process directly affected by ultrasound. These additional influences confound an already complex problem. Experimentation to investigate delivery in live animals at this early stage would be highly premature and prohibitively expensive, though it will be necessary later to test for an immune response. A wide range of transdermal drug delivery literature has utilised Franz diffusion cells (described in chapter 2.1.1) for *ex vivo* study of delivery. To allow for direct comparison the work presented in this chapter has implemented a similar setup.

This chapter represents the combination of the optimised ultrasound parameters and vaccine loaded gel formulation in an *ex vivo* model to verify the delivery of ovalbumin (as a vaccine analogue) into freshly harvested porcine skin. The first objective was to determine if the parameters optimised for transport were also sufficient to enhance the permeability of the stratum corneum (SC). Other researchers have demonstrated the utility of inertial cavitation for increasing the permeability of the SC as outlined in Chapter 1 of this thesis. Permeability increases in the skin have been quantified by changes in electrical resistance, a widely used method in literature (Tezel, Sens et al. 2001). This method was used to quantify permeability increase at the previously optimised parameters, and determine whether a

significant alteration of skin permeability was achieved. Following re-optimisation of the ultrasound parameters to facilitate permeability increases in addition to transport, the coupling gel described in chapter 4 was applied to the skin simultaneously with ultrasound, and delivery of both drug and nanoparticles into the skin was quantified.

The permeability study presented in this chapter was obtained under the supervision of Professor Samir Mitragotri at the University of California, Santa Barbara on an overseas research visit. The author also wishes to acknowledge and thank Byeong Hee Hwang at the Mitragotri Lab at UC Santa Barbara for his valuable assistance and discussion.

5.1 Skin Permeability and Ex vivo transdermal delivery study

Work presented in Chapter 3 led to the identification of ultrasound parameters optimised for cavitation-enhanced molecular transport through a hydrogel. However, when applied to skin, the ultrasound must assist molecular transport and also the permeabilisation of the SC. As discussed in Chapters 1 and 2, ultrasound has been used for permeabilisation of the skin by other researchers and this work has concluded that shockwaves, microstreaming, and microjets produced during inertial cavitation are among the primary mechanisms for permeability enhancement of the skin surface (Wolloch and Kost 2010). Consequently, the parameters optimised for transport were tested on *ex vivo* porcine tissue to investigate the associated permeability enhancement. Decreases in electrical resistance of the skin were measured and used to quantify increases in skin permeability following ultrasound exposure. Ultrasound parameters were therefore re-optimised for skin as opposed to a hydrogel.

Following the re-optimisation of ultrasound parameters, we next developed an ultrasound assisted transdermal vaccine delivery system in order to demonstrate delivery in an *ex vivo* model. This study aimed to assess and quantify delivery of a fluorescently labelled vaccine analogue (ovalbumin) and fluorescently labelled nanocups to also assess their passage through the skin under the influence of ultrasound. Ultrasound was applied to the skin using the same setup as shown in figure 5.1, with fluorescently labelled OVA and nanocups present in the coupling gel. Through the utilisation of a fluorescent skin surface marker, the penetration depths and dose distribution in the skin samples were assessed using multi-photon microscopy, and later histological sectioning. Additionally, the skin conductivity enhancement ratio was determined for each ultrasound exposure, and PCD data was acquired as previously described to monitor inertial cavitation levels in the coupling gel during ultrasound exposure.

5.1.1 Materials and methods

5.1.1.1 Skin tissue source

Porcine skin was chosen as a model for human skin based on its similarities to human skin in terms of structure, thickness and cellular composition (Jacobi, Kaiser et al. 2007). In addition, the speed of sound through porcine tissue (reported as 1710 ± 60 m/s (Cantrell, Goans et al. 1978)) is comparable to that of human skin (1498-1650 m/s) (Moran, Bush et al. 1995): given that it also has similar density, the characteristic impedance is thus similar, ensuring comparable transmission of ultrasound into the skin. Experiments were performed on full thickness porcine skin harvested from the medial thigh of the animals immediately after abattoir sacrifice (female Landrace pigs, weighing 40–50 kg). Hair on the surface of the skin was trimmed with scissors and fat was removed from the underside. Shaving was not performed as this would affect the integrity of the SC. Skin was then cut into smaller (50x50 mm) pieces, wrapped in aluminium foil and stored in a 4°C fridge for up to 3 days. Prior to an experiment, skin was mounted in a Franz diffusion cell (shown in figure 5.1 (b))

5.1.1.2 Re-characterisation of ultrasound source

In order to provide ultrasound coupling, the vast majority of *in vitro* and *ex vivo* ultrasound experiments have been performed with both the ultrasound source and the intended ultrasound target submerged in a solution, or most commonly water. Prolonged immersion of skin in solution produces macerations of the cornified layers of the skin and increases permeability (Scheuplein 2010). Therefore, placing skin in solution greatly influenced the results of experiments looking to quantify the permeability increases in skin due to ultrasound alone. Additionally, depending on the delivery site, immersion in water may not be clinically feasible. Introduction of the water based solution immediately before and removal straight

after ultrasound treatment minimised these effects. Nonetheless, water was still required in the form of an ultrasound couplant between the ultrasound source and target.

To satisfy both the requirements of ultrasound coupling and maintenance of skin integrity, a coupling cone was used for these experiments (figure 5.1). This watertight cone was fitted onto the ultrasound transducer and shaped to match the outer envelope of the spherically focussed sound field, resulting in a conical shape. Acoustically transparent Mylar plastic was used to cover the opening of the cone. For coupling, the cone was filled with degassed filtered water, and so the skin was not immersed for long periods of time. The focus of the ultrasound was positioned within the donor compartment of the Franz diffusion cell.

Due to the introduction of the coupling cone, changes in the ultrasound field were expected. Therefore, the modified ultrasound field beyond the cone (and particularly the focal region) was re-characterised. Characterisation was performed with the same US parameters and hydrophone described in section 3.2.2, and the results are shown in figure 5.1. Use of the matching cone altered the shape of the focus and yielded a reduction in peak rarefactional pressure amplitude on the order of 42%.

5.1.1.3 Gel Administration in the Permeability Study

As the objective of this part of the study was to determine permeability increases in the skin as a result of ultrasound exposure, a vaccine analogue was not used. Instead, the gel couplant described in Chapter 4 was used without any form of cavitation nuclei. Cavitation nuclei were not used in the coupling gel to facilitate the selection of ultrasound parameters that did not rely on their presence. Gel (4 ml) was filled in the donor compartment of height 15 mm, positioned below a therapeutic ultrasound transducer with a water-filled applicator cone designed to ensure that the focus lay 2-5 mm above the skin (figure 5.1)

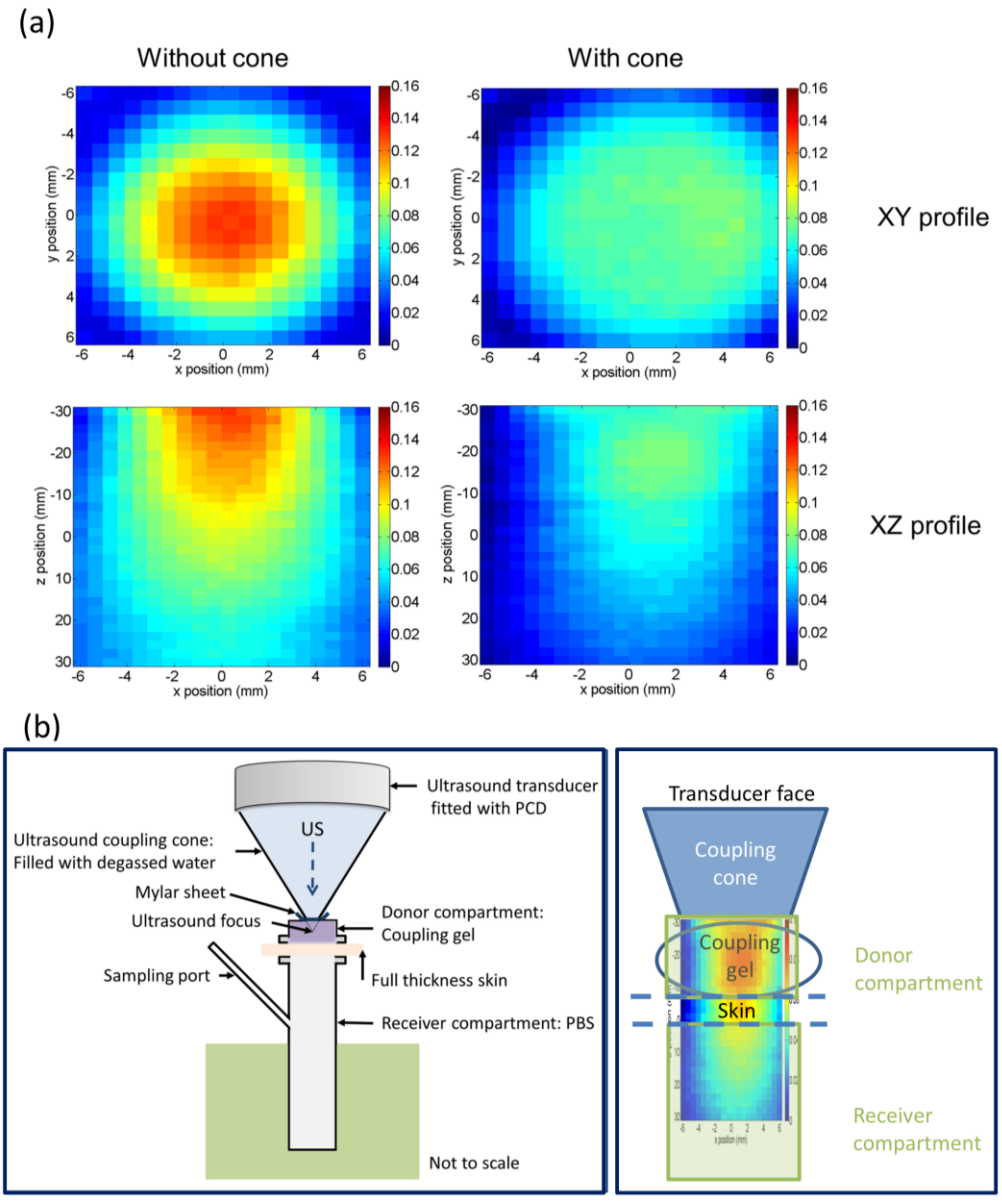

Figure 5.1: (a) Comparison of ultrasound field produced by 256 kHz transducer without (left panels) and with (right panels) coupling cone in the axial (top panels) and transverse (bottom panels) planes. Colour bars indicate peak negative pressure in MPa. (b) Schematic of experimental setup with ultrasound field. A coupling cone filled with degassed, deionised and filtered water was used to couple the ultrasound transducer to the gel in the donor compartment through an acoustically transparent mylar sheet. The ultrasound focus was placed at the centre of the donor compartment. Electrical current was measured via insertion of electrodes into the sampling port and the donor compartment before and after ultrasound exposure.

5.1.1.4 Ultrasound Exposure Parameters – Permeability Study

In an attempt to further optimise ultrasound parameters for skin permeability enhancement, the total exposure time (number of pulses) was increased to find settings at which there was a measureable permeability increase in the skin. Pressure was not altered due to concerns regarding damage caused by prefocal cavitation of the water in the coupling cone. Duty cycle remained unaltered due to heating concerns; a higher duty cycle may have led to heating capable of causing skin damage. The ultrasound parameters implemented in this study were therefore 256 kHz frequency, 1 MPa peak negative focal pressure, 10% duty cycle with a 10 ms pulse (2560 cycles) every 100 ms (10 Hz PRF) for varying numbers of pulses from 0 to 1000.

5.1.1.5 Electrical Resistance/Conductivity Measurements

The current gold standard in detection and monitoring of skin permeability *in vitro* is the comparison of the "conductivity" of the skin (Mitragotri and Kost 2001). In order to determine the permeability increase in the skin during each condition, the electrical resistance of the skin was used to determine conductivity enhancement ratios for each ultrasound exposure. Cu/CuCl electrodes were introduced in the donor and receiver compartments to measure the electrical resistance of the skin before and after ultrasound exposure. To measure the electrical resistance, an AC electrical field at 100 mV and 10 Hz, was applied across the electrodes for a short time (typically, for 5 s) with a signal generator (model HP 4116 A, Hewlett Packard). The electric current through the skin was then measured with an ammeter (Texas Instruments), and the electrical resistance was calculated by Ohm's law. Skin resistivity was obtained by multiplying the skin electrical resistance (measured experimentally) by the skin area (1.77 cm^2). Skin conductivity was calculated by taking the reciprocal of resistivity (Mitragotri, Edwards et al. 1995). Measurements were taken with PBS in both the donor and receiver compartments prior to and

immediately following ultrasound exposure and each treatment in the delivery study (Tezel, Paliwal et al. 2005).

5.1.1.6 Delivery Study - Gel/Drug administration

OVA (A5503, Sigma-Aldrich, UK) was firstly conjugated with FITC dye using the Fluorotag FITC conjugation kit (FITC1, Sigma-Aldrich, UK). The absorbance of the conjugated samples was measured at 280 and 495 nm and the fluorophore/protein molar ratio was calculated. FITC-OVA was then added to each gel (+/- cavitation nuclei) at a testing concentration of 1.5 mg/ml.

In order to make the NCs fluorescently visible, they were labelled with anthracene, a fluorescent dye with excitation peak at 362 nm (ultraviolet region) and emission peak at 407 nm (blue region)(Kwan, Coviello et al. 2015). Anthracene was selected because its fluorescence spectra have no overlap with the fluorescence spectra of the FITC tagged to the OVA molecules. Fluorescent nanocups were added to the OVA-FITC laden gel at a concentration of $5x10^9$ particles/ml as in the optimal formulation described in chapter 4. 4 ml of OVA and nanocup laden gel was placed in the donor compartment of the Franz diffusion cell (as in figure 5.1) immediately following resistivity measurements and prior to ultrasound exposure.

5.1.1.7 Delivery Study - Therapeutic Ultrasound Setup and Experimental Groups

Ultrasound parameters (265 kHz frequency, 1 MPa PRFP, 10 ms pulse duration, 10 Hz pulse repetition frequency, 90 s exposure duration) were selected on the basis of previous work to maximise acoustic emissions associated with inertial cavitation. Experimental groups were as shown in table 1. Three replicate samples were taken for each group.

Table 1: Delivery study treatment groups.

Group	**Treatment**
Negative control – OVA in gel with NCs	Gel placed on skin for 90 s. No ultrasound exposure
Pretreatment with nanocup gel	Skin pretreatment with gel with nanocups **(no OVA)** placed on the skin and exposed to US (256 kHz, 1 MPa PRFP, 10 ms pulse duration, 10 Hz PRF, 90 s exposure duration), before application of liquid OVA for 90s.
OVA in gel with US exposure	OVA in gel **without** NCs placed on skin. 90 s US exposure (as above)
OVA in gel with nanocups with US exposure	OVA in gel with NCs placed on skin. 90 s US exposure (as above)
Positive control 1	Skin pre-treatment with 1% w/v sodium dodecyl sulphate (SDS) solution and US (as above) before application of OVA in gel with NCs.
Positive control 2	Skin pre-treatment with 1% w/v sodium dodecyl sulphate (SDS) solution before application of OVA in gel with NCs. No ultrasound exposure.

Acoustic emissions were recorded throughout exposures using a 5MHz passive cavitation detector. Emissions originating from the coupling gel and skin were post processed as previously described. Positive control samples were not imaged due to the denaturation of OVA-FITC in the presence of SDS, rendering it non-fluorescent.

5.1.1.8 Delivery Study - Microscopy

5.1.1.8.1 Multi-photon microscopy

Multi photon microscopy (MPM) was used to image the skin samples to assess penetration of fluorescently labelled OVA and NCs. Immediately following ultrasound exposure, the areas of skin samples subjected to ultrasound were "painted" with fluorescent red 2 µm diameter latex beads (SpheroTech, USA) to demarcate the skin surface. 2 µm diameter beads were chosen as these were too big to diffuse through the skin and therefore acted as markers for the skin surface to visualise and quantify the penetration depths of both OVA-FITC and nanocups in the skin. The concentration of the bead solution was arbitrarily chosen based on the amount of beads available for all samples. A higher concentration would have allowed for the skin surface to be completely covered with beads, imaged as a continuous surface, but because of the modest concentration, the "surface" of the skin was demarcated as a number of points, which were used to extrapolate a skin surface in Matlab software.

A modified BioRad Radiance 2100 MP Multiphoton Microscope (Zeiss; Jena, Germany), was used for 3D imaging. Near infrared (NIR) laser beams (lambda = 800 nm) were obtained from a tunable 76 MHz femtosecond pulsed Ti:sapphire laser (Mira 900-F, Coherent, Ely, UK) pumped by a 10 W multiline argon ion laser (Verdi; Coherent). A Nikon S Fluor 20X objective (NA = 0.75) was used for all images. The emission filters selected were: 495 nm for blue, 525 nm for green, and 595 nm for red. 3 dimensional, 3 colour images were obtained of xy dimension 389x389 µm up to 1.5 mm deep (z-slice resolution 1.95 µm) into each skin sample. 3D representations were generated from the data acquired using Imaris software (Bitplane, USA).

Data was post processed using Matlab software. The algorithm implemented obtained an extrapolated skin surface from the red beads, and then measured the depths in each column of the 3D image between this skin surface and every voxel containing OVA-FITC (stained green) or nanocup (stained blue) to obtain a distribution of depths. The depth distribution was then weighted according to the fluorescence intensity of each voxel analysed, with a view to giving the intensity distribution of the OVA-FITC and nanocup in each measured area of the skin.

5.1.1.8.2 Histological Sectioning of Skin

After imaging of the skin with MPM, samples were snap frozen in OCT medium and histologically sliced (slice thickness: 15 μm) without any further staining protocols. This was performed for verification of delivery depth and investigation of any histological damage to the skin surface. Sliced samples were viewed using a fluorescence microscope (Nikon Eclipse Ti). A Nikon S Fluor 10X objective (NA = 0.3), 4X objective (NA = 0.2) and 20X objective (NA = 0.45) was used to acquire fluorescence images.

5.2 Results and Discussion – Ultrasound Parameter Re-optimisation for Skin Permeability

Figure 5.1 shows that the ultrasound field is altered as a direct result of the presence of a coupling cone. Although the size and shape of the *axial* focus remains the same, the ultrasound pressure at the focus is reduced. The dimensions of the coupling cone were restricted due to the geometry of the setup. As a result, some reflection was present in the near field causing interference in the ultrasound en-route to the focus. In the transverse plane, the size and shape of the focus outside the opening of the cone was altered, and the focal pressure reduced. As a result of the reduction in pressure, a recalibration was performed to determine the new voltage input required to the transducer to produce a peak negative acoustic pressure of 1 MPa at the focus. The new input voltage was determined as 248.8 V (peak to

peak), (an increase of 113.4 V from 135.3 Vpp without the cone) and was used for the investigations presented in this chapter.

Increases in the skin conductivity enhancement ratio with increasing ultrasound exposure time are shown in figure 5.2(a). As total exposure time increased, the conductivity enhancement ratio also increased, indicating an increase in skin permeability. This relationship is observed to plateau for exposure times in excess of 70 s up to 100 s, which was the maximum time tested. Increasing conductivity enhancement ratios were expected at longer exposure durations because the duration of inertial cavitation activity had also increased. Exposure times in excess of 100 s were not tested because it was believed that maximum permeability increases had been achieved. We therefore demonstrated that skin permeability can be effectively increased by increasing ultrasound exposure time up to 90 s. In order to verify that permeability increases were not occurring due to heating, temperature changes in the donor compartment were also measured. A temperature elevation of 0.14°C was observed over the whole 90s exposure time (at a 10% DC and 1.4 MPa peak negative pressure), which does not represent significant heating (figure 5.2(b)). On the basis of these results, total ultrasound exposure time was increased from 10 s to 90 s to allow sufficient permeabilisation of the skin in addition to molecular transport.

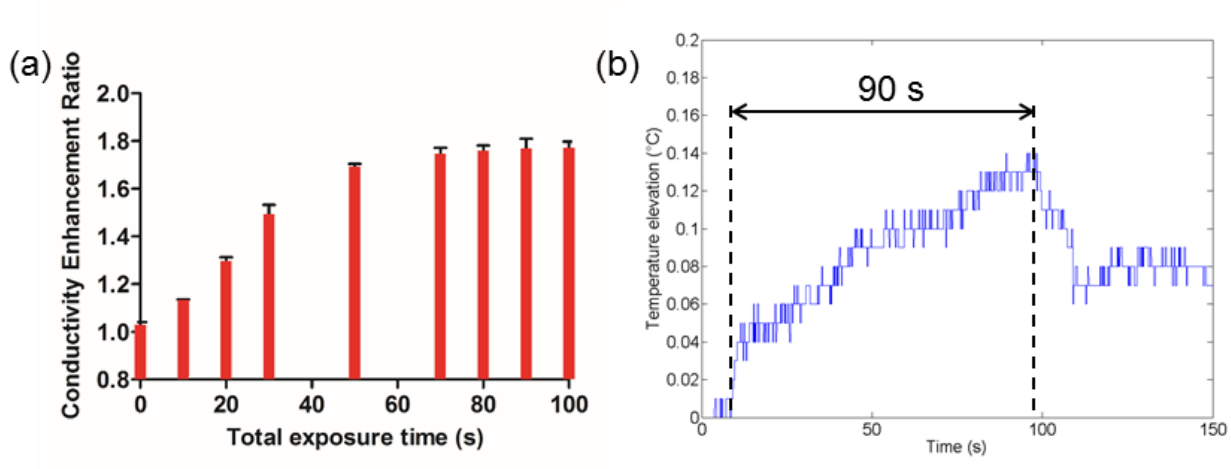

Figure 5.2: (a) Effect of increasing exposure time on permeability of porcine skin. As the PRF of the signal was 10 Hz, the total number of pulses ranged from 0 (at 0 ms exposure time) to 1000 pulses (at 100 s exposure time) (n=5, standard deviation shown). Ultrasound parameters were otherwise constant at 1 MPa peak negative focal pressure, 10% DC and 10 Hz PRF. Cavitation nuclei were not included in the couplant of this study.(b) Temperature elevation due to ultrasound in the donor compartment of the Franz diffusion cell over a 90s exposure (1.4 MPa peak negative pressure, 10% DC)

5.3 Results and Discussion – Quantification of delivery into the skin

5.3.1 Skin Permeabilisation

Changes in electrical conductivity of the skin are shown in figure 5.3. In the absence of both ultrasound and chemical penetration enhancers, there was no significant change in skin conductivity. Ultrasound exposure in the absence of NCs also produced no detectable skin permeability enhancement. Small but detectable changes were observed, however, in the presence of ultrasound **and** NCs, regardless of whether OVA was present. Chemical permeabilisation (in the absence of US) showed a significant (9.5-fold) increase in conductivity enhancement, and the addition of US further significantly increased the permeability of the skin to 12-fold.

In this study, this method was used to assess permeability increases in the skin caused as a result of ultrasound exposure. Previous work has shown that skin permeability is enhanced in the presence of inertial cavitation (Tang, Wang et al. 2002; Tezel, Sens et al. 2002). It follows therefore that couplants that favour inertial cavitation occurrence (such as those containing cavitation nuclei) are likely to cause a greater increase in skin permeability, especially as heating mechanisms have been eliminated as a possible reason for permeability enhancement (figure 5.2(b)).

This was observed in the results of this study. SLS has been widely studied as a chemical transdermal penetration enhancer because it is able to readily and reversibly disrupt the barrier properties of the skin, particularly the SC (Som, Bhatia et al. 2012). This effect was seen in the current study, where the most significant (12-fold) increase in skin permeability was observed simply upon exposure to US in the presence of SDS. Increased permeability in the presence of SDS **and** ultrasound was likely due to cavitation in the SDS solution, as shown in figure 5.4. The main drawback with the use of chemical penetration enhancers however, is skin irritation resulting from an inflammatory response to the chemical and the damage it causes. In contrast, an inflammatory response in the skin to ultrasound has never been observed. Consequently, assuming a suitable delivery profile is achievable with the small but observable permeability change associated with US skin treatment with NC-Gel (either as a pre-treatment or simultaneously applied with the vaccine), this is a preferable option to the chemical penetration enhancer. We have also demonstrated that ultrasound at the clinically acceptable and achievable settings used in this study show a noticeable trend towards skin permeabilisation.

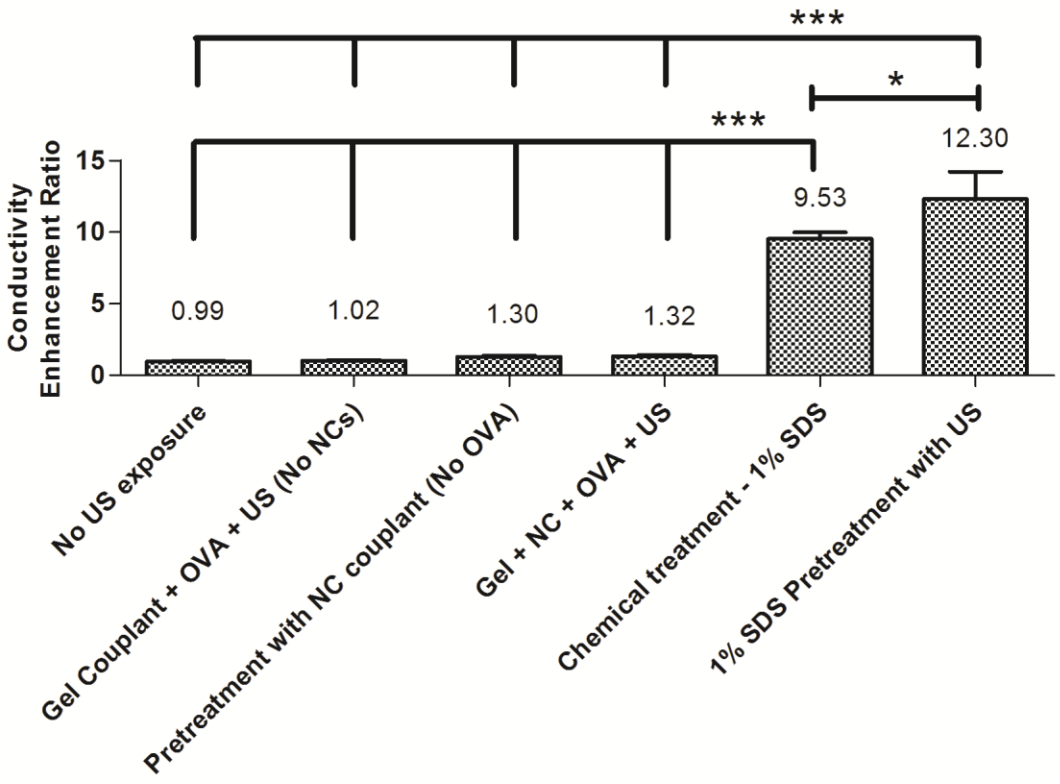

Figure 5.3: Skin conductivity enhancement ratios for each skin treatment. Average values are shown above each data bar. (n=3) (* denotes $p<0.05$, *** denotes $p<0.001$)

5.3.2 Acoustic Monitoring of Inertial Cavitation Activity

Broadband acoustic emissions originating from the donor layer and skin are shown in figure 5.4. Spectrograms in figure 5.4 (a-c) give a representation of the magnitude and temporal distribution of the frequency content of broadband energy emissions as exposures progress (for a single representative sample in each experimental group). Broadband emissions when the gel did not contain any form of cavitation nuclei was sparse and of low magnitude (figure 5.4(a)), whereas in the presence of NCs, cavitation was sustained and of high magnitude throughout the exposure duration (figure 5.4(b and c)). Pre-treatment with SDS in the donor compartment showed more broadband emissions than in the gel alone, but these emissions were significantly lower when NCs were present in the gel couplant (figure

5.4(d)). The average total emission energy for each condition is shown in figure 5.4(d). As expected, the total energy is significantly lower in the absence of NCs. Variability between samples is lower in the absence of NCs.

The increase in the magnitude of broadband emissions detected in the presence of NCs is due to the presence of cavitation nucleation sites in the form of nanobubbles on the NC surface. Cavitation nucleation in gel that did not contain NCs required either more energy to occur, or a nucleation site (such as a pocket of air entrapped within the gel) to be present in the ultrasound focus. In the absence of NCs this was much less likely, and inertial cavitation events were energetically more difficult to achieve. This led to their scarcity and resulted in sparse, low energy emissions as shown in figure 5.4(a).

Conversely, gel that was plentifully supplied with NCs, and therefore cavitation-ready nanobubbles, showed emissions indicative of many cavitation events within the ultrasound focus. Furthermore, the cavitation events were sustained over the exposure period. Previous studies have shown that NC particles entrap gas on their crevice-like concave surface that detaches from the particle before undergoing uncontrolled expansion and collapse (Kwan, Coviello et al. 2015). Gas from collapsed bubbles may then dissolve into the gel, or may coalesce with other gas to once again form a bubble capable of an inertial cavitation event (Kwan, Coviello et al. 2015) Furthermore, all of the entrapped gas on a single NC may not be drawn out in a single cavitation event, allowing for more than one “event per nanoparticle”. Recent work has explored this possibility and shown the utility of super-hydrophobic cavitation nuclei (typical contact angle >160°) to nucleate hundreds of times without deactivation. However, this is only possible if the microjet resulting from the collapse of the bubble is not directed into the crevice (Borkent, Gekle et al. 2009). Due to their size, the NCs provide a high cavitation density in the gel that is within the ultrasound focus. Additionally, plentiful inertial cavitation events within the focus generate microstreaming effects which cause convection currents within the gel that circulate the

NCs, replenishing the supply of cavitation nucleation sites in the ultrasound focus. It is believed that the combination of these effects give the NCs the capability to produce sustained high energy acoustic emissions, indicative of inertial cavitation. These results confirm the increased amount of inertial cavitation present during insonation in the presence of NCs, and combined with the permeabilisation results, add credence to the conclusion that permeability increases in the skin are a result of increased amounts of inertial cavitation.

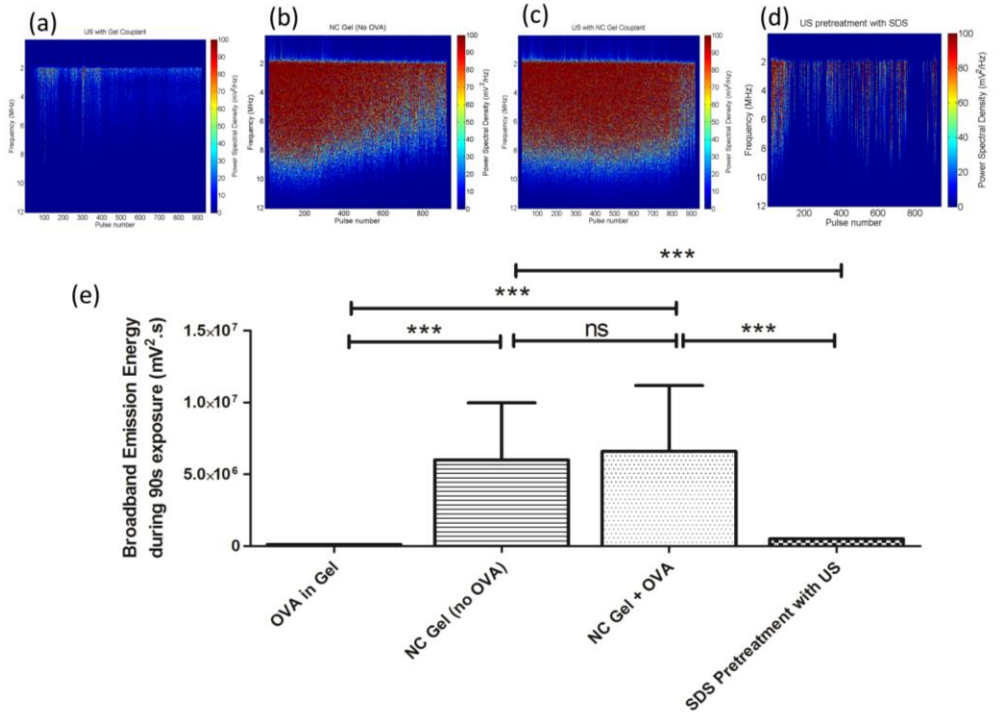

Figure 5.4: (a-d) Representative frequency spectrograms of the magnitude and temporal distribution of broadband acoustic emissions for the experimental groups exposed to US, as detected by the PCD. (e) shows total broadband energy emissions over the entire 90s (900 pulse) exposure period), calculated as the sum of the integrals of the filtered Fourier Transforms for each pulse in the exposure. (n=3) (*** denotes $p<0.005$ using a one way ANOVA analysis)

5.3.3 Vaccine and Nanocup Delivery Visualisation

Microscopy was used in this study for visualisation of the OVA and NC passage through the skin. Fluorescence labelling permitted visualisation in both 2- and 3-dimensions. From these images, it was possible to estimate dose depth and distribution of OVA and NCs in porcine skin.

5.3.3.1.1 Multiphoton microscopy (3D)

Multi-photon microscopy (MPM) is a specialised fluorescence imaging technique that provides distinct advantages for three dimensional imaging of biological tissue. The effective sensitivity of fluorescence microscopy, especially with thick specimens, is limited by out-of-focus flare. This limitation is reduced in a confocal microscope, where a pinhole rejects out-of-focus fluorescence. However, excitation light generates fluorescence around the focus and causes photobleaching. Furthermore, the penetration depth in confocal microscopy is limited by the absorption and scattering of the excitation light by the specimen before reaching the current plane of focus.

MPM avoids these problems by utilising multi-photon excitation of fluorophores. The underlying principle of this technique is based on the probability that multiple low-energy photons can arrive 'simultaneously' at a fluorophore and through interactions with it, induce an electronic transition normally excited by a single high-energy photon (Williams, Zipfel et al. 2001). Since the energy of a photon is inversely proportional to its wavelength, the two absorbed photons have a wavelength about twice that required for one-photon excitation. For example, a fluorophore that normally absorbs ultraviolet light (~350 nm wavelength) can also be excited by two photons of near-infrared light (~ 700 nm wavelength) if both reach the fluorophore at the same time (within an interval of about 10^{-18} s). Because two-photon excitation depends on simultaneous absorption, the resulting fluorescence emission varies with the square of the excitation intensity. This quadratic relationship between excitation and emission means that the emission generated by a fluorophore excited by two photons at

700 nm is exactly the same as if it was excited by one at 350 nm, and gives rise to many of the significant advantages associated with two-photon excitation microscopy.

In order to produce a significant number of two-photon absorption events (in which both photons interact with the fluorophore at the same time), the photon density must be approximately one million times that required to generate the same number of one-photon absorptions. The consequence is that extremely high laser power is required to generate significant two-photon-excited fluorescence. This power level is achieved by the focusing of pulsed lasers, in which the photons are only spatially dense enough to generate significant two-photon excitation in the focus, while the average laser power (and spatial density of the photons) outside of the focus remains fairly low. As a result, only those fluorophores in the focus are excited at any given time, preventing photobleaching in the sample. Additionally, because there is no absorption in out-of-focus specimen areas, more of the excitation light penetrates through the specimen to the plane of focus. The increased light penetration is also because red and infra-red light employed in a multiphoton technique undergoes less scattering then light of shorter wavelengths. The result is greatly increased specimen penetration, which is generally two or three times greater than is possible with confocal microscopy. Based on these advantages, MPM was used to image sections of skin after treatment to track the fluorescent molecules through the skin and determine penetration depths to the order of 1 mm.

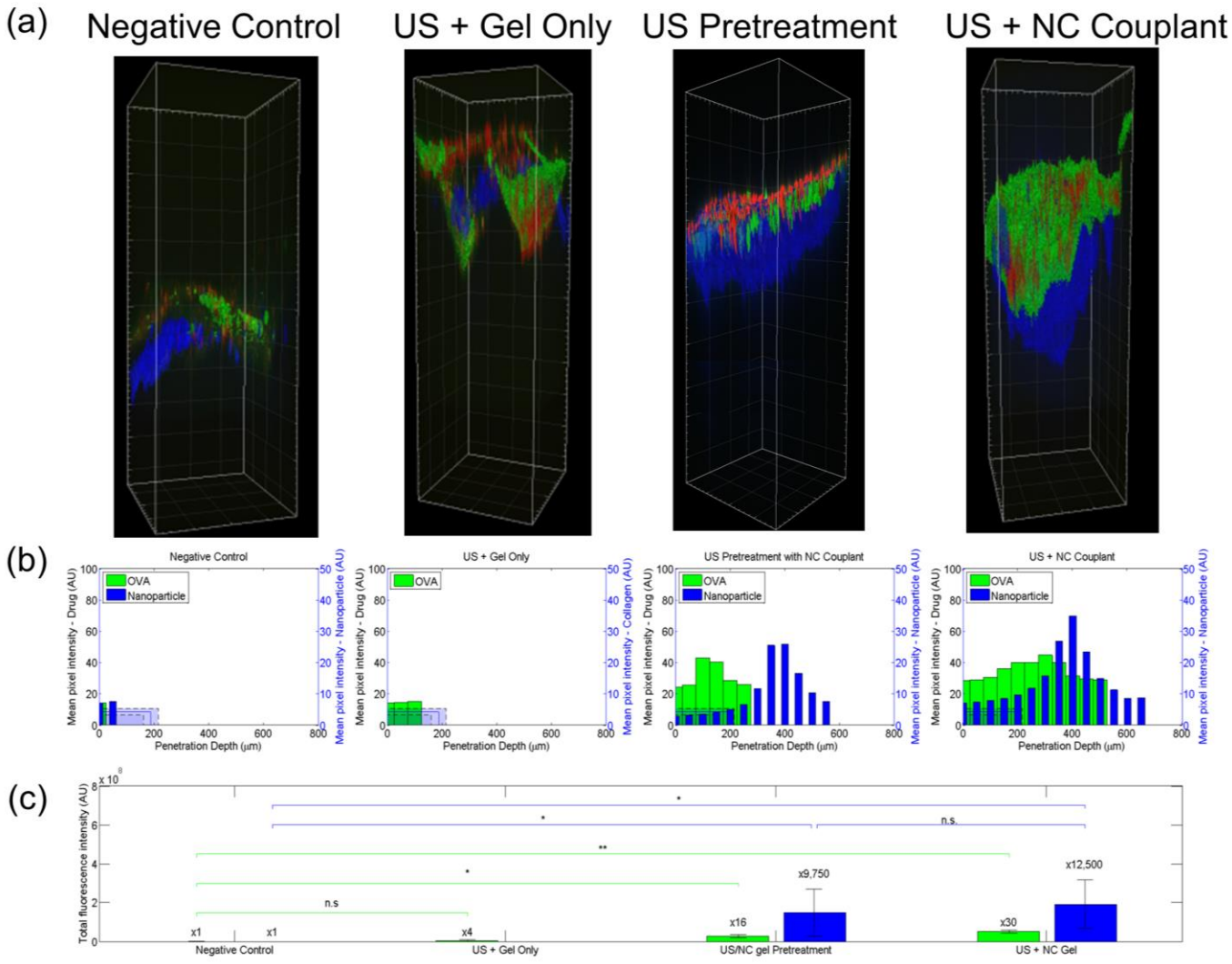

Figure 5.5: (a) 3D Visualisations of OVA and NC penetration in a single representative sample of each of the four treatment groups that were visualised. OVA = green, NCs = blue, and skin surface = red. Each square on the surrounding grid is 100 µm x 100 µm. Ultrasound exposure direction is vertically down through the images. (b) Quantitative OVA and NC distribution profiles for a single representative sample within each treatment group. Shaded regions represent mean±1SD of signal that may have originated from collagen in the skin rather than NCs. (c) overall OVA and NC delivery doses for each treatment group, showing enhancements in dose delivery relative to the control (n=3). ANOVA used to compare means within groups *indicates $p<0.05$, ** indicates $p<0.01$ and n.s. represents a non-significant result.

Figure 5.5 shows qualitative and quantitative results for OVA and NC penetration in the four different treatment groups examined in this study. 3D image representations are shown in row (a) and give an at-a-glance summary of the difference in delivery for the four treatment conditions. In the negative control image, OVA (stained green) and NCs (stained blue) are seen to penetrate the skin surface (stained red) very sparsely, and to a maximum depth of approximately 100 μm. With the addition of ultrasound, more penetration (in dose as well as depth) is seen (figure 5(a) – US + Gel Only). However, most of the increased drug dose overlaps with the red regions, indicating that large amounts of drug did not traverse further than the skin surface. When US+ NCs were used to pre-treat the skin there was minimal increase in OVA delivery, however the NC penetration was considerably increased, with penetration depths of up to 550μm. Finally, when OVA was applied simultaneously with US and NCs, OVA penetration depth increased substantially to 500 μm, and OVA dose was also markedly increased. Nano-cups in this group also penetrated to depths of 600-700 μm.

Visual assessment of the MPM images enables qualitative comparison of delivery, however it does not provide a quantitative assessment of the penetration achieved in each condition by OVA and NCs. For this purpose, Matlab algorithms were developed to mark the skin surface demarcated by the red beads and assign this as the skin surface with a depth of 0. Penetration of drug and NC was then measured through each column of voxels of the complete 3D image from this modified skin surface. Figure 5.5 (b) shows histograms of all the depths measured for each fluorescent entity, weighted for pixel intensity to show where the concentration was highest within the distribution. These histograms show that OVA and NC penetration in the absence of ultrasound was sparse and shallow – reflected by low pixel intensity and poor penetration depth (figure 5.5 (b) – Negative control). In the absence of NCs, OVA delivery from gel with ultrasound exposure was also shallow, reaching depths of up to 150μm (figure 5.5(b) – US + Gel Only). Pretreatment with ultrasound and NC-enriched gel resulted in separate distributions of OVA and NCs (figure 5(b) – US Pretreatment with NC Couplant). Ultrasound exposure

with NC-enriched gel enabled the NCs to penetrate deep into the skin as well as permeabilise the skin, due to inertially collapsing bubbles on particle surfaces. The penetration depth of OVA was also enhanced approximately 2-fold due to the permeabilisation effect, but as OVA penetration was reliant on diffusion (as opposed to convective transport during US exposure), it was not able to penetrate as deeply as the NCs. Upon the application of OVA simultaneously with US and NCs, microstreaming mechanisms due to inertial cavitation were able to further provide an active transport mechanism for the OVA molecules. As a result, significant enhancements (approximately 2-fold) were seen in the penetration depth of OVA in the simultaneous application US+NC couplant group.

Despite the absence of NCs, fluorescence in the blue spectrum was observed. This was due to the autofluorescence of collagen in the skin, which has been shown to fluoresce in the blue region upon excitation with UV light (excitation/emission range: 270-370 nm/ 405-460 nm) (König, Schenke-Layland et al. 2005). In order to investigate the extent to which fluorescence emissions from collagen alone could be visualised in the skin at the microscopy settings used, 9 separate skin samples in the absence of any treatment were examined. The average pixel intensity and mean maximum penetration depth of the collagen detected in these samples was determined at the same settings used for image acquisition. The average pixel intensity was found to be 8.56±2.04 AU, and the mean maximum penetration depth was 187.96±27.11 µm. Consequently, in order to ensure that collagen signal was not mistaken for signal originating from the NCs, it was assumed that signal in the blue channel at any point less than 187.96±27.11 µm deep, and of intensity less than 8.56±2.04 AU may be collagen, and this is represented by light blue shaded areas on each distribution in figure 5.5(b). These values were superimposed on the raw data as opposed to subtracted from the raw datasets because the collagen fluorescence varied with each skin sample, so subtraction of a mean value from all the skin samples would not provide a fair representation of the results.

The final histogram (figure 5.5(b) – US + NC Couplant) shows the distribution of OVA and NCs in the US + NC couplant treatment group. Both OVA and NCs show markedly higher dose (proportional to intensity) and penetration depth than in the other two treatment groups. OVA distribution shows a peak at around 300 μm, indicating that the highest dose of OVA was delivered at this depth. The peak for NCs was deeper, at around 400 μm, and there was significant NC fluorescence in the area outside of the expected collagen range. It was noted in samples within this treatment group that that the penetration depth of NCs was always higher than that of the OVA when ultrasound and cavitation related mechanisms were responsible for transport. This is hypothesised to be due to the NCs ability to "self-propel" in an ultrasound field as a nanobubble repeatedly inertially cavitates on their surface. As a result, and in contrast to the OVA molecules, NCs do not appear to be reliant upon only the microstreaming effect of inertial cavitation.

The observation that deeper penetration is always seen with the NCs compared to OVA has led to some discussion regarding drug loading of the NCs themselves. Research investigating the feasibility of this and any effects on drug molecules due to such close proximity to violent inertial cavitation events is currently being performed. For the purposes of this study however, co administration of OVA with the NCs was believed to be sufficient for an epidermal vaccine delivery application.

Overall OVA and NC dose calculated as a function of fluorescence intensity is shown in figure 5.5(c). Dose was calculated simply as the sum of the intensities of all the green or blue fluorescent voxels in a 3D image stack. Three samples per treatment group were analysed, and significant enhancements in delivery were observed in both the mean OVA dose and NC dose in the US+ NC Couplant (OVA = 30-fold enhancement, NCs = 12,500-fold enhancement) compared to the control, demonstrating enhanced delivery of both entities. With cavitation-enhanced ultrasound pre-treatment alone, the overall OVA concentration increased 16-fold compared to control, whilst with cavitation-enhanced delivery the

overall OVA concentration increased 30-fold relative to control. At first glance, it would thus seem that active transport during delivery only accounts for a further 2-fold increase over permeabilisation alone. However, it is worth noting that no OVA was delivered to depths greater than 250 microns in the pre-treatment group, whilst the increased concentration delivered by cavitation-enhanced transport reaches depths of up to 550 microns. Even though there is still a significant advantage of cavitation-enhanced transport during delivery in terms of overall dose delivered, it is most transformative in terms of mediating a previously unachievable penetration depth. NC dose and delivery profile in the cavitation-enhanced ultrasound pre-treatment group was similar to that seen in the simultaneous US+NC+OVA treatment group, as from the point of the NCs, they had seen the same ultrasound conditions and were unaffected by the application of the OVA.

Although figure 5.5(c) can be used to compare OVA and NC dose in the skin samples, an absolute dose delivered per ultrasound treatment cannot be calculated from this data due to the sampling method. It is important to note that the x and y dimensions of the 3D volume images acquired are around 400 µm, so every image samples only a small percentage of the insonated area. Previous work has demonstrated the formation of dermal localised transport regions when ultrasound is used to permeabilise the skin. Due to this observation, it cannot be assumed that dose in the 3D volume sampled is the same throughout that sample of skin. A potential method for determination of absolute OVA dose to the skin is an ELISA immunoassay of skin tissue homogenate to identify the OVA concentration in the skin, and this methodology has been applied in *in vivo* studies presented in chapter 6 of this thesis. Testing of tissue homogenate is viable in *ex vivo* and even short term *in vivo* animal studies, however this is not feasible for delivery in humans. Non-invasive methods of dose determination into the skin are currently under investigation and beyond the scope of this work.

5.3.3.1.2 Histological Sectioning (2D)

In addition to visualisation in 3D using MPM, histological sectioning of the skin samples after imaging with MPM was performed in order to verify (1) the penetration seen with the MPM, and (2) that there was no visible skin damage as a result of ultrasound exposure. Figure 5.6 shows co-registered images of histological sections of porcine skin from each of the three treatment groups. The images are orientated such that the SC is the uppermost layer in the skin and the ultrasound is being applied from the top of the images downwards. Bright-field images show three clear differentiated layers with an intact SC in all three treatment groups. This demonstrates that there was no lasting damage to the skin as a result of ultrasound exposure. Column 2 (figure 5.6) shows the OVA penetration at different depths within the skin for all three treatment groups. In the negative control image (top), FITC-labelled OVA is only present on the surface of the skin within the SC, and with minimal penetration into the epidermis. Upon the introduction of US, fluorescence from the OVA-FITC is present not only on the SC, but also within the epidermal layer, indicating that some delivery has taken place. However, the fluorescence intensity seen in the US + Gel + NCs group is much higher, and demonstrates once more the utility of ultrasound and NCs for the delivery of OVA into the skin. Large high-intensity fluorescent regions (red arrows) indicate “clumping” of the OVA as opposed to homogenous delivery over an area, as seen in the 3D MPM images.

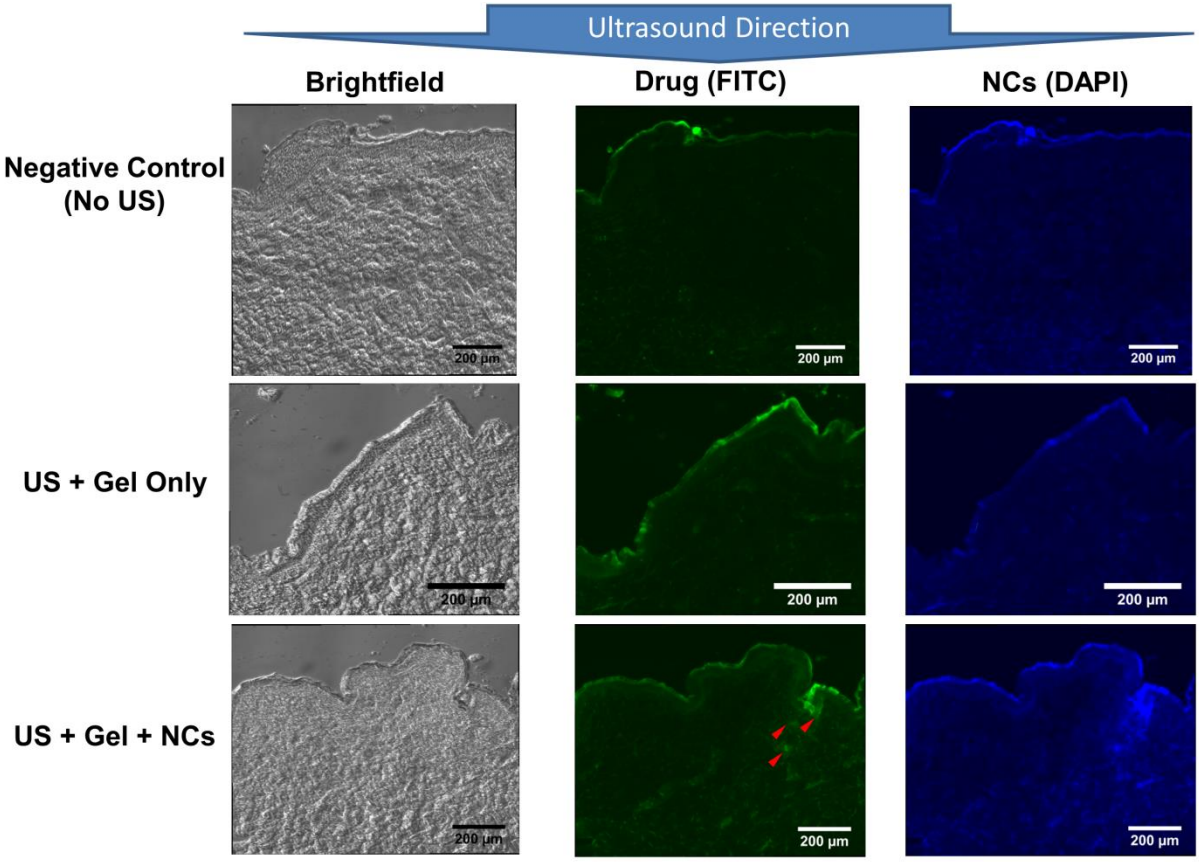

Figure 5.6: Representative co-registered histological sections of skin from each of the three treatment groups (rows). Direction of ultrasound exposure is shown by the blue arrow. Columns show brightfield images (left) to illustrate skin structure and the position and depth of the SC, epidermis, and dermis. Centre and right columns show OVA penetration and NC penetration respectively. Red arrows indicate large high-intensity fluorescent regions showing local "clumping" of the OVA.

Images of NC penetration in the histological slices are shown in figure 5.6 (right column). All three treatment groups show significant fluorescence throughout due to high background fluorescence in the skin itself. High-intensity regions that are markedly different to the negative control image are only seen in the US + Gel + NCs group, indicating this is the only group where there was significant NC penetration that is visible over the background signal.

Although it is tempting to directly compare these images to the MPM data quantitatively, there are a number of reasons why this is not possible. Firstly, the sample size does not encompass the entirety of the acoustic window. 10 cross-sectional slices of tissue 10µm thick were removed for observation from a 30 mm x 30 mm piece of tissue. Although attempts were made to sample sections from the entire insonated area, this methodology cannot capture the complete delivery profile and give a reliable measure of OVA or NC dose delivered. Secondly, photo-bleaching had an impact on attempts to quantitatively derive delivery dose from intensity. The protocols involved in histological sectioning require the sample to be exposed to ambient lighting conditions. Despite efforts to keep samples wrapped in aluminium foil and the use of relatively photo-stable dyes, photo-bleaching in the samples was possible. Finally, the skin has autofluorescence which varies not only between samples, but also within them. Although the FITC-OVA was well visualised by its dedicated filter set, the DAPI filter utilised for the visualisation of the NCs was sub-optimal, resulting in higher background fluorescence emissions from collagen and other skin components. As a result, the contribution of the background skin fluorescence was significant. Because the levels of background fluorescence are so variable, quantitative analysis of the intensities of these images will not provide reliable dose data. To avoid this issue in the future, skin could be photobleached prior to treatment, so that the background fluorescence intensity level is known as 0. Alternatively radiolabelling of OVA and/or NCs could be utilised instead of fluorescence if facilities were available.

5.4 Summary

Work presented in this chapter aimed to demonstrate model vaccine delivery using the proposed ultrasound assisted vaccination system in biological tissue. Porcine skin was chosen as an *ex vivo* model as it has many structural and acoustic similarities with human skin. Initially, a reoptimisation of ultrasound parameters was performed as it became evident that the initial 10 s exposure time, which

had initially been optimized to enable cavitation-mediated *transport*, was not sufficient to permeabilise the skin to the extent to which it could be measured by electrical resistance measurements. However, a measureable skin permeability increase was achieved when the exposure time was extended to 90 s. Therefore, the total ultrasound exposure time was extended for all subsequent experiments.

For demonstration of delivery, skin was insonated in the presence of fluorescently stained OVA and nanocup nanoparticles. OVA was selected as a model vaccine because it has been shown in many pre-clinical studies to be capable of producing an immune response. Detection of an immune response was not an objective of the work presented in this chapter, but as this objective was to be addressed in later work (described in chapter 6), it was believed to be sensible to use a vaccine candidate that could be carried forward into *in vivo* studies.

Results demonstrated that OVA was effectively delivered from gel embedded with NCs and exposed to US up to 500 µm deep in the skin, compared to a penetration depth of only 0-50 µm in the absence of NCs or ultrasound. Penetration depth was also compared to a pre-treatment group, where skin was pre-treated with NC-enriched gel, and the OVA was applied as a solution following the removal of gel and ultrasound. OVA transport was therefore reliant on diffusion, and therefore was limited to around 200µm. Electrical conductivity measurements of the skin before and after ultrasound exposure in the presence of NCs showed evidence of increased skin permeability. Passive acoustic monitoring data from the ultrasound focus showed significantly higher levels of inertial cavitation present when NCs were present in the coupling media. As inertial cavitation is believed to be the mechanism for both skin permeabilisation and assisted molecular transport, these results indicated that conditions were conducive to delivery. MPM and histological examination of the porcine skin samples after ultrasound exposure simultaneously with OVA application confirmed this hypothesis, showing OVA penetration of up to 500 µm, and NC penetration to up to 700 µm. These depths place both OVA and the NCs

throughout the epidermis and the upper dermal layers, meaning that OVA would have had access to immunogenic Langerhans cells in the skin and be capable of eliciting an immune response. Drug loading the NCs has been suggested, and will be further investigated elsewhere. In order to exclude heating effects as a possible mechanism for enhanced permeability and transport, the total temperature elevation during the 90s exposure time was measured and demonstrated as insignificant (0.14°C).

In conclusion, the work presented in this chapter has shown the utility of US in combination with NCs for the epidermal delivery of OVA in an *ex vivo* porcine model. The depths and doses achieved are, in theory, sufficient for transdermal vaccine delivery to be successfully performed. The remaining work in this thesis evaluates the ability of this complete ultrasound-assisted transdermal vaccination system to elicit an immune response *in vivo* .

References:

Borkent, B. M., S. Gekle, et al. (2009). "Nucleation threshold and deactivation mechanisms of nanoscopic cavitation nuclei." Physics of Fluids (1994-present) **21**(10): 102003.

Cantrell, J. H., R. E. Goans, et al. (1978). "Acoustic impedance variations at burn–nonburn interfaces in porcine skin." The Journal of the Acoustical Society of America **64**(3): 731-735.

Jacobi, U., M. Kaiser, et al. (2007). "Porcine ear skin: an in vitro model for human skin." Skin Research and Technology **13**(1): 19-24.

König, K., K. Schenke-Layland, et al. (2005). "Multiphoton autofluorescence imaging of intratissue elastic fibers." Biomaterials **26**(5): 495-500.

Kwan, J. J., C. M. Coviello, et al. (2015). "Ultrasound-responsive gas-stablizing nanocups for tumor mapping and enhancement of drug delivery." ACS Nano **In submission**.

Mitragotri, S., D. A. Edwards, et al. (1995). "A mechanistic study of ultrasonically-enhanced transdermal drug delivery." J Pharm Sci **84**(6): 697-706.

Mitragotri, S. and J. Kost (2001). "Transdermal delivery of heparin and low-molecular weight heparin using low-frequency ultrasound." Pharm Res **18**(8): 1151-1156.

Moran, C. M., N. L. Bush, et al. (1995). "Ultrasonic propagation properties of excised human skin." Ultrasound in medicine & biology **21**(9): 1177-1190.

Scheuplein, R. J. (2010). Permeability of the Skin. Comprehensive Physiology, John Wiley & Sons, Inc.

Som, I., K. Bhatia, et al. (2012). "Status of surfactants as penetration enhancers in transdermal drug delivery." Journal of pharmacy & bioallied sciences **4**(1): 2.

Tang, H., C. C. Wang, et al. (2002). "An investigation of the role of cavitation in low-frequency ultrasound-mediated transdermal drug transport." Pharm Res **19**(8): 1160-1169.

Tezel, A., S. Paliwal, et al. (2005). "Low-frequency ultrasound as a transcutaneous immunization adjuvant." Vaccine **23**(29): 3800-3807.

Tezel, A., A. Sens, et al. (2002). "Investigations of the role of cavitation in low-frequency sonophoresis using acoustic spectroscopy." Journal of Pharmaceutical Sciences **91**(2): 444-453.

Tezel, A., A. Sens, et al. (2001). "Frequency dependence of sonophoresis." Pharm Res **18**(12): 1694-1700.

Waller, J. M. and H. I. Maibach (2005). "Age and skin structure and function, a quantitative approach (I): blood flow, pH, thickness, and ultrasound echogenicity." Skin Research and Technology **11**(4): 221-235.

Williams, R. M., W. R. Zipfel, et al. (2001). "Multiphoton microscopy in biological research." Current Opinion in Chemical Biology **5**(5): 603-608.

Wolloch, L. and J. Kost (2010). "The importance of microjet vs shock wave formation in sonophoresis." Journal of Controlled Release **148**(2): 204-211.

6. Cavitation-Enhanced Transdermal Vaccine Delivery and Immune Response in Vivo

In the work presented thus far, it has been shown that the proposed ultrasound-assisted transdermal vaccine delivery system is able to deliver detectable doses of FITC-labelled ovalbumin (OVA) to a depth of around 500 µm in *ex vivo* porcine skin. Additionally, it has been shown that cavitation-enhancing NCs are vital to achieve this level of OVA penetration depth and that the NCs themselves travel further into the skin than the FITC-labelled OVA, despite being over 70 times larger in size. Such penetration may be the result of cavitation-mediated self-propulsion of the particles deeper into the tissue.

In addition to demonstrating a favourable delivery profile of OVA in skin tissue, it is also important to demonstrate a therapeutic response. In the context of vaccine delivery, a therapeutic response can be defined as the elicitation of an immune response *in vivo*. The aim of this chapter is therefore the attainment and characterisation of an *in vivo* immune response to the model antigen OVA as a result of ultrasound-assisted transdermal vaccination using the system developed and optimised in this thesis.

In addition to reporting the longer term *in vivo* immune response to ultrasound assisted transdermal vaccination in mice, the delivery and distribution of fluorescently tagged OVA, NCs and an immunisation adjuvant, CpG, were examined in a short term study similar to the work presented in chapter 5. Blood and skin samples were taken from mice immediately post-delivery to assess safety and delivery. In a longer-term (41 day) study, the immune response of the mice treated with the ultrasound assisted system was compared to that elicited when OVA was administered by injection or with the aid of chemical transdermal penetration enhancers. Blood samples were taken from the mice to quantify antibody titres. Beyond the use of a hydrogel to deliver the vaccine and of nanoparticles to enhance inertial cavitation, a key innovation of both studies was the fact that inertial cavitation activity was measured in all mice during delivery using the previously described passive cavitation detection system.

OVA was selected for the work presented in this chapter due to its well documented ability to elicit an immune response in mice (O'Hagan, Jeffery et al. 1993; Tew, Wu et al. 1997; Zhang, Liu et al. 2003; Allan 2008; Li, Peng et al. 2011). Most studies detail work in BALB/c mice, a widely used albino, laboratory bred strain of mice commonly used for immunology, therefore BALB/c mice were used in this study.

An immunologic adjuvant is defined as *"any substance that acts to accelerate, prolong, or enhance antigen-specific immune responses when used in combination with specific vaccine antigens"* (Sasaki and Okuda 2000). In this study, CpG oligodeoxynucleotides (CpG ODN) were used for this purpose. CpG ODN are short single-stranded synthetic DNA molecules containing a cytosine triphosphate deoxynucleotide ("C") followed by a guanine triphosphate deoxynucleotide ("G"), linked by a phosphate linker ("p"). When these CpG motifs are unmethylated, they act as immunostimulants. CpG ODN was selected over other adjuvants (such as aluminium salts and oil based entities) as it is readily soluble in water and small in size, allowing transport within micro-streams formed during ultrasound exposure in the gel. Additionally, studies have shown it to be an effective adjuvant for inducing T-cell immunity in BALB/c mice when co-administered with OVA (Maletto, Rópolo et al. 2002).

The *in vivo* study presented in this chapter is therefore presented as two halves. An initial short-term study was performed to determine the delivery effectiveness of OVA, CpG and NCs in a manner similar to the work presented in chapter 5. Additionally, analysis of the OVA content in the gel couplant was performed before and after ultrasound exposure in an attempt to quantify the dose leaving the gel and entering the skin. In complement, OVA content within the skin immediately after treatment was also quantified. Acoustic, multi-photon microscopy (MPM) and histological analyses were performed as in chapter 5.

The second half of the *in vivo* study aimed to identify the presence of specific anti-OVA IgG in mouse serum 14 days after treatment. A widely used sandwich ELISA technique was implemented to determine and compare antibody levels in the treatment group against positive and negative controls to determine whether an immune response had been successfully elicited.

6.1. Methods and materials

6.1.1. Study design and experimental groups

40 five-week-old BALB/c female mice were obtained from the Biomedical Services Unit at the John Radcliffe Hospital (Oxford, UK). These 40 mice were divided into two 20 mice treatment groups consisting of a "Delivery and Distribution" (DD) arm and an "Immune Response" (IR) arm (figure 6.1). The purpose of the DD arm was to examine the penetration and passage of labelled OVA and NCs into murine skin, therefore these mice were culled on the day of treatment so that treated skin could be excised. Mice in the IR arm of the study were examined for the provocation of an immune response as a result of OVA treatment after 14 days. Blood samples were taken at 30min after treatment on day 0, and on day 14 and day 35 of the study for detection of anti-OVA antibodies. Retreatment to boost was performed on day 21. Individual experimental groups and the rationale for their selection are outlined in table 6.1.

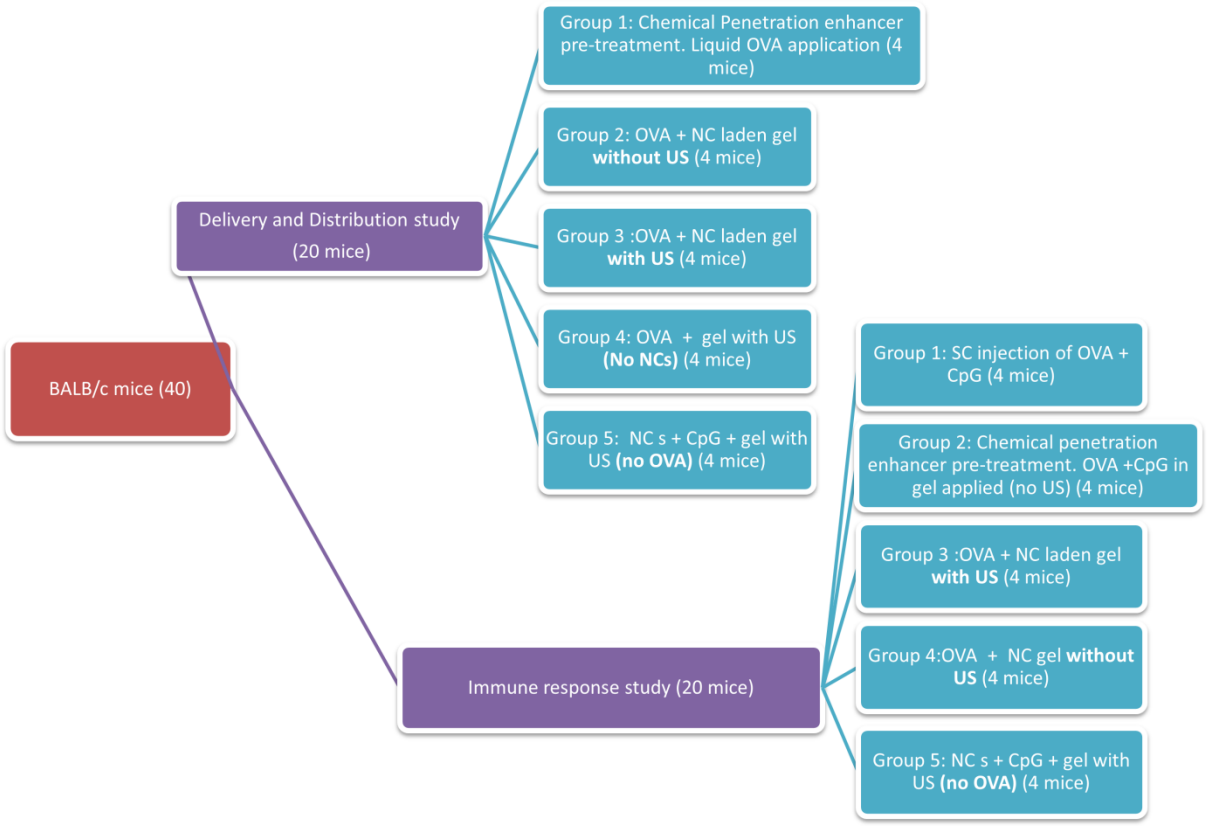

Figure 6.1: Experimental summary of ultrasound-assisted transdermal vaccination study design. 40 female BALB/c mice were divided into two lots of five groups of four (n=4) for the delivery and distribution study and the immune response study. Mice in the delivery and distribution study were bled 30 min after treatment, and culled immediately after to harvest the treated skin. Mice in the immune response study were treated at day 0, with a booster treatment on day 21 of the study. Mice were bled 30 min after treatment on day 0, at day 14 & on day 35 before sacrifice on day 42. Key: OVA = ovalbumin protein, NCs = nanocups, US = ultrasound.

Table 6.1: Experimental groups and rationale for selection.

Experimental Group	Description of Treatment	Rationale for Selection
Delivery and Distribution Study		
1. Chemical Penetration enhancer pre-treatment.	7% SDS applied to the skin for 120 s. Liquid FITC-OVA solution was then applied for 90 s.	Positive control. Chemical Penetration enhancers are used for skin permabilisation in current transdermal delivery studies (Cevc and Vierl 2010).
2. FITC-OVA + F-NC laden gel without ultrasound	FITC-OVA and F-NC laden gel applied to skin for 90 s, with no ultrasound exposure	Negative control for the effect of ultrasound on delivery
3. FITC-OVA + F-NC laden gel with US	FITC-OVA and F-NC laden gel applied to skin in the presence of ultrasound for 90 s.	Experimental condition
4. FITC-OVA + gel with US	FITC-OVA gel without F-NCs applied to the skin in the presence of ultrasound for 90 s.	Control condition to test for the significance of NCs
5. NCs +FITC- CpG + gel with US	Gel containing only NCs and FITC labelled CpG was applied with ultrasound for 90 s. There was no OVA present in this study	Group to examine the passage of CpG alone through the skin.
Immune Response Study		
1. SC injection of OVA and CpG	Subcutaneous injection of OVA (10 µg/mouse) with CpG (10 µg/mouse) in 100 µl PBS	Injection is the current gold standard for vaccine delivery.
2. Chemical Penetration enhancer pre-treatment	7% SDS applied to the skin for 120 s. OVA and CpG laden gel was then applied to the treated area for 90 s. (No US)	Chemical penetration enhancers are the current gold standard for transdermal delivery of drugs.
3. OVA + NC + CpG laden gel with US	OVA and NC laden gel with CpG applied to skin in the presence of ultrasound for 90 s.	Experimental condition
4. OVA + NC + CpG laden gel without ultrasound	OVA and NC laden gel with CpG applied to skin for 90 s, with no ultrasound exposure	Negative control for immune response to OVA+CpG on skin surface
5. NCs + CpG + Gel with US	Gel with only NCs and CpG applied to skin and insonated for 90 s	Negative control to determine the immune response in the absence of OVA

6.1.2. Couplant preparation

FITC-OVA and NCs stained with 9-anthracene (9AC-NCs) were prepared as outlined in chapter 5 (section 5.2.1). FITC-CpG and unlabelled CpG were obtained from Source Biosciences (Nottingham, UK) and reconstituted in sterile PBS. As both the FITC-OVA and 9AC-NCs were in liquid solutions, their addition to the 0.5% gel previously used significantly reduced gel viscosity from 2.9 Pa.s to around 0.5 Pa.s. For this reason, the gel concentration was increased to 2% so that leakage from the donor compartment was minimised. The viscosity of the 2% formulation was measured experimentally as 3.38 Pa.s. In order to keep gel viscosity and OVA concentration constant, deionised filtered water was added to the gel formulations that did not contain FITC-OVA or 9AC-NCs to replace the volume of fluid that would have been added otherwise. Exceptions to this were study group 1 from the DD study and groups 1 and 2 from the IR study, as liquid OVA was used in the absence of US. The OVA concentration in all of the formulated gels used on day 0 of each study was 1 mg/ml.

OVA and NCs used in the immune response study were untagged to prevent the presence of the dyes affecting the immune response. For the booster treatment, lower viscosity gel (0.5%, 0.5 Pa.s) was used to maximise the possibility of microstreaming mechanisms to enhance OVA transport into the skin. Additionally, OVA concentration in the booster gel was increased to 2.5 mg/ml and CpG dose per mouse was increased to 30 μg to increase the possibility of a measureable anti-OVA antibody in blood samples. Gel recipes for each study arm and treatment are shown in table 6.2.

Table 6.2: Gel formulations.

Delivery and Distribution Study				
Study group	FITC-OVA solution (2 mg/ml) (for n=4)	9AC -Nanocup solution (for n=4)	2% gel (for n=4)	FITC-CpG
1	8 ml (4 mg/mouse)		0	0
2	8 ml (4 mg/mouse)	4 ml (1 ml/mouse)	4 g (1 g/mouse)	0
3	8 ml (4 mg/mouse)	4 ml (1 ml/mouse)	4 g (1 g/mouse)	0
4	8 ml (4 mg/mouse)	0 (1 ml H_2O/mouse)	4 g (1 g/mouse)	0
5	0 (2 ml H_2O/mouse)	4 ml (1 ml/mouse)	4 g (1 g/mouse)	40 µg (10 µg/mouse)

Immune Response Study – Treatment 1 (day 0)				
Study group	OVA (unlabelled) solution (2 mg/ml) (for n=4)	Nanocup (unlabelled) solution (for n=4)	2% gel (for n=4)	CpG (unlabelled) required
1	40 µg (10 µg/mouse)	0	0	40 µg (10 µg/mouse)
2	8 ml (4 mg/mouse)	0	0	40 µg (10 µg/mouse)
3	8 ml (4 mg/mouse)	4 ml (1 ml/mouse)	4 g (1 g/mouse)	40 µg (10 µg/mouse)
4	8 ml (4 mg /mouse)	4 ml (1 ml/mouse)	4 g (1 g/mouse)	40 µg (10 µg/mouse)
5	0 (2 ml H_2O/mouse)	4 ml (1 ml/mouse)	4 g (1 g/mouse)	40 µg (10 µg/mouse)

Immune Response Study – Treatment 2 – Boost (day 21)				
Study group	OVA (unlabelled) solution (5 mg/ml) (for n=4)	Nanocup (unlabelled) solution (for n=4)	0.5% gel (for n=4)	CpG (unlabelled) required
1	200 µg (50µg/mouse)	0	0	120µg (30µg/mouse)
2	8 ml (10mg/mouse)	0	0	120µg (30µg/mouse)
3	8 ml (10mg/mouse)	4 ml (1 ml/mouse)	4 g (1 g/mouse)	120µg (30µg/mouse)
4	8 ml (10mg/mouse)	4 ml (1 ml/mouse)	4 g (1 g/mouse)	120µg (30µg/mouse)
5	0 (2 ml H_2O/mouse)	4 ml (1 ml/mouse)	4 g (1 g/mouse)	120µg (30µg/mouse)

6.1.3. Ultrasound setup and mouse model

A 9 cm^2 area at the side of the mouse abdomen (above the hind leg) was shaved and depilated (using Veet hair removal cream) 24 hours prior to treatment to allow (1) hair removal for effective sealing of the donor compartment, and (2) time for the skin barrier to recover from the depilatory treatment. Immediately prior to treatment, the mice were sedated with anaesthesia (2% isofluorane and 98% oxygen; flow rate at 2 L/min) and the donor compartment was placed onto the skin surface and secured using masking tape. 4 mL of the coupling gel formulation was filled into the donor compartment and the

transducer lowered down onto the mouse to allow for ultrasound transmission. The cone was filled with 0.2 µm pore-size filtered degassed deionised water before ultrasound treatment commenced.

Mice in groups 3, 4 and 5 of the DD study, and groups 3 and 5 of the IR study were subjected to US exposure for a total exposure time of 90 s. The ultrasound parameters were 256 kHz frequency, 1 MPa peak negative acoustic pressure, 10% duty cycle (10 ms on, 90 ms off) at a pulse repetition frequency of 10Hz. The setup described in chapter 5 (section 5.1.1) was modified to ensure a watertight seal between the cone and the donor compartment, and the donor compartment and the skin of the mouse. Modifications to the cone are shown in figure 6.2. In the first modification, the end of the cone was sealed with a plastic cap sealed with a sheet of mylar to prevent water leakage onto the mouse. This plastic cap was lowered onto a modified donor compartment containing the vaccine with a shaft with an O ring on the surface that was to rest on the anaesthetised mouse. Using this setup, the ultrasound field and focus position within the donor compartment remained identical to the characterisation shown in figure 5.1.

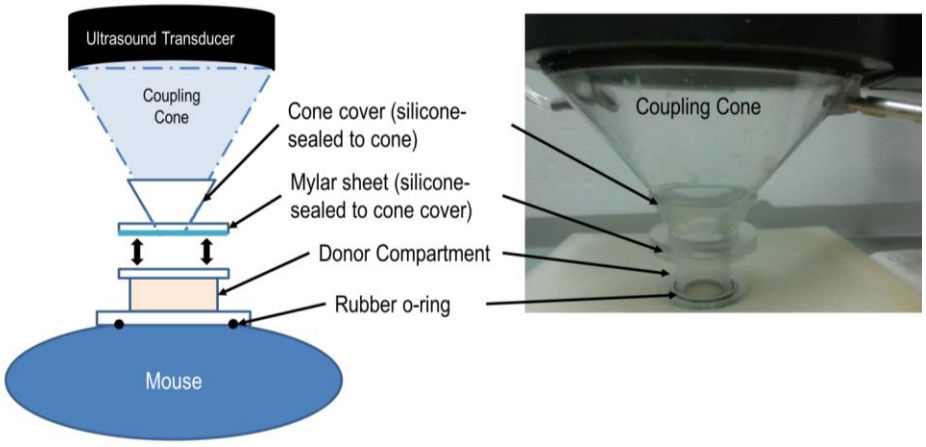

Figure 6.2. Modified *in vivo* ultrasound setup (left: schematic, right: photograph). Two new parts were added. The first on the end of the cone to prevent water leakage, and the second was a modified donor compartment to prevent the leakage of gel around the mouse due to the uneven surface.

6.1.4. Investigations

6.1.4.1. Delivery and Distribution Study

6.1.4.1.1. Measurement of OVA content in donor gel

In an attempt to track and quantify the delivery of the OVA to the skin, a purchased OVA Enzyme-linked immuno-sorbent assay (ELISA) kit (Agro Bio, Germany) was used to quantify levels of OVA in samples of donor gel taken before and immediately after treatment, so that transfer of OVA into the skin might be measured in terms of its loss from the donor layer.

6.1.4.1.2. Monitoring of acoustic emissions from couplant

Acoustic emissions from the ultrasound focus (positioned within the donor gel) were recorded for each ultrasound exposure. An identical setup to that used in chapter 5 was implemented, and the same algorithm used to filter out harmonic emissions and quantify broadband emissions.

6.1.4.1.3. Excised skin studies

Within 10 minutes following treatment, mice were sacrificed and the skin in the treatment area excised. Skin from one mouse from each experimental group was fixed in formalin for histology. Skin from the second and third mice in each group was flash frozen in liquid nitrogen for tissue ELISA to identify the OVA dose in the skin (described in “OVA dose in excised skin” below). The fourth skin sample was placed in a petri dish, refrigerated at 4°C, and subjected to MPM analysis within 3 hours. Following MPM analysis, this sample was also flash frozen in nitrogen for OVA ELISA.

<u>Histological studies</u>

Skin sections were fixed in formalin solution (10%, Product HT501128, Sigma Aldrich, UK) immediately after harvest. Alternate sections were sliced and stained with H&E to detect skin damage. Slides were imaged on a Nikon Ti microscope (CFI S Fluor 40x objective, NA = 0.9)

OVA dose in excised skin

Skin sections that had been flash frozen were first rinsed in ice-cold phosphate buffered saline (PBS) (Sigma-Aldrich, UK) to remove blood, and then weighed and homogenised. PBS was added to the samples at a concentration of 1 mL PBS/100 mg skin and homogenised on ice. The resulting suspension was sonicated on ice with an ultrasonic cell disruptor (Microson Ultrasonic cell disruptor, Misonix, NY, USA) and then centrifuged for 5 min at 5000 x g. The supernatant was removed and stored at -20°C until assay. An OVA Enzyme-linked immuno-sorbent assay (ELISA) kit (Agro Bio, Germany) was used to quantify levels of OVA in the tissue homogenate.

MPM analysis

One skin sample from each group was imaged using MPM as described in chapter 5.2. Immediately before imaging, fluorescent red 2 µm beads were once again used to demarcate the skin surface. Due to the small size of the tissue samples, only two areas per skin sample were imaged. Image stacks were analysed for depth distribution of OVA and NCs using the same algorithm implemented in chapter 5.2.

6.1.4.2. Immune Response Study

6.1.4.2.1. Treatment regimen

As stated previously, two treatments in the IR study were performed. The first treatment, on day 0 of the study used a gel formulation identical to the short term DD study, except that the OVA and NCs were no longer fluorescently tagged. The fluorophores were eliminated as these would not be present in clinical use, and because tracking was not required for the purposes of the study. Treatment was performed as described in the DD study, with a 90 s exposure at 1MPa PRFP/256kHz frequency, and following treatment the skin was wiped clean with a damp paper towel. Treatment 2 was performed as a booster to treatment 1, on day 21 of the study (figure 6.3).

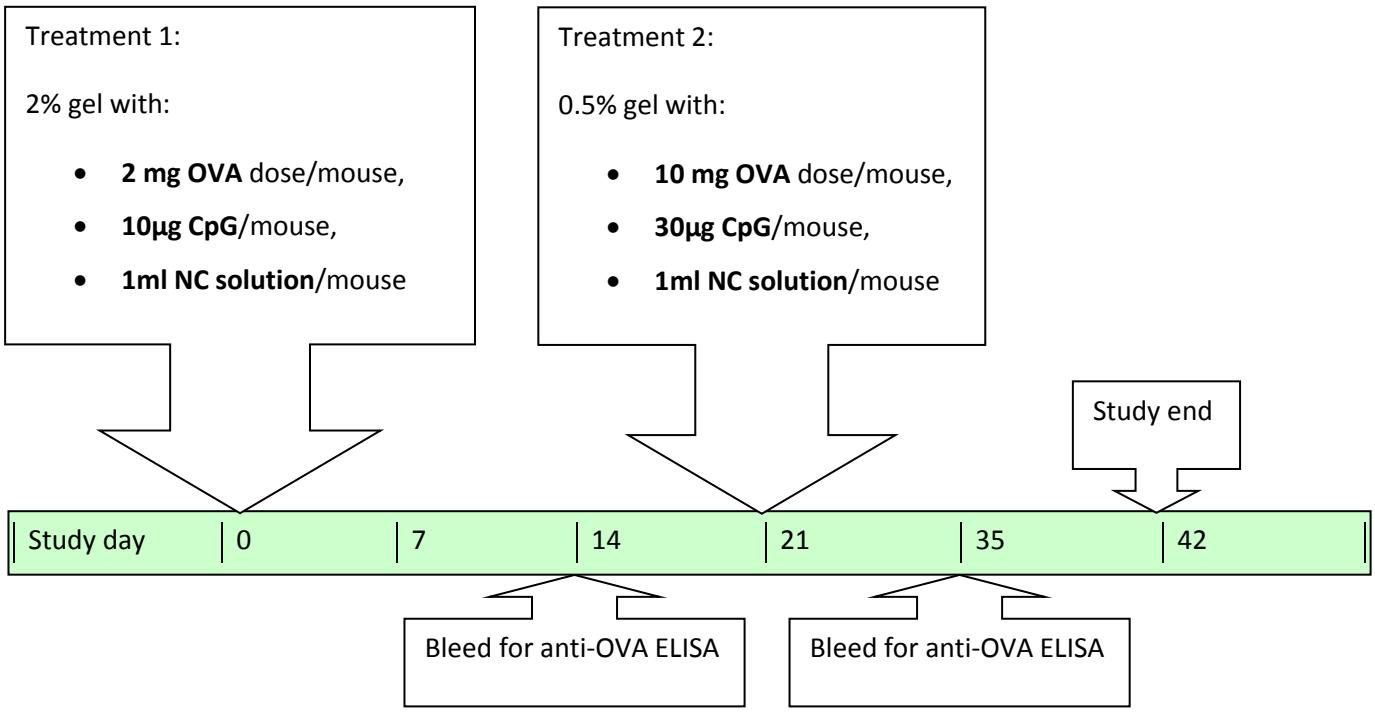

Figure 6.3: Timeline for immune response study.

6.1.4.2.2. Detection of complement response

For the detection of a complement response to the vaccine, CpG or the NCs after treatment, a purchased C3a ELISA detection kit (OptEIA, BD Biosciences, CA, USA) was used for quantitative determination of C3a-desArg in murine serum samples taken 30 min after treatment. Complement response is part of the innate immune system and activates within minutes of pathogen detection, and therefore, if a complement response is present, it is detectable 30 min after treatment.

6.1.4.2.3. Detection of specific immune response to OVA

In order to determine whether an immune response specific to OVA had been elicited in the mice, blood samples (20 µL) were taken from each mouse on day 0 (before treatment as a baseline), day 14 (to examine the levels of anti-OVA antibody produced in response to treatment 1) and day 35 (to examine a

response to booster treatment). Blood was diluted in 180 µL PBS (1:10 dilution) and centrifuged for 3 minutes at 3000 rpm. The supernatant was removed and frozen at -20°C prior to analysis.

An enzyme linked immunosorbent assay (ELISA) was used to reliably and sensitively determine the binding, and therefore the presence and levels of, antibodies to proteins of interest. The purpose of ELISA in this study was to detect the levels of specific anti-OVA IgG antibodies present in the blood serum. OVA was diluted to 1 µg/mL and 50 µL of this solution was added to each well of a Nunc-Immuno Maxisorb flat-bottom 96-well plate (Fisher Scientific, UK). The plate was sealed with a transparent plastic plate sealer and incubated overnight at 4°C. Following incubation, the plate was washed with PBS-Tween (0.5%) 6 times to remove any unbound OVA. Bovine serum albumin (5% w/v) was used as a blocking agent, and 50 µL of diluted serum was added to the wells and incubated for 1 hour at room temperature before removal.

Serum samples (1:10 dilution) were diluted further for testing to 1:20 dilution in PBS and after the removal of the BSA solution, 50 µL was added to each well. Each serum sample was tested in triplicate and every experimental group contained serum from at least 3 ($n \leq 3$) mice. The samples were sealed and incubated for 1.5 hours at room temperature before the plate was washed 6 times with PBS-Tween. Goat anti-mouse IgG secondary antibody-HRP (Santa Cruz, USA) was diluted 1:5000 in PBS and 50 µL added to each well before 1 hour incubation at room temperature. Following incubation, the plate was washed 6 times with PBS-Tween and 50 µL of TMB substrate (80091; Alpha Diagnostic International Inc., US) was added to each well and left to develop at room temperature for 30 min. 50 µL of stop solution (80100; Alpha Diagnostics International Inc., US) was added to each well. All ELISA plates were read at absorbance wavelength 450 nm on a FLUOstar Omega plate reader (BMG Labtech, Germany). One way ANOVA Bonferroni multiple comparison tests were performed for all samples at the same

concentration; the results are represented by *, ** and *** corresponding to $p< 0.05$, 0.01, and 0.001 respectively.

6.2. Results and Discussion

6.2.1. OVA delivery study

The OVA delivery study had two main aims: (1) investigation of whether the treatments caused damage the skin to the point of irritation and injury, and (2) identification of the delivery profile of ovalbumin *in vivo.* Determining the delivery profile of OVA was necessary in order to correlate the amount of delivered OVA to the response elicited in the mouse. For this purpose, a number of investigations were used to assess (1) treatment safety, (2) OVA penetration depth, and (3) OVA penetration dose relative to controls. Treatment safety, i.e. the damage to the skin surface, was assessed using histological sectioning and staining to allow visualisation of the skin surface immediately following treatment, and treated groups were compared to control skin with no treatment. Next, delivery profile was examined in 3D using MPM (as described in chapter 5) and delivery depth was determined from the 3D images using the same algorithms implemented in chapter 5. In order to determine penetration dose, the transfer of OVA from the couplant to the skin was investigated by measuring the OVA content in (1) the couplant before and after ultrasound treatment to identify if any OVA had moved, and (2) the skin itself following treatment to determine dose efficiency of the procedure. Finally, acoustic emissions from the coupling gel during treatments that involved ultrasound exposure were examined to determine any correlation between delivery and inertial cavitation activity in the gel.

6.2.1.1. Treatment safety

In any proposed transdermal treatment application, the treatment must not cause irreversible or functional damage to the skin surface to the point where it is unable to protect the body from incoming pathogens. For this reason, SC integrity was assessed after each treatment. Possible causes of skin damage in this experiment included (1) damage caused by mechanical mechanisms from ultrasound exposure and inertial cavitation, or (2) chemical disruption from agents in the gels or skin pre-treatment. Figure 6.4 shows cross sectional histological sections of treated skin stained with hematoxylin and eosin (H&E) stain to enable visualisation of the different skin layers and structures within them. Panel (a) shows non-treated skin with SC intact and the epidermis and dermis clearly demarcated for comparison.

Assessment of the damage caused by ultrasound exposure can be performed by comparing images in panels (c) and (e) to panel (a). Panel (c) (without US exposure) shows minor disruption of the uppermost layers of the SC probably caused by the application of a wet gel to the skin surface causing occlusion and therefore some disruption when compared to non-treated skin. This extent of disruption is present in all of the gel treatment groups regardless of ultrasound application and was undetectable on visual examination of the skin pre-excision. Additionally minor SC damage on this order heals within hours, and can therefore be assumed to be non-harmful. The lack of significant difference between panels (c) and (e), indicates that US application did not cause structural damage to the SC, even in the presence of NC mediated high levels of inertial cavitation (figure 6.4(e)).

Among the currently used transdermal permeability enhancement modalities, chemical penetration enhancers are known for causing irritation and damage to the skin. Chemical permeability enhancement is performed with the aim of reducing the barrier properties of the SC, and despite being reversible in most cases, causes vulnerability to external pathogens. Healing time from chemical insult from this treatment can also take several days, leaving the skin vulnerable for a considerable amount of time

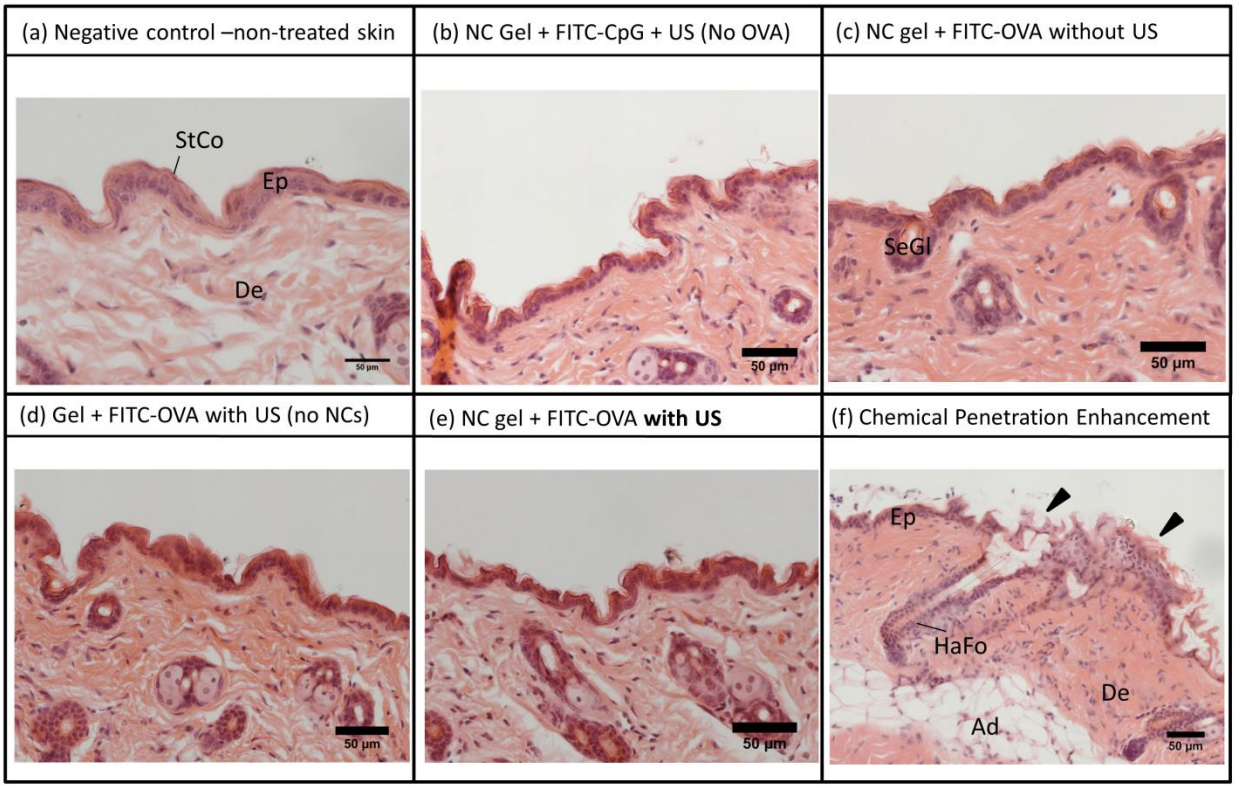

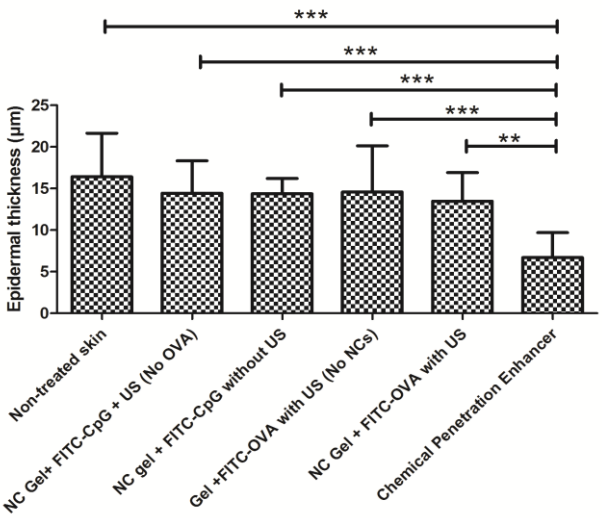

Figure 6.4: (Top) Cross sectional images of Haemotoxylin and Eosin stained histological slides of murine skin after each of the treatment regimens tested. In all images, ultrasound was applied from the top downwards onto the skin surface. Key: StCo = Stratum corneum, Ep = Epidermis, De = Dermis, Ad = Adipose tissue, HaFo = Hair follicle, SeGl = Sebaceous gland. (Left) Comparison of epidermal thicknesses between treatment groups. *** and ** represent $p<0.001$ and $p<0.01$ respectively in one way ANOVA test.

(Wang, Olson et al. 2000). Chemical damage to the SC was demonstrated in this study (figure 6.4f, arrows). Application of SDS to the skin as a pre-treatment resulted in SC breakdown to the point where it was no longer attached to the skin, and in some cases, epidermal detachment occurred (shown by arrows, figure 6.4(f)). On this basis, the epidermal thicknesses of skin in the different treatment groups were examined using ImageJ. Comparison of epidermal thickness reveals that the epidermis in the chemical penetration enhancer group was significantly decreased compared to every other treatment group, without any significant differences between the other groups (figure 6.5).

From the results of this investigation, 7% SDS when used as a chemical penetration enhancer is unsuitable for use due to skin damage and safety concerns. In contrast, US application appeared to do no damage to the SC and resulted in the desired short-term disruption necessary for transdermal vaccine delivery.

6.2.1.2. 3D Delivery profile and OVA penetration depth

In order to quantify penetration depth, the same MPM methodology presented in chapter 5 was used. One notable difference observed when switching from a porcine to murine model was that murine skin is much thinner than porcine skin, so epidermal depths were on the order of 20 µm, as opposed to 100 µm in pig skin. Penetration depths in murine skin were therefore much smaller than in porcine skin (as shown in figure 6.5), but this does not mean that the vaccine did not reach its intended target. Furthermore, due to the thinness of the murine skin samples, the z resolution used to obtain these 3D datasets (5 µm per z slice though the depth of the stack) was not fine enough to capture exact delivery profiles for OVA and the NCs. This methodology used could be improved in subsequent experiments, but for this study it was useful to give an overall qualitative indication of the OVA delivery distribution.

Qualitative evidence of low dose transfer was apparent in these images, however doses of OVA (observed as green in figure 6.5) were substantially lower than those seen in the porcine experiments

presented in chapter 5. This is most likely to be because the gel used in the murine study was 4 times more viscous than the gel used in the porcine delivery studies. Increased gel viscosity was due to ease of use with the mouse, as a more viscous gel was less likely to leak out of a holder during ultrasound exposure. However, increased viscosity undoubtedly hindered the acoustic microstreaming mechanisms that promoted OVA delivery. In future experiments, optimisation of the gel holder will allow use of the less viscous gel formulation. Significant differences in OVA delivery were not detected in the absence of US or NCs. OVA penetration in skin subjected to chemical pre-treatment was significantly higher than the other control groups. Penetration of OVA to depths of around 150 µm (figure 6.6) is hypothesised to be due to the removal of the epidermal layer, and therefore boundary of the SC, as shown in figure 6.4. Delivery in the US assisted vaccine delivery group was also substantial, and quantitative analysis of the penetration depth performed in MATLAB (figure 6.6) showed that the penetration depth was around 200 µm.

Due to their smaller size and ability to self-propel in the presence of inertial cavitation, NCs have been shown to travel deep into the skin upon ultrasound exposure. In this study, NCs were seen to consistently travel at least as far and in greater amounts than OVA. In the ultrasound assisted transdermal vaccine delivery system group, the highest dose of NCs was found at around 300 µm depth, which is into the dermis of murine skin. Vaccine loading of the NCs would represent one of the next key areas of research in the development of this system.

As discussed in chapter 5, natural collagen in the skin was also visualised in the blue channel, and therefore figure 6.5b includes shaded blue regions where fluorescence in the blue channel cannot be verified as either collagen or cups. Mean intensity and depth for collagen auto-fluorescence was calculated as described in chapter 5. In the groups that did contain NCs there was substantial signal beyond this range, therefore NC signal was still detectable over the collagen auto-fluorescence.

Upon examination of the passage of FITC-labelled CpG through the murine skin (figure 6.5, leftmost column), there was some penetration of both NCs (blue) and CpG (green). This is thought to be the result of three effects in combination. Firstly, US was used to induce cavitation in the gel to propel the CpG molecules into the skin. Secondly, NCs were present to enhance this effect, and they themselves have been observed to pass through the skin with relative ease. Finally, the molecular weight of CpG oligonucleotides is 6.3 kDa; approximately a tenth of the molecular weight of OVA (45 kDa), making the microstreaming-assisted passage of CpG through the gel much more effective than that of OVA.

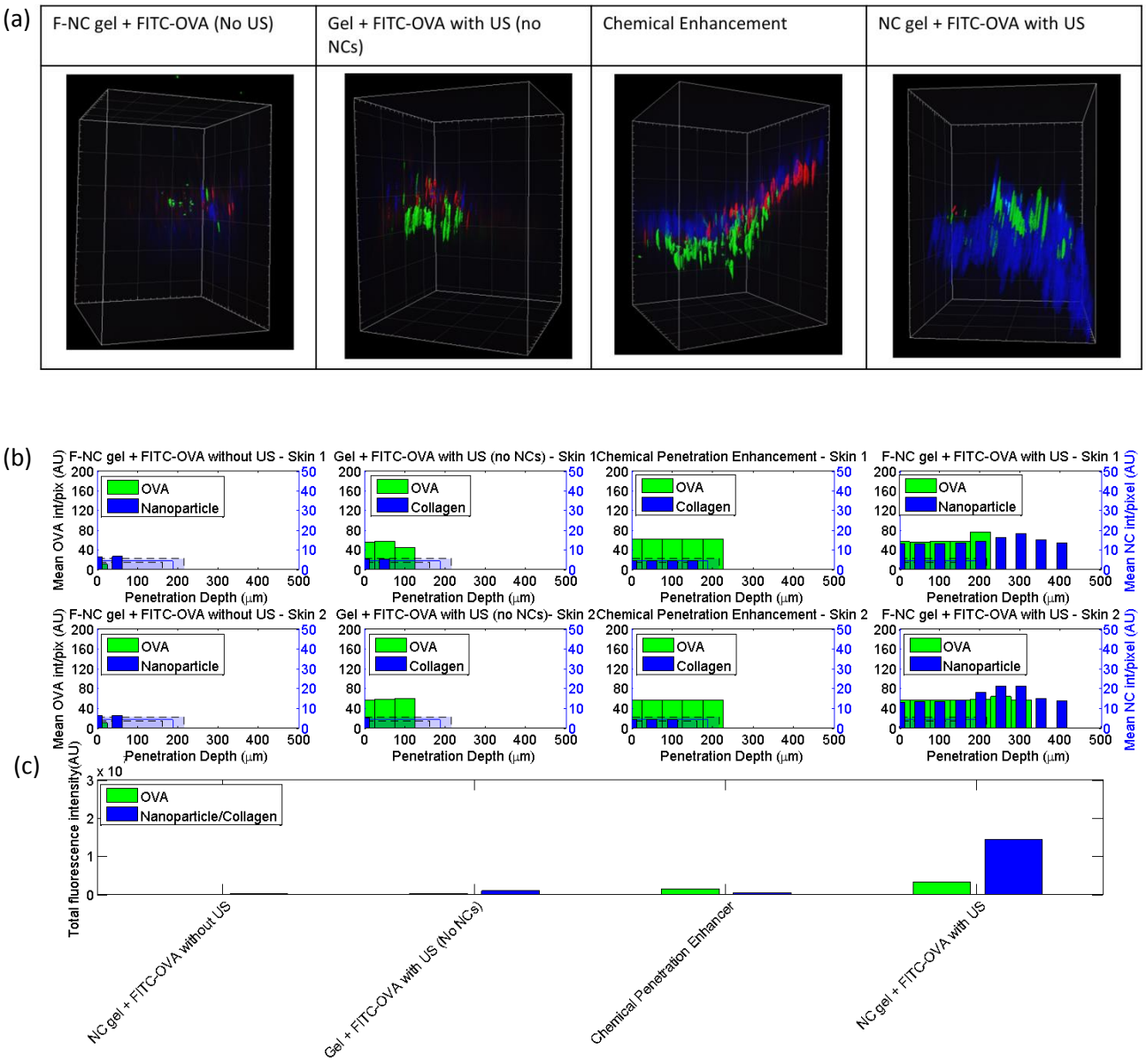

Figure 6.5: (a) 3D profiles of a single representative image stack from each OVA treatment group. Quantitative analysis of depth for each treatment (b) and dose (c) for each treatment condition involving OVA. 2 skin areas were sampled from each treatment group. Shaded blue box represents the background fluorescence of collagen, determined from the average depth and intensity of collagen in untreated samples in the absence of NCs (dotted lines and shaded areas represent 1 standard deviation from the mean).

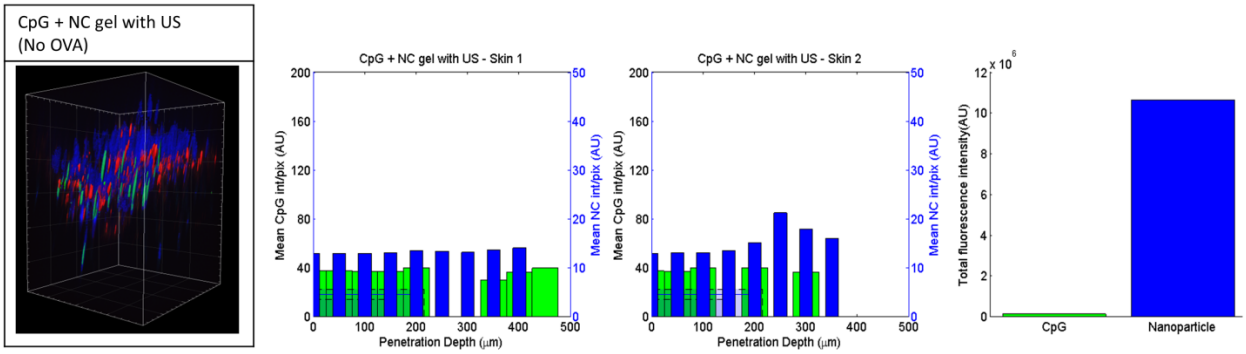

Figure 6.6: (left) 3D profile of a single representative image stack from the CpG (no OVA) treatment group. (middle and right): Quantitative analysis of depth for CpG/NC treatment (as in figure 6.5).

6.2.1.3. OVA dose delivery

6.2.1.3.1. OVA removal from couplant

In a vaccine delivery modality where there is expected to be a dose efficiency (meaning only a percentage of the administered dose will reach its therapeutic target), it is of paramount importance to have a methodology to non-invasively monitor the amount of vaccine that is delivered that is independent of the therapeutic effect of delivery. With a view to tracking the OVA delivery in this experiment, OVA concentration in the couplant was measured before and after treatment to investigate whether there were any detectable differences. The results of this investigation are shown in figure 6.7.

There were no statistical differences detected in the coupling gels before and after ultrasound treatment in all treatment groups except the transdermal vaccination group (OVA and NC gel with US), meaning that if some OVA had been transferred to the skin in these groups, the amount was below the resolution of the assay used. The one significantly different result ($p = 0.038$, two tailed T-test) was associated to the US-assisted system developed in this thesis and showed a concentration decrease from 1 mg/ml to 0.91 mg/ml in the gel, representative of a 9% decrease in OVA content. Because no

significant differences existed between any of the other groups, it was initially assumed that the delivery efficiency was very low.

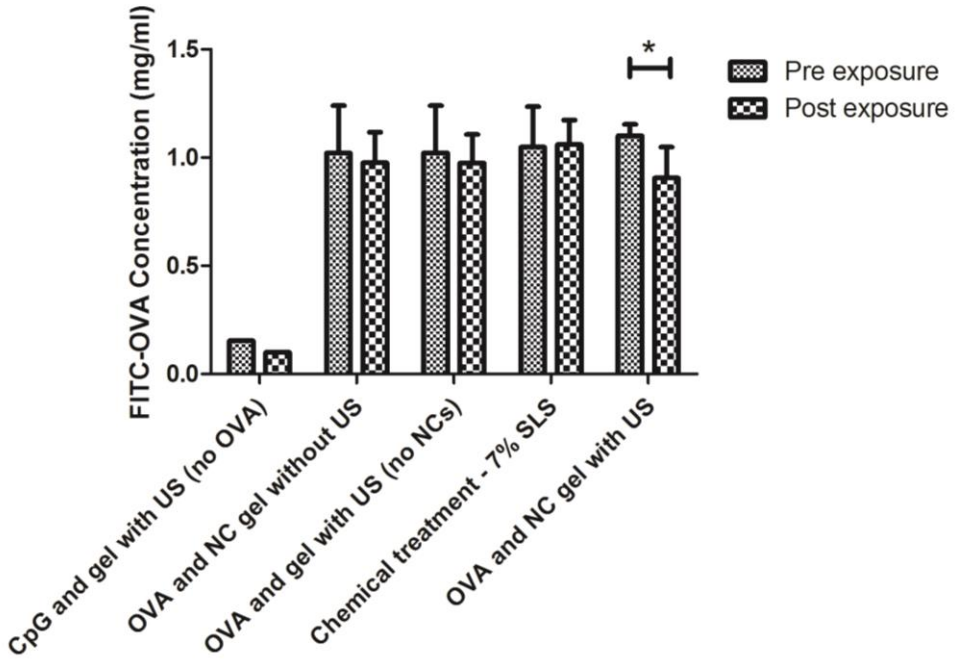

Figure 6.7: Concentration of OVA in the coupling gel before and after ultrasound exposure for each of the treatment conditions. * represents $p<0.05$ using a one tailed Student's T-test. n=4 for each group except the CpG and gel with US (No OVA) group, where n=2.

6.2.1.3.2. OVA dose in excised skin

Previous results recording the removal of OVA from the coupling gel suggested that substantial amounts of OVA were not moving into the skin during ultrasound application. However, to characterise this further, OVA content in the skin was examined. As described in the methods section, the same OVA detection ELISA kit was used to quantify OVA levels in homogenised skin samples from the mice, taken 5 minutes after treatment. Results of this investigation are shown in figure 6.8. It is worth highlighting that in order to remove excess OVA and avoid artificially high readings, mouse skin was wiped with a damp

paper towel after treatment, therefore OVA concentration detected may represent an underestimate of the true OVA transfer due to removal of superficially delivered OVA.

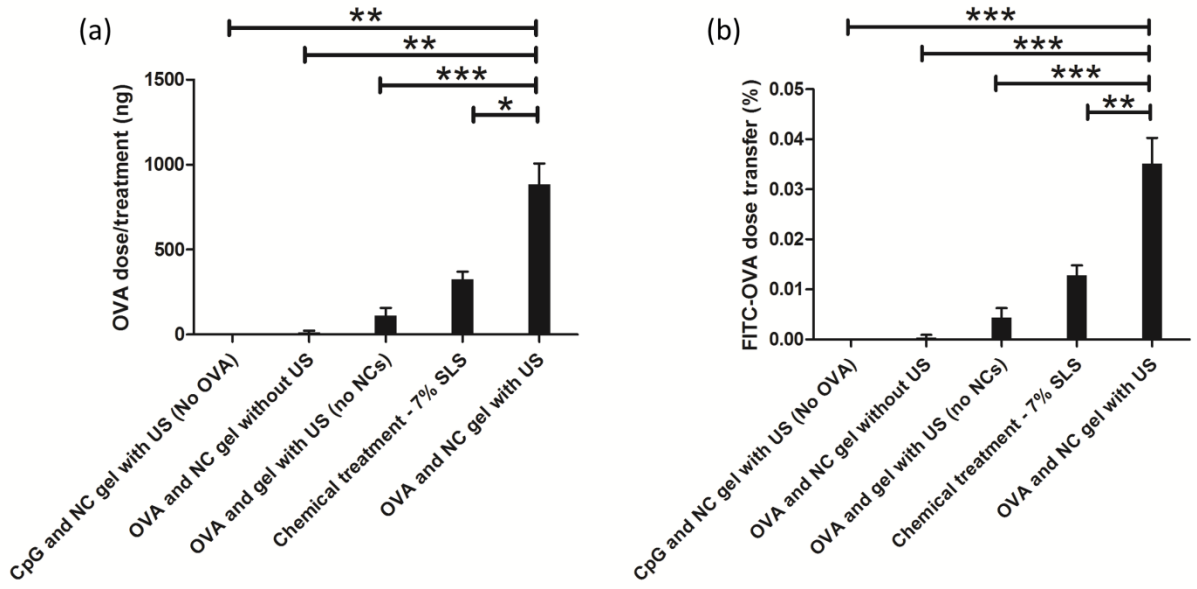

Figure 6.8: (a) Average OVA dose delivered in a single mouse for each treatment examined. (b) FITC-OVA dose transfer of OVA from the couplant to the skin, used as a measure of delivery efficacy. *, ** and *** represent p values of <0.05, 0.01 and 0.001 respectively using a one way ANOVA with Bonferroni multiple comparisons tests. n=4 for each group except the CpG and gel with US (No OVA) group, where n=2.

Figure 6.8(a) shows the average OVA dose achieved to the skin (regardless of skin sample size) in each treatment group. The dose delivered to the skin is zero in the treatment group that contained no OVA, and this result confirms the reliability of the assay that was used. Application of the gel to the skin in the absence of ultrasound showed some delivery (on the order of 10's of nanograms), but this was not statistically different to the no OVA group, indicating this treatment regimen's lack of utility. Upon the application of US but in the absence of cavitation inducing nanoparticles, OVA delivery increased further (on the order of 100 ng), but once again this result was not statistically different to either of the

previous two groups. The addition of chemical penetration enhancer pre-treatment increased dose approximately 3-fold, but delivery was highest (nearly 1 μg) in the ultrasound assisted vaccine delivery group, which was substantially (3-fold) and statistically ($p<0.05$) higher than the chemical penetration enhancer group, as well as every other group tested.

A delivery dose of 1 μg per treatment is comparable with delivery dose seen in other ultrasound assisted vaccination techniques. A previous *in vivo* study showing transdermal delivery of tetanus toxoid vaccine using low frequency (40 kHz) ultrasound as a pre-treatment prior to the application of a vaccine loaded patch for 2 hours showed a delivery dose of 1.3 μg, which generated an immune response comparable to that induced by a 10 μg subcutaneous injection (Tezel, Paliwal et al. 2005). Compared to alternative methods of transdermal vaccine delivery, 1 μg per treatment represents a low dose, mostly because delivery methods such as microneedles have a very high delivery efficiency. However, in a separate study, dose sparing with microneedles was specifically studied in mice with OVA as the model vaccine. At low dose (1 μg), specific antibody titers from microneedles were one order of magnitude greater than subcutaneous injection and two orders of magnitude greater than intramuscular injection (Matriano, Cormier et al. 2002). The same study also showed that for higher OVA doses (20-80 μg) the delivery method did not affect the immune response, and high levels of antibody titres (showing that a sufficient dose of antigen had been delivered) had been achieved. Clinically relevant vaccine doses in humans vary widely, depending on factors such as the vaccine and the age of the patient. The clinically delivered vaccine dose using the ultrasound assisted vaccine delivery system described in this thesis is also directly affected by the skin of the patient. Therefore, the assessment of whether doses achieved with this system are clinically useful will depend on these factors.

Figure 6.8(b) translates the doses delivered in each treatment from figure 6.8(a) into the percentage of the total dose in the coupling gel that was delivered into the skin. The same trend is observed, with the

ultrasound-assisted vaccine delivery system showing the highest dose transfer. Moreover, upon comparison to figure 6.5, the same trend is observed, with the greatest amount of OVA being removed from the coupling gel in the same group that the highest concentration is present in the skin.

However, the extremely low dose transfer efficiency (at best, 0.04% of the total), and the significant discrepancy between a 9% decrease in OVA concentration (representing an OVA loss of 22,500 ng) in the couplant and the ~800 ng average dose found in the skin in the ultrasound assisted transdermal vaccination group is a cause for concern. Hypothesised reasons for these discrepancies include that a substantial amount of OVA was resting on the surface of the skin (having left the gel during treatment) and was wiped off the skin and lost immediately after treatment. Poor ultrasound coupling between the gel applicator and cone, or applicator and mouse may have caused low ultrasound transmission resulting in substantially decreased inertial cavitation activity and therefore reduced delivery. Distortions of the acoustic field in the presence of the mouse may have also resulted in significant reflections of the ultrasound. Additionally, low dose transfer efficiency may be related to the size and shape of the gel applicator itself. Although the US focus encompassed around 80% of the gel layer and beyond, OVA molecules at the top of the gel may not have had sufficient time or propulsion to move down and enter the skin. Future designs of a gel application device will be shorter in height to allow easier passage and therefore more efficient transfer of the vaccine contained in the gel to the skin.

6.2.1.4. Acoustic emissions from couplant

In the treatments that involved ultrasound exposure, the passive cavitation detector (PCD) fitted inside the HIFU transducer (as described in chapter 3) was used to passively monitor cavitation emissions from the HIFU focus to quantify the amount of inertial cavitation activity occurring. Figure 6.9 shows spectrograms of acoustic emissions during all treatments where US was used. Additionally, in an attempt to try to correlate broadband emissions from the focus to delivery dose, the delivered OVA doses are also displayed on all the spectrograms except those where OVA was not delivered.

As shown in previous work described in chapter 5, the addition of nanoparticles to the coupling gel increased both the power and duration of broadband emissions; characteristic of increased inertial cavitation activity. Additionally, higher power and duration of broadband emissions resulted in greater delivery of OVA to the skin by at least an order of magnitude.

Particularly of note is the fact that in this study, gel viscosity was increased from 0.5 Pa.s to 3.38 Pa.s. This was done to prevent leakage from the gel holder before and during ultrasound application. However, as a result of increased gel viscosity, cavitation mechanisms such as microstreaming were dampened, and this effect can be seen by comparing the second row of spectrograms in figure 6.9 to the spectrogram in figure 5.4(b) as both are plotted on the same colour scale. Both represent the same couplant conditions except for the altered gel viscosity, and it can be seen that both the power and duration of broadband acoustic emissions at the focus are reduced when gel viscosity is increased. It is hypothesised that the delivery of OVA was therefore also adversely affected by the increased gel viscosity, which may have contributed to the low OVA transfer efficiency.

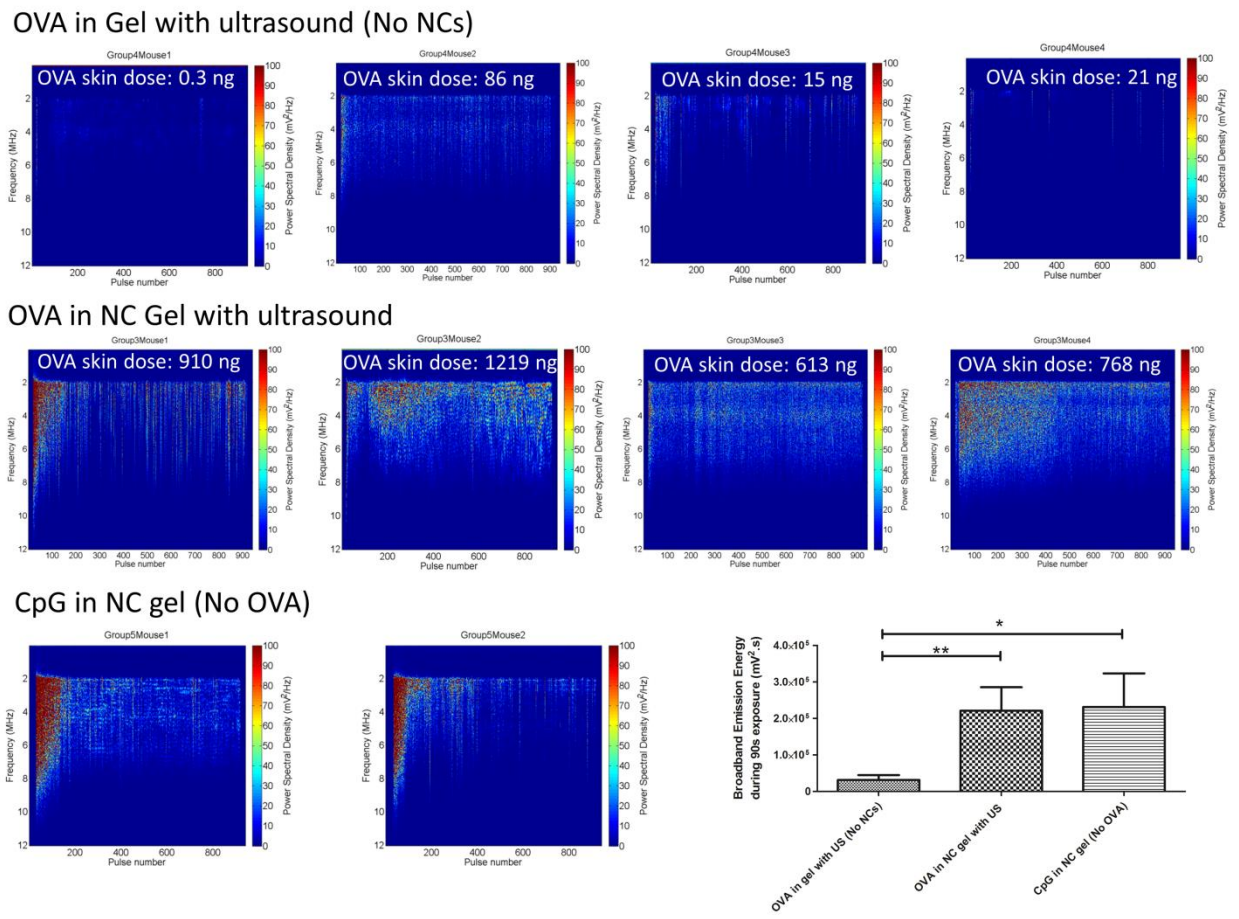

Figure 6.9: Acoustic emissions from the HIFU focus for each of the treated mice in the short term delivery study. Gels were exposed to 256 kHz ultrasound at a PRFP of 1 MPa for 90s. Pulse length was 10ms, and PRF was 10Hz. Acoustic emissions were recorded using a PCD, the focus of which was coaxially aligned with the HIFU focus. Received PCD signals were 2 MHz high-pass filtered before amplification (28dB) and presented in spectrograms as frequency content across each pulse, which also corresponds to exposure time (900 pulses = 90s at 10Hz PRF). Bar chart (bottom right) shows average and SD of total broadband acoustic emissions for each treatment condition.

6.2.2. OVA Immune Response *in vivo*

The main long term *in vivo* study aim was to investigate whether an immune response could be elicited with the ultrasound assisted transdermal vaccine delivery system. The elicitation of the immune response was assessed by a comparison of the levels of specific anti-OVA IgG antibodies in mouse blood at 14 days after treatment versus before any treatment. The initial treatment at day 0 of the study was identical to that described in the short term study, except that the OVA and NCs were not labelled. A higher viscosity (2%) gel was also used. Quantification of anti-OVA IgG in treated mice at day 14 (using the ELISA technique outlined above), showed that levels were not significantly different from day 0 in any treatment group except the direct injection positive control.. Therefore, a vaccine boost was administered on day 21 of the study, with a higher OVA concentration (2.5 mg/ml vs. 1mg/ml), a higher CpG dose (30 μg/mouse vs. 10 μg/mouse) and the gel viscosity was decreased to 0.5% from 2% to allow better exploitation of microstreaming-mediated transport. All of these measures were put in place to maximise the likelihood of OVA delivery. Between day 0 and day 14 of the study, the experimental setup was optimised so that a less viscous gel would not leak out of the holder, and therefore use of the 0.5% gel was possible. Blood was taken on day 35 (14 days after the boost) to re-examine anti-OVA antibody levels.

In addition to identifying a specific immune response to OVA, blood taken from mice 30 min following treatment was also assayed for serum levels of C3a to determine if a complement response had occurred in response to the treatment. Acoustic emissions were also examined from the booster treatment to compare the differences in broadband activity in the gel formulations of varying viscosity.

6.2.2.1. Identification of a specific immune response

The primary objective of the work performed in this chapter was to demonstrate a specific anti-OVA immune response as a result of ultrasound-assisted transdermal vaccine delivery in an *in vivo* model. A sandwich ELISA technique was used to quantify levels of anti-OVA IgG in the day 35 serum samples, and average absorbance readings (over 4 mice) for each treatment group are shown in figure 6.10.

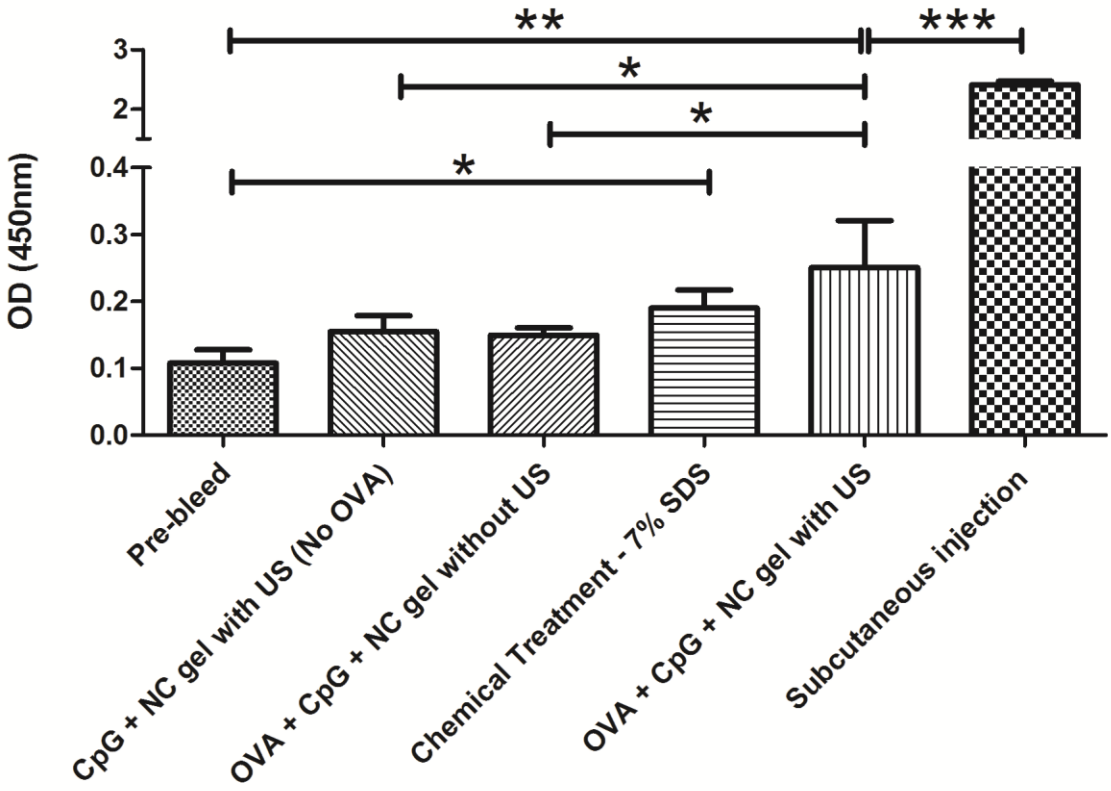

Figure 6.10: Anti-OVA IgG antibody levels in all of the treatment groups on day 35 of the study. Mice were bled and serum diluted in PBS before being applied to a Nunc Maxisorp 96 well plate for analysis using a standard anti-OVA ELISA technique as described in methods. OD = optical density (absorbance). n=4, standard deviation shown, significant differences determined by one-way ANOVA Bonferroni multiple comparison tests. ***, ** and * = $p< 0.05, 0.01, 0.001$ respectively.

In this study, optical density (absorbance) was used as a proxy for antibody concentration for the purposes of comparison between treatment groups. Determination of endpoint titres was attempted, but due to the low levels of antibody in the serum (samples were diluted to only 1:20 dilution for ELISA) it was not possible to identify the entire sigmoidal curve and reliably determine endpoints in terms of absorbance signal. However, because statistically significant differences exist between absorbance levels for different treatment groups, it is hypothesised that a response, albeit small, was in fact observed. This conclusion is strengthened by the data from the short term study, which suggested that there was a very low dose transferring to the skin at all, leading to the low response.

Figure 6.10 shows that in the absence of OVA and US, there were no significant differences in antibody levels compared to the pre-bleed (non-treated) mice, indicating that treatment in these groups had not been successful. The lack of OVA was the reason for the lack of response in the no OVA group. In the absence of US (and therefore permeability enhancement of the SC) the vaccine remained on top of the skin and did not gain access to epidermal Langerhans cells. Only the chemical penetration enhancement, the ultrasound and NC assisted transdermal vaccination, and the subcutaneous injection groups showed significantly different antibody levels to the pre-bleed mice, demonstrating successful delivery. In this study, subcutaneous injection was used as the positive control, and illustrates the antibody response at 100% dose delivery. Interestingly, the ultrasound/NC assisted system outperformed the chemical penetration enhancer group, which represented the transdermal treatment positive control. These results indicate that for a relatively low dose transfer from the couplant to the skin, a detectable specific immune response could be mounted. Unfortunately, it was not possible to detect the exact dose transfer for the booster treatment in this study as the mouse skin could not be excised without sacrifice of the mouse. Future studies will aim to address this issue to identify the relationship between dose delivered and cavitation response at the parameters used in the booster treatment. This investigation therefore serves as a proof of concept study that the ultrasound assisted

transdermal vaccination system developed in this thesis is capable of mounting a detectable and specific immune response to OVA.

6.2.2.2. Complement response to treatment regimes

The complement system is composed of a large number of distinct plasma proteins that react with each other to label pathogens for destruction (opsonization) by phagocytes and induce a series of inflammatory responses that help to fight infection. The complement cascade can be activated in three distinct ways on pathogen surfaces that depend on different molecules for their initiation, but the pathways converge to generate the same set of effector molecules (Janeway, Travers et al. 2001).

C3a is a complement fragment that acts on specific receptors to produce local inflammatory responses. When produced in large amounts it can induce a generalised anaphylactic shock, and so is often termed an anaphylotoxin (Janeway, Travers et al. 2001). In this study, C3a concentration was specifically examined to verify *in vivo* that none of the administered components (the NCs in particular) were causing such a response. Figure 6.11 demonstrates no significant differences in C3a concentration in serum between all of the treatment groups, indicating the absence of a complement response, and therefore inflammation, to the nanocups, OVA and CpG. It was especially important to verify that the cavitation-enhancing NCs did not cause complement activation and therefore would not bias immune responses to NCs as opposed to the administered OVA. Previous studies have demonstrated that immune responses to OVA to involve both production of anti-OVA specific antibodies on a humoral level, and $CD4^+$ and CD8 T- cell responses at the cellular level, with an absence of complement activation, therefore the result of this study is consistent with other work.

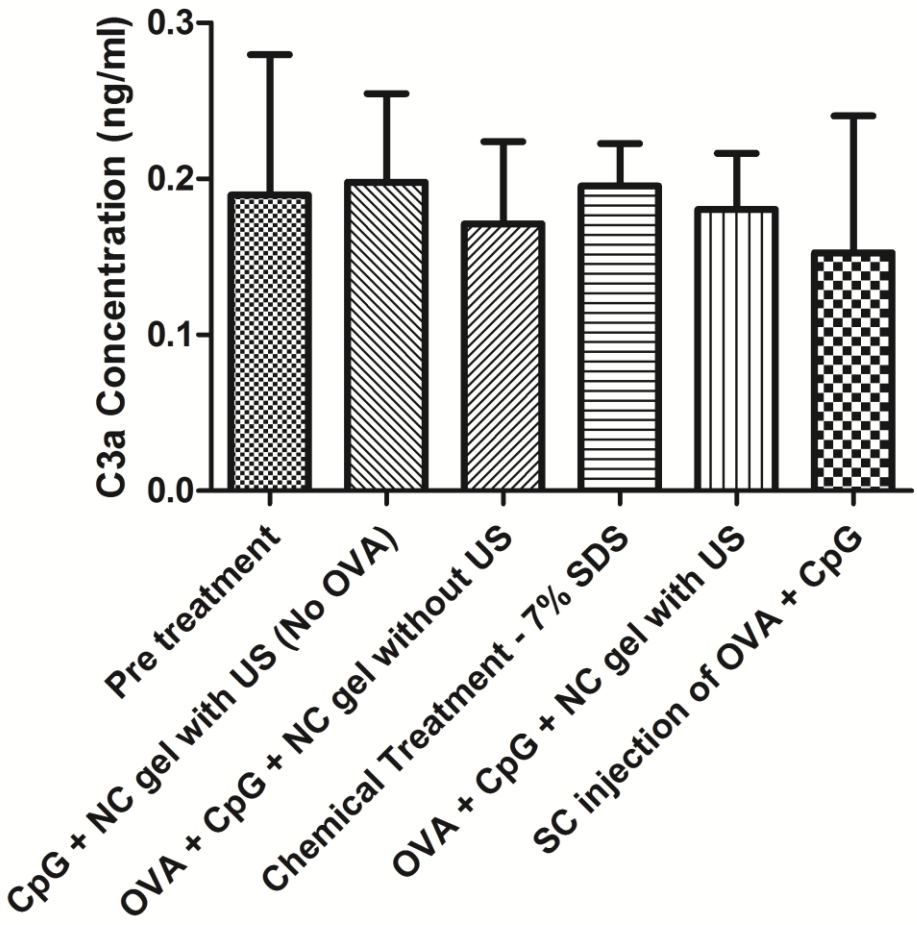

Figure 6.11: Complement concentrations in mouse serum 30 mins after treatment in all of the treatment groups, compared to the non-treated (pre bleed) mice. Serum was diluted in PBS and a C3a detection kit was used to quantify levels in post-treatment serum. For all groups, n=4, error bars show standard deviation.

6.2.2.3 Acoustic emissions from booster treatment (day 21)

As mentioned previously, the increased gel viscosity in the initial treatment is likely to have decreased the levels of inertial cavitation, and therefore levels of OVA transport within the gel. Figure 6.12 shows spectrograms from all of the treatments performed in the booster regimen with ultrasound. Upon comparison with figure 6.9, it can immediately be seen that the power and duration of broadband

acoustic emissions is greater with the lower viscosity gel. Bar graphs on each of these figures show the total broadband energy released during a single treatment for each group, and demonstrate that the total energy released when the lower viscosity gel is used is an order of magnitude higher (figure 6.12) than when the higher viscosity gel is used (figure 6.9), even in the presence of NCs. Therefore, it is hypothesised that both the absolute dose, and the dose transfer from the gel would have been higher in this booster treatment than in the initial treatment. As mentioned previously, unfortunately it was not possible to quantify (by way of a short term study) the dosage efficiency and absolute delivered dose, but this will be a topic of further study.

Both treatment groups represented in figure 6.12 incorporated NCs in the gel, and it is clear that emission spectra from sample to sample (even within the same gel sample over multiple treatments) can vary widely. This could be a result of NCs being inhomogeneously dispersed throughout the gel, with areas of higher and lower concentrations and therefore periods of time when many NCs were activated and periods where NCs were sparse. Additionally, if the majority of the NCs were in the upper region (nearest the transducer) of the gel and were insonated and depleted in the first part of the exposure, the broadband emissions from the remainder of the exposure would have been markedly reduced (as in Group3 Mouse1 spectrogram in figure 6.12).

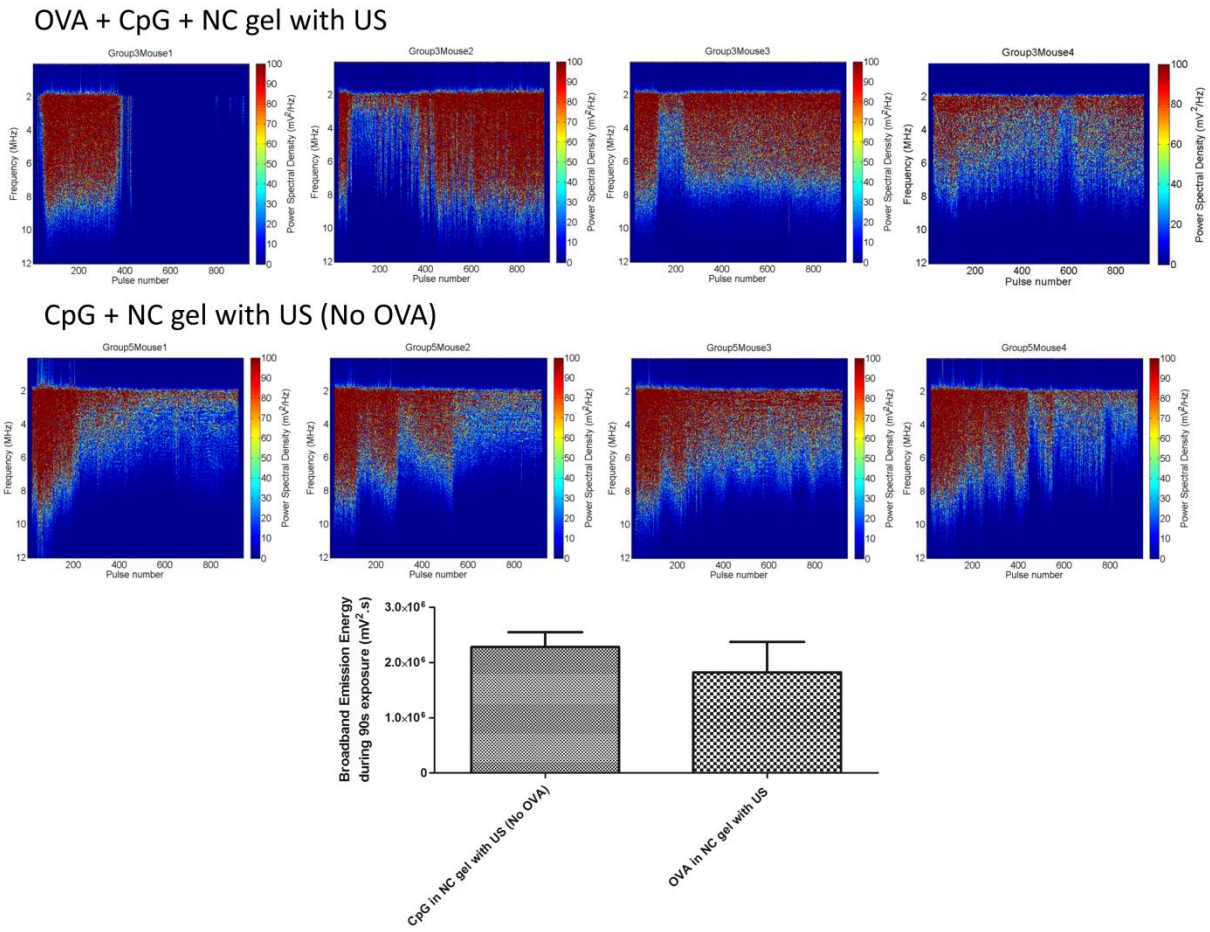

Figure 6.12: Acoustic emissions from the HIFU focus for each of the treated mice in the booster treatment of the long term immune response study. Row 1 (top) represents the ultrasound assisted transdermal vaccination system group, and row 2 (middle) is the response with NC gel and CpG in the absence of OVA. Gel viscosity for these experiments was 0.5 Pa.s. Bar chart (bottom) shows average and SD of total broadband acoustic emissions for each treatment condition.

6.3. Summary

In summary, the short term OVA delivery and distribution study has shown that the use of US with NC mediated-cavitation to assist transdermal delivery of OVA does not do any long term or severe damage to the skin, and is suitable for use for this application. In contrast, the alternative transdermal approach of chemically perturbing the skin caused considerable damage.

The delivery profile of OVA was quantified using identical MPM protocols to those used in chapter 5. Delivery was less substantial both in depth and dose, but this was a result of the thinness of murine skin compared to porcine. Penetration was greatest in the chemical pre-treatment group due to chemical removal of the epidermis, but there was substantial delivery in the US assisted transdermal treatment to depths of up to 200 μm. NCs were consistently seen to penetrate deeper than OVA, and this is thought to be due to their ability to self-propel upon exposure to ultrasound. The passage of FITC-labelled CpG (adjuvant) was also examined, and was seen to penetrate to depths of 300-400 μm owing to its smaller size and propensity to be transported through acoustic micro-streaming processes. An attempt was made to track the delivery of OVA by measuring changes in OVA concentration in the coupling gel before and after ultrasound, but any changes in OVA concentration were below the resolution of the assay used. In terms of quantification of dose delivered, it was observed that around 0.04% of the dose present within the gel was found in the skin, when ultrasound and NCs were used. Although low compared to direct injection, this level was substantially (2-fold) and significantly ($p<0.01$) greater than the level of transfer achieved using the alternative transdermal approach of chemical disruption of the SC.

The level may be so low because (1) the size and shape of the gel applicator may fail to fully exploit the micro-streaming effects of ultrasound exposure, and (2) loss of OVA due to wiping of the skin following treatment. In future studies, increasing the dose efficiency of this system represents a key area of study.

Analysis of acoustic emissions showed that when NCs were present, broadband emissions from the HIFU focus were both more powerful and longer in duration than in gel without NCs. The presence of NCs in the gel, and therefore higher levels of broadband emissions originating from inertial cavitation events at the focus also coincided with significantly higher OVA dose delivery to the skin.

The long term immune response study demonstrated that despite what is believed to be a relatively low dose transfer of OVA from the couplant to the skin, a detectible level of OVA specific antibodies were detected in the mouse serum in response to an initial dose + booster treatment of ultrasound/NC assisted transdermal vaccination. Additionally, following the booster, the ultrasound/NC assisted transdermal vaccination system developed in this thesis outperformed the current gold standard in transdermal delivery (chemical penetration enhancers) in terms of eliciting a specific anti-OVA response. The absence of a complement response to any of the administered agents (OVA, NCs or CpG) demonstrated that a harmful inflammatory response was not instigated. Acoustic data from the booster treatment with a low viscosity, high dosage gel showed increased levels of inertial cavitation, leading to the conclusion that decreased gel viscosity is more conducive to inertial cavitation (indicated by increased broadband emissions) and therefore higher levels of delivery.

It is hoped that optimisation of the technologies and approaches described here will help the field of transdermal vaccination progress so that reliable and robust needle free vaccination can be achieved.

References:

Allan, S. (2008). "Vaccines: Explaining alum: immunologists' dirty little secret." Nat Rev Immunol **8**(5): 320-320.

Cevc, G. and U. Vierl (2010). "Nanotechnology and the transdermal route: A state of the art review and critical appraisal." Journal of Controlled Release **141**(3): 277-299.

Janeway, C. A., P. Travers, et al. (2001). Immunobiology: the immune system in health and disease, Churchill Livingstone.

Li, N., L.-h. Peng, et al. (2011). "Effective transcutaneous immunization by antigen-loaded flexible liposome in vivo." International journal of nanomedicine **6**: 3241.

Maletto, B., A. Rópolo, et al. (2002). "CpG-DNA stimulates cellular and humoral immunity and promotes Th1 differentiation in aged BALB/c mice." Journal of Leukocyte Biology **72**(3): 447-454.

Matriano, J., M. Cormier, et al. (2002). "Macroflux® Microprojection Array Patch Technology: A New and Efficient Approach for Intracutaneous Immunization." Pharmaceutical Research **19**(1): 63-70.

O'Hagan, D. T., H. Jeffery, et al. (1993). "Long-term antibody responses in mice following subcutaneous immunization with ovalbumin entrapped in biodegradable microparticles." Vaccine **11**(9): 965-969.

Sasaki, S. and K. Okuda (2000). The Use of Conventional Immunologic Adjuvants in DNA Vaccine Preparations. DNA Vaccines. D. Lowrie and R. Whalen, Humana Press. **29:** 241-249.

Tew, J. G., J. Wu, et al. (1997). "Follicular dendritic cells and presentation of antigen and costimulatory signals to B cells." Immunological reviews **156**(1): 39-52.

Tezel, A., S. Paliwal, et al. (2005). "Low-frequency ultrasound as a transcutaneous immunization adjuvant." Vaccine **23**(29): 3800-3807.

Wang, J. F., M. E. Olson, et al. (2000). "Molecular and Cell Biology of Skin Wound Healing in a Pig Model." Connective Tissue Research **41**(3): 195-211.

Zhang, X. Y., X. G. Liu, et al. (2003). "Anti-T-cell humoral and cellular responses in healthy BALB/c mice following immunization with ovalbumin or ovalbumin-specific T cells." Immunology **108**(4): 465-473.

7. Conclusions and Future Work

7.1. Conclusions

The exploitation of inertial cavitation for ultrasound-assisted vaccine delivery presents a number of major advantages that are not offered from other modalities. In addition to being safe, inexpensive, and non-invasive, cavitation-mediated transdermal delivery has the capability to simultaneously deliver therapy whilst being monitored remotely; it is a marker of its own success.

The primary objective of this thesis was the development of a non-invasive ultrasound-assisted transdermal vaccination system that was also immunologically effective. Previous literature in the ultrasound assisted transdermal vaccination field, notably journal articles by Professor Samir Mitragotri and his research group, previously demonstrated (1) successful permeabilisation of the SC with acoustic cavitation mechanisms, and (2) activation of the Langerhans cells by ultrasound exposure. However, all published studies had done so with liquid delivery systems which are not practical, and where investigators were not overly concerned about drug transport. The work presented in this thesis aimed to address these issues.

A gel vaccine dosage formulation was chosen over a liquid based product in order to mimic current clinically approved and established ultrasound coupling formulations. In Chapter 1, fundamental principles of vaccine delivery and the different delivery routes were discussed, followed by an in-depth analysis of opportunities and limitations with respect to the transdermal route. Although previous literature has shown that Langerhans cells resident in the epidermis are capable of eliciting a systemic immune response, the stratum corneum (SC) is widely recognised as the major barrier to the vaccine entry. Therefore, SC permeabilisation techniques were assessed for effectiveness and potential. Together, this literature suggested that upon safe permeabilisation of the SC, transdermal vaccine delivery represented a viable delivery route.

Chapter 2 discussed the possibility of using inertial cavitation mechanisms instigated by ultrasound to achieve the required permeabilisation of the SC. Here we mentioned the basic physical principles governing ultrasound wave production and propagation. The ways in which ultrasound interacts with biological tissues was reviewed, which indicated that inertial cavitation is effective at permeabilising the skin surface. However, these studies did not investigate the capability of inertial to increase the *transport* of a drug or vaccine into the skin.

An ultrasound-assisted transdermal vaccine delivery system is a combination of two distinct elements: (1) a dosage form that contains the vaccine in a formulation from which it can be transdermally delivered, and (2) an ultrasound source that facilitates increased skin permeability and enhances vaccine transport from the dosage form into the skin. Chapter 3 addressed the ultrasound source and successfully demonstrated that ultrasound-induced inertial cavitation was able to enhance the transport of molecules of size similar to vaccine molecules through a tissue mimicking hydrogel. Other mechanisms, such as acoustic radiation force and small levels of heating (< 2°C increase in temperature) had little impact on transport. The work presented in Chapter 4 aimed to select a suitable combination coupling gel and dosage medium for an ultrasound assisted transdermal vaccine delivery system. Formulations were examined for consistent acoustic properties within and between batches. Cavitation thresholds of gels were identified and compared. A formulation was selected based on acoustic and chemical properties of native gel. This chapter also demonstrated the utility of cavitation nuclei to decrease the cavitation threshold. By producing the same level of acoustic emissions from a medium at much lower pressures, the system required less than 50% of the power requirement with cavitation nuclei than without. Nanocups (NCs), a novel gas-stabilising solid nanoparticle, were shown to be highly effective at generating inertial cavitation and lowering thresholds and were recommended for use, particularly as they were confirmed to have no adverse chemical effects on the vaccine within the gel.

Following the acoustic characterisation results, vaccine stability within the different gel formulations was investigated. Three separate analyses for protein structure demonstrated that BSA and OVA are stable to ultrasound exposure at the optimised exposure parameters within all of the gel formulations, both with and without cavitation nuclei. Therefore, the acoustically superior NCs were formulated within the optimal gel formulation.

Work presented in chapter 5 demonstrated vaccine delivery using the proposed ultrasound assisted vaccination system in biological tissue. Initially, a re-optimisation of ultrasound parameters was performed as the initial 10 s exposure time chosen to enable enhanced transport was insufficient for skin permeabilisation. desired measurable but small permeability increase reflected by a 15% change in conductivity was achieved with an exposure time of 90 s, therefore the total ultrasound exposure time was extended for all subsequent experiments. Results demonstrated OVA penetration of up to 500 μm, and NC penetration to up to 700 μm depth beyond the skin surface. At these depths, both OVA and NCs are distributed throughout the epidermis and the upper dermal layers. Therefore, OVA penetration was sufficient to access immunogenic Langerhans cells in the epidermis. An ultrasound pre-treatment group was also introduced to the demonstrate the utility of ultrasound to both permeabilise and aid active transport of the vaccine into the skin: OVA penetration depth when molecules were reliant on diffusion through US permeabilised skin was less than 50% of that observed when active transport of OVA molecules could occur due to simultaneous exposure of gel and OVA to ultrasound on the skin surface. The limited increase in OVA penetration observed with US pretreatment alone counters the idea that channels created by the penetration of the nanocup projectiles are primarily responsible for the enhanced penetration of OVA. Our results suggest that inertial cavitation needs to be occurring at the same time as OVA delivery, and confirms our initially proposed mechanism of cavitation-mediated microstreaming as the primary means of enhanced mass transport into the skin.

Such *ex vivo* data provided a compelling case for *in vivo* investigation to test for the elicitation of an immune response as a result of delivery. Chapter 6 presents the two arms of the *in vivo* study: (1) a short term study examined the delivery profile of OVA and NCs in murine skin achieved through ultrasound-assisted transdermal vaccination compared to the current transdermal gold standard treatment – chemical penetration enhancers and (2) a long-term study that tested for an OVA-specific antibody response in the mice two weeks after vaccination and compared it to the current gold standard in vaccine delivery - subcutaneous injection. The short term OVA delivery study showed that the use of US with NC mediated-cavitation to assist transdermal delivery of OVA does not do any long term or severe damage to the skin, in contrast to the alternative transdermal approach of chemically perturbing the skin which caused considerable damage. Delivery was less substantial than the *ex vivo* study both in depth and dose, but this was a result of the increased gel viscosity used in the murine study to prevent leakage of the vaccine gel formulation from the holder. Penetration depth was greatest in the chemical pre-treatment group due to chemical removal of the epidermis, but there was also substantial delivery in the US assisted transdermal treatment to depths of up to 200 µm. NCs consistently penetrated the skin deeper than OVA, due to both their size allowing them to be carried in microstream currents in the gel as well as their ability to self-propel upon ultrasound exposure. The FITC-labelled CpG (adjuvant) was seen to penetrate to depths of 300-400 µm owing to its smaller size and propensity to be transported through acoustic micro-streaming processes. OVA dose in skin immediately after treatment was significantly ($p<0.05$) higher in the ultrasound assisted transdermal vaccination group than the chemical penetration enhancer (positive control) group, showing effective delivery of doses up to 1 µg. In clinical terms, this is a modest dose, but bearing in mind the mechanism of delivery, there is a strong possibility that increasing the ultrasound exposure time would result in proportional delivery increases. In terms of dose efficiency however, the dose delivered to the skin was around 0.04% of the applied dose. Although low compared to direct injection, this level was substantially (2-fold) and significantly ($p<0.01$) greater

than the level of transfer achieved using the alternative transdermal approach of chemical disruption of the SC. Low dose efficiency was attributed to (1) the size and shape of the gel applicator which failed to fully exploit the micro-streaming effects of ultrasound exposure, and (2) loss of OVA due to wiping of the skin following treatment. Analysis of acoustic emissions showed that when NCs were present, broadband emission energy from the HIFU focus over the whole treatment was an order of magnitude more powerful and remained sustained compared to gel without NCs. Significant increases in OVA dose delivery were also seen when NCs were present in the gel.

The long term immune response study demonstrated that despite a relatively low dose transfer of OVA from the couplant to the skin, a detectible level of OVA specific antibodies were produced *in vivo* in response to an initial dose and booster treatment of ultrasound/NC assisted transdermal vaccination. Additionally, following the booster, the ultrasound/NC assisted transdermal vaccination system developed in this thesis outperformed the current gold standard in transdermal delivery (chemical penetration enhancers) in terms of eliciting a specific anti-OVA response. Acoustic data from the booster treatment with a low viscosity and high dosage gel showed increased levels of inertial cavitation. We thus concluded that decreased gel viscosity is more conducive to inertial cavitation (indicated by increased broadband emissions) and therefore higher levels of delivery. A low viscosity gel is, however, superior to a fluid because of the clinical applicability and approved regulatory status of gels.

In summary, ultrasound induced inertial cavitation is capable of not only permeabilising skin, but also enabling active transport of molecules. Additionally, heating and mechanical effects of inertial cavitation do not adversely affect the structural integrity of protein molecules such as OVA and BSA when suspended in a gel formulation, even when the gel is seeded with cavitation-enhancing nanoparticles. Through exploitation of this effect, it has been shown that model vaccine molecules (such as OVA) can be delivered to the epidermis *ex vivo,* where it is possible to trigger a systemic immune response via the

Langerhans cell network. The size of NCs allow them to be transported via microstreams formed in a medium during ultrasound exposure) as well as due to the propulsion provided by bubbles collapsing on their surface. In combination, this enables greater penetration during ultrasound exposure into tissues than a molecule reliant on diffusion and active transport through micro-streaming. Additionally, due to their size, they travel relatively unhindered (compared to cavitation nuclei such as talc) through the pores of the skin extracellular matrix.

Finally, not only is the ultrasound-assisted vaccine delivery system developed in this thesis capable of favourable delivery profiles, but these delivery profiles were shown to result in a vaccine specific antibody response *in vivo* that was significantly higher than that of all the other transdermal delivery methods tested, serving as a proof-of-concept for a transdermal vaccine delivery system. Although the delivery efficiency, and the antibody response was not as large as subcutaneous injection, there is a large scope for system optimisation.

The ultrasound assisted vaccination approach taken in this thesis offers a number of advantages over other methods of vaccine delivery via the skin. Once optimised, the system presented in this thesis will represent a significant improvement upon other ultrasound assisted methods as it has demonstrated the exploitation of ultrasound for both permeabilisation and molecular transport purposes. Microneedles are by far the most developed non-ultrasound technology in this field and represent a key competitor to the ultrasound-assisted system as they are capable of efficiently delivering large doses of a number of vaccines to the epidermis. However, despite eliminating the pain associated with conventional injections, they can still cause inflammation and local irritation, possibly leaving the skin prone to infection, whereas skin permeabilisation as a result of cavitation has been shown to heal within hours.

The key usability advantages of this system are therefore that it eliminates sharps waste from vaccinations, is non –invasive, and involves the use of a clinically relevant and easily used gel formulation. Furthermore, potential exists for delivery to variable depths depending on the therapeutic and its site of action within the skin. Delivery concentration could also be varied as a function of US amplitude, duty cycle and treatment duration for the same gel formulation. Further research will focus towards a gel formulation that does not require cold storage, therefore also eliminating these costs from the current vaccination process. The key barrier to this technology is the variability in performance. Thus far, the system has only been tested and characterised with OVA as a model vaccine, and the use of other molecules as well as the skin condition at the treatment site, are very likely to affect the delivery profile. Further research towards methods of dose control is therefore necessary before clinical translation of this technology. Other key areas of future work are discussed in section 7.2. The optimisation of the technologies and approaches described will help the field of transdermal vaccination progress so that reliable and robust needle free vaccination can be achieved.

7.2. Future Work

The first stages of the development of an ultrasound-assisted vaccination system, with evidence that delivery and vaccine-specific immune response is achievable *in vivo* are presented in this thesis. In future studies, increasing the dose efficiency of this system represents a key area of study. Optimisation of (1) the ultrasound application system and parameters, and (2) the vaccine application form are believed to be the key steps in achieving a higher dose efficiency.

The current ultrasound application system consists of a large focussed transducer with a coupling cone attached, driven by a complex sequence of numerous pieces of equipment. Use of an unfocussed transducer capable of producing a peak negative focal pressure of 1 MPa would increase the treatment area (by introducing an US field as opposed to a focus), and therefore the amount of vaccine transferred

per treatment. Secondly, if the transducer itself is designed with a short (up to 1 cm) near field distance, a coupling cone would not be required and the vaccine-loaded coupling gel would be sufficient to provide ultrasound coupling to the skin. The equipment used to drive the transducer itself requires miniaturisation and simplification to optimise it for this application. Such optimisation would allow the system to be implemented in a primary care, or even at-home setting.

With an improved transducer, a re-optimisation of ultrasound parameters represents an area of further study. The pulse durations and PRF used in this thesis were chosen primarily to prevent heating in Chapter 3, and carried through the studies when a therapeutic effect was demonstrated. These parameters may offer scope for optimisation for minimum power requirements (if a shorter pulse/lower PRF achieves the same effect) whilst producing maximum inertial cavitation energy in a given gel formulation.

Vaccine-loaded coupling gel application in this study was performed using a gel chamber at the focus of the ultrasound transducer. The gel chamber was of height 20 mm, which although was greater than the length of the ultrasound focus at 256 kHz, represented a very long distance for OVA molecules positioned at the top of the chamber to travel to reach the skin prior to delivery. Remodelling the dimensions of the gel chamber to decrease height and increase surface area in contact with skin is hypothesised to increase delivery efficiency from the gel into the skin.

The gel formulation itself also represents a further area of study. The NC concentration used in this work was the maximum concentration achievable at the time. Although it has been shown to be effective for the studies performed, it may be possible to achieve the same effect with a lower concentration, which would decrease the cost of the gel component. Conversely, recent developments show that higher concentrations of NCs can be achieved, therefore increasing the concentration of NCs to investigate increased delivery with a decreased vaccine dose also offers potential cost savings. The *in vivo* study

showed that the gel viscosity is a key factor in delivery dose and response. Two gel viscosities were used in this work; (i) 0.5% to mimic the concentration in clinically approved coupling gels, and (ii) 2% to account for the addition of NC and OVA solutions. However, experimentation at other concentrations may enable a more favourable trade-off between gel viscosity and vaccine delivery.

The ability to monitor inertial cavitation and acoustic emissions during treatment represents a highly attractive opportunity for non-invasive remote feedback on delivery in real-time. The work described in this thesis shows that delivery is achievable only in the presence of inertial cavitation. Therefore finding a way to correlate acoustic emissions during treatment to delivery dose would be a highly valuable tool to remotely assess the effectiveness of delivery using this treatment.

Once optimised, the ultrasound-assisted vaccine delivery system described in this thesis offers great potential for the development of non-invasive delivery platform that is applicable over a wide range of vaccines. One of the largest areas of future work will involve the optimisation of ultrasound parameters and gel formulations for different types of vaccines to ensure that inertial cavitation-related mechanisms are exploited to their greatest potential. Following this final optimisation stage, this system offers the capability to deliver a vast number of vaccines without any of the current disadvantages associated with injections. Additionally, this system offers the capability for self-administration of vaccines, offering the potential to increase compliance rates. Currently, there are no vaccinations or delivery systems that can be administered or used by the patient themselves. Through miniaturisation and simplification of the ultrasound hardware and by packaging the vaccine dosage form in a “patch” form it is hoped that this system can be expanded to vaccines and drugs to enable a home-use drug and vaccine delivery platform.

Appendix A

Gel production protocol

Ingredients (per 100g of gel)

Polyacrylic acid (gel) powder	0.5g
Trometamol – Trizma Base	0.5g
Propylene glycol	20.0g
Deionised water	100.0g

Procedure:

1. In a mortar, mix the polyacrylic acid powder with the polypropylene glycol, adding the liquid gradually and grinding throughout. The mixture should be homogenous, with minimal lumps.
2. In a separate beaker, mix the Trometamol and DI water. Stir to dissolve. *The solution should be colourless and transparent when mixed.*
3. Mix the two solutions from (1) and (2) together, adding (2) to (1) gradually and mixing in the mortar.
4. Weigh the total (mixed) solution.
5. Leave the solution at room temperature for at least 5 hours. The Carbomer will swell.
6. After 5 hours, reweigh the total solution. Water will have evaporated off, so restore to pre-swelling weight with DI water.

Gel degassing

7. Place the gel under vacuum for around 8 hours.
8. Transfer to centrifuge tubes and centrifuge for 4 min at 4000rpm to remove residual bubbles.